

FENWICK PROJECT OF

Candida L. Desjardins

(Name)

A Remote and Non-Contact Measurement of the Blood
Pulse Waveform with a Laser Doppler Vibrometer

(Project Title)

Edward J. Soares, Ph.D.

ADVISOR
NAME(S) AND
SIGNATURE(S)

De-Ping Yang, Ph.D.

READER
NAME(S) AND
SIGNATURE(S)

Leon Claessens, Ph.D.

**A Remote and Non-Contact Measurement of the
Blood Pulse Waveform with a Laser Doppler
Vibrometer**

Table of Contents

	Page Numbers
I. Abstract	1
II. Introduction	2-3
III. Background	4 - 46
a) Lasers	
(i) What Is a Laser and How Does It Function?	4-14
(ii) Laser Safety	156
(iii) Interferometers	16-20
b) Lasers in Medicine	
(i) Laser Tissue Interactions	21-23
(ii) Medical Applications of Lasers	24-35
c) Cardiology	
(i) The Heart and How it Functions	36-37
(ii) Blood Pressure	38
(iii) Cardiac Parameters	39-40
d) Relevant Mathematics	
(i) First Derivative Test	41
(ii) The Fundamental Theorem of Calculus	42
(iii) The Fourier Transform and Filtering	43-44

IV. Methods and Results	45 - 94
a) Experimental Setup	45-47
b) Data and Analysis	48-61
c) Human Subject Trials	62-70
d) University of Massachusetts Medical School Clinical Trials	71-76
e) Principal Component Analysis	77-84
f) Related Projects	85-88
g) Applications	89-94
V. Future Work	95 - 97
VI. Conclusions	98
VII. Appendices	
a) References	x-x
b) Figures and Tables	88-92
c) Antonelli, L., Desjardins, C., Soares, E., “A remote and non-contact method for obtaining the blood-pulse waveform with a laser Doppler vibrometer” submitted to the proceedings SPIE Photonics West: BiOS, January 2007.	
d) Human Participant Consent Form	93-94
e) Human Participant Health Questionnaire	95-96
f) List of Equipment Used	97

I. Abstract

The use of lasers to remotely and non-invasively detect the blood pressure waveform of humans and animals will provide a powerful diagnostic tool. Currently, blood pressure measurement tools are not useful for burn and trauma victims, and animals require catheterization to acquire accurate blood pressure information. The purpose of the LDV sensor method and apparatus invention is to remotely and non-invasively detect the blood pulse waveform of both animals and humans. This invention is used to monitor an animal's or human's skin in proximity to an artery using laser radiation from a laser Doppler vibrometer (LDV). This system measures the velocity (or displacement) of the pulsatile motion of the skin, indicative of physiological parameters of the arterial motion in relation to the cardiac cycle.

Tests have been conducted with an LDV that measures surface velocity, and a signal-processing unit, with enhanced detection obtained with optional hardware including a retro-reflector dot. The blood pulse waveform is obtained by integrating the velocity signal to get skin surface displacement using standard signal processing techniques. Continuous recording of the blood pulse waveform collects data containing information on cardiac health and can be analyzed to identify important events in the cardiac cycle, such as heart rate, and the timing of peak systole and of the dicrotic notch. The results presented will include plots of the blood pulse waveform measured at various arterial locations, and under different stress conditions. In addition, the blood pulse waveforms of a smaller animal will be presented.

II. Introduction

A laser Doppler vibrometer (LDV) was used to remotely and non-invasively record the arterial blood pulse waveform (BPW) of both small animals and humans. A laser beam is directed on the skin surface above a palpable artery in order to measure the velocity of the pulsatile motion of the skin surface. The resulting waveform can be monitored in real-time and recorded for further analysis of the patient's physiological condition. Qualitative analysis can be done on the morphology of a patient's waveform in respect to heart muscle contractions, valve operations, and the timing of various cardiac cycle events. This LDV technique has been used to measure the blood pulse waveform over various palpable arteries including the carotid, radial, femoral, brachial, pedal, popliteal, posterior tibial, and facial arteries of human subjects. Such a non-contact method of measuring the blood pulse waveform is particularly useful in cases where limited contact to the patient is desired, such as with trauma or burn victims, and neonatal patients.

The laser light from the LDV is reflected from the skin's surface, and the light undergoes a Doppler shift due to the surface motion along the axis of the laser beam as the artery underneath the skin contracts and expands. The light is then detected by the LDV's interferometer system and it is demodulated to obtain the skin surface velocity. The integration of this skin velocity waveform yields the displacement of the skin surface's movement, which we define as the *blood pulse waveform*.

This project investigates the use of a laser Doppler vibrometer for the non-contact measurement of the arterial blood pulse waveform of humans and animals. Experimental data is presented to demonstrate the feasibility of a non-contact, laser-based detection

method of measuring the blood pulse waveform. Analysis will also be presented to provide the insight on the type of information that can be extracted from the blood pulse waveform measured with a laser Doppler vibrometer.

III. Background

a) Lasers

(i) What is a Laser and How Does It Function?

LASER: Light Amplification by Stimulated Emission of Radiation

Light:

The light emitted by lasers is electromagnetic radiation, thus it has a wave nature consisting of vibrating electric and magnetic fields. These waves are disturbances that transmit energy from one place to another. Waves are characterized by their frequency, the number of cycles per second of oscillation of the electric or the magnetic field, and their wavelength, the length over which the wave repeats itself. The wavelength can also be described as the distance between the peaks of the wave. We can relate these two quantities by the following:

$$\lambda \times f = c \quad (1)$$

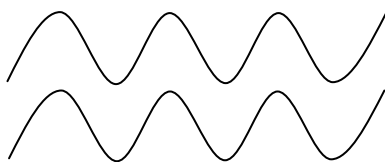
where f is the frequency, λ is the wavelength, and c is the speed of light (3.00×10^8 m/s).

Besides the wave properties of light, electromagnetic radiation has particle-like properties. Light acts as if it is consisted of discrete amounts of energy called photons, where photon energy increases as the wavelength of light decreases. In most light-matter interactions, the particle nature of light dominates over the wave nature [5].

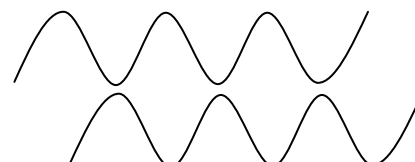
Laser light properties are very different from the properties of conventional light sources. Laser light can be characterized by the following properties; directivity, coherence, brightness, and monochromaticity. At large distances, the light from a laser

will gradually broaden due to diffraction so that it is not a perfectly parallel flux of light. This phenomenon is known as directivity, and because of it, laser light can be focused to a diameter only a few times the size of its wavelength. The small divergence angle of the beam allows the light to be focused to very small dimensions and thus greater intensities. The brightness of a beam is the power emitted per unit surface area per unit solid angle. The brightness of a beam doesn't change as it propagates; however, focusing may increase the irradiance (power/area) [5].

Coherence is the property of laser light which distinguishes it from ordinary light sources. A coherent beam of light has the same wavelength, the same direction, and the same phase. Unlike conventional light sources, the light emitted from a laser beam is almost purely sinusoidal over a long period of time, rather than a succession of irregular pulses. If the light waves all have the same wavelength in the beam, then it is monochromatic light. The phase of the waves refers to their positions with respect to one another [5]. If two waves are in phase, their peaks are perfectly lined up in space and time. If the waves are shifted with respect to one another, they are out of phase by a given degree, as shown by the following:



IN-PHASE



OUT OF PHASE BY 180°

Spatial coherence describes the phase of waves at two different points at a given instant in time such that the light at the top of the beam is coherent with the light at the bottom of

the beam. If two waves in a beam remain coherent for a long period of time as they move past a given point, then the light is temporally coherent. Thus, the two waves stay in phase for many, many wavelengths. Coherence is the property of light that causes laser speckle. Laser speckle is produced when laser light is scattered from a diffusing surface [5].

Amplification by Stimulated Emission:

All lasers contain material capable of amplifying radiation. The laser (or active) medium is the optical amplifier capable of sustaining stimulated emission because of its atomic structure, whether it be a solid, liquid, or a gas laser medium. It is the collection of atoms and molecules that can be excited to a state of an inverted population ratio, the state where more atoms are in an excited than a lower energy state. Without excitation, there are normally more atoms in the laser medium which are in lower energy levels than in high energy levels. Once the medium is excited in such a way that the atoms in upper energy levels outnumber those in the lower levels, the light incident on the medium will be amplified by stimulated emission. In 1917, Albert Einstein proposed that stimulated emission was responsible for amplifying radiation [5].

There are two types of energy emission which must be distinguished; spontaneous emission and stimulated emission. The higher energy level atoms within the laser can emit energy via spontaneous emission. During spontaneous emission, excited states of atoms only remain for short periods of time and eventually the atom will release the extra energy as a photon of light and returns back to its ground state. Stimulated emission occurs when an excited atom collides with a spontaneously emitted photon and returns

down to its ground state. This action emits two photons of light, the original photon that came in, and a photon from its jump down. The two photons released from stimulated emission travel in the same direction as the photon that originally came in, which explains the directivity of lasers since the beam only travels in one direction [5].

In summation, spontaneous emission has no photons coming in but one photon coming out, and with stimulated emission, there is one photon coming in and two photons coming out. The following diagram demonstrates amplification by stimulated emission.

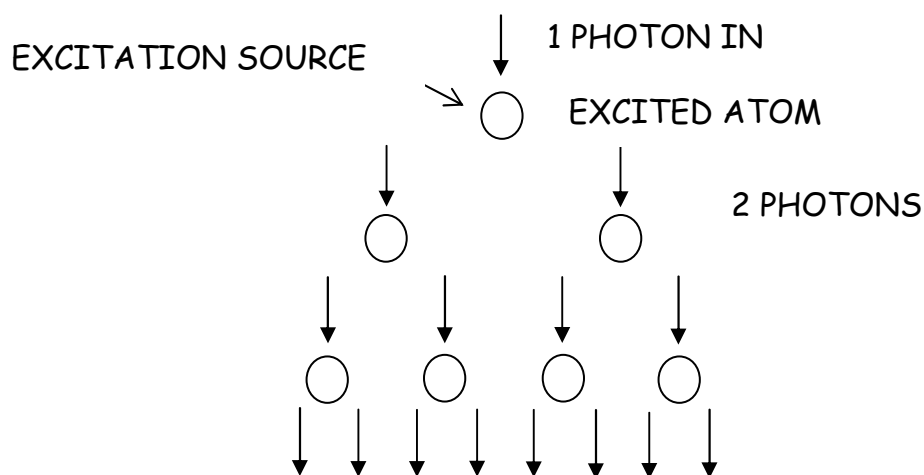


Figure 1 – Diagram of amplification by stimulated emission

After exposure to an excitation source in the laser medium, a photon moving south will strike an excited atom, and two photons are released traveling south. The two photons going south then strike two more excited atoms, which release four photons moving south and so forth. This doubling phenomenon is the amplification of laser light [5].

The laser scheme below demonstrates the concept of amplification and also explains the properties of laser light as well. Each laser produces its beam by combining

stimulated emission, a resonant cavity, and a pump source used as an excitation mechanism.

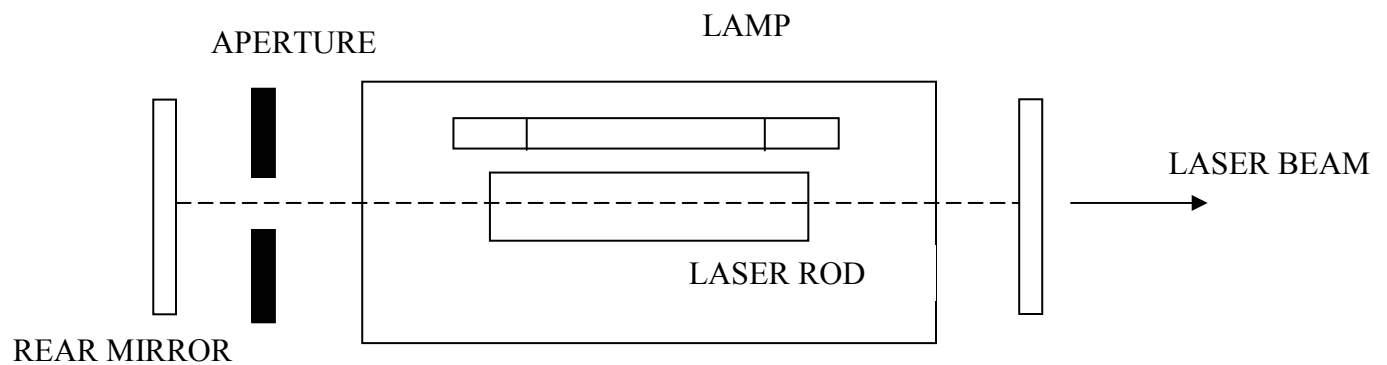


Figure 2 (a) – Laser Scheme [5]

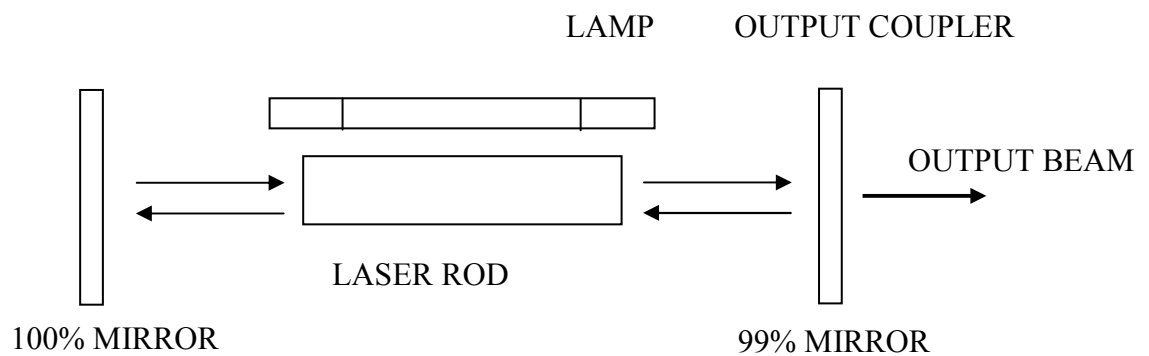


Figure 2 (b) – Typical Resonant Cavity

Every laser has a cavity with at least two mirrors at the ends filled with lasable material. One of the mirrors is 100% reflective so that all of the photons bounce back off of the mirror and into the medium for more amplification to occur. The other mirror is only partially reflective so that some of the photons bounce back into the medium, while the

others go through the mirror to create the output usable laser beam. Thus, the beam will oscillate between the mirrors, but will only exit one way [5].

In particular, I studied the Helium-Neon (He-Ne) laser and its functions. The following table summarizes its properties:

Active Medium	Neon Gas
Most common output wavelength	632.8nm
Power Range	0.1mW – 100mW
Pulsed or CW	CW (continuous wave)
Excitation	Electrical
Polarization	Unpolarized or Linearly Polarized

Table 1 – He-Ne laser properties

The following is a diagram of a He-Ne laser:

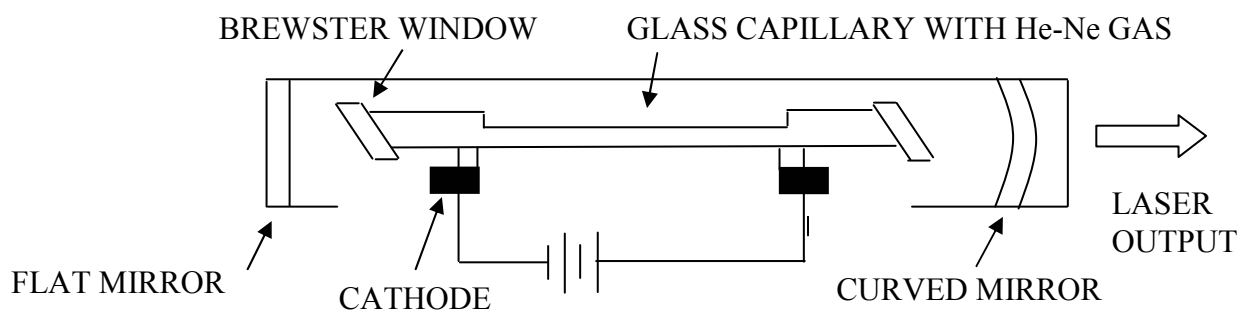


Figure 3 – He-Ne laser scheme

The population inversion mechanism for a He-Ne laser is electrical, with helium being excited by an electron impact, then transferring its energy to neon atoms. The lasing medium used is a mixture of helium and neon gas (about 90% helium and 10% neon), which is enclosed within the glass capillary, which is between the two mirrors. As mentioned above, one mirror is partially reflective, and the other is fully reflective. In

order to maintain population inversion, the atoms must be able to easily collide, thus the diameter of the glass capillary tube must be small to ensure a high collision rate.

However, smaller tubes limit the output power, so a balance must be made. Overall, the laser is a function of the medium mixture, the pressure, the tube diameter, and the tube current. Gas lasers are successful and widely used in industry because they are compact, portable, and easy to use [5].

Optical Components:

Optical components help to manipulate the output beam so that it can be used in various ways. Optics can help to achieve many desired effects, such as reflecting light with mirrors, refracting or focusing light with lenses, and wavelength selection by altering polarization. Geometrical optics deals with the particle nature of light having straight line propagation and particle-like dynamics. Physical optics deals with the wave properties of light, exhibiting diffraction and interference effects [5].

There exist three fundamental laws of geometrical optics:

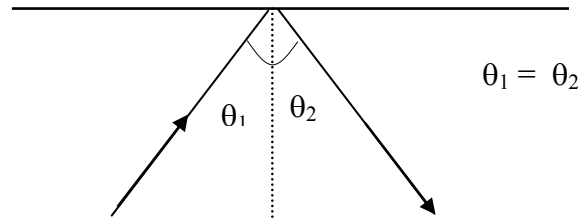
The Law of Rectilinear Propagation:

Unless it passes through a different medium, light travels in a straight line.



The Law of Reflection:

For a specular reflection, the angle of incidence is equal to the angle of reflection.

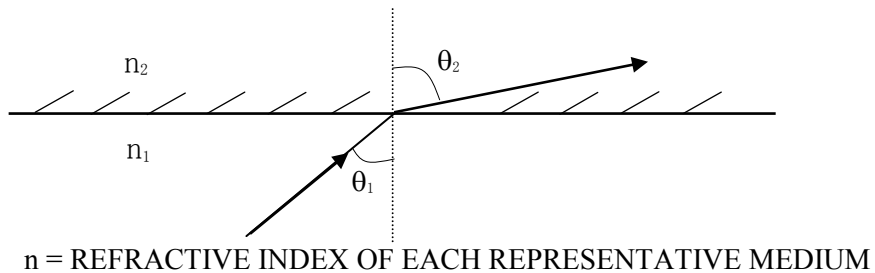


The Law of Refraction (Snell's Law):

When a light ray passes at an oblique angle from a medium of a lesser to a greater optical density (refractive index), it will bend toward the normal. Conversely, a ray passing from a medium of greater refractive index to a lesser, the ray is bent away from the normal,

$$n_1 \sin\theta_1 = n_2 \sin\theta_2. \quad (2)$$

θ_1 = ANGLE OF INCIDENCE, θ_2 = REFRACTED ANGLE



The refractive index is the measure of the speed at which light travels through a material.

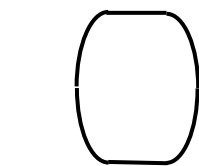
As a reference, the refractive index, n , in a vacuum is defined to be equal to one. For all other materials, the refractive index is:

$$n_{\text{material}} = c_{\text{vacuum}} / c_{\text{material}}, \quad (3)$$

where this ratio is usually greater than one. Taken from Handbook of Chemistry and Physics, the refractive index of our atmosphere, $n = 1.0002926$, is small enough that refractive indices of solids are measured relative to the air rather than to a vacuum of $n = 1.0$. The refractive index depends on the nature of the material being studied as well as the wavelength of light passing through it. In general, as the material density increases, the refractive index increases [5].

Lenses are great tools when working with light. The most common lenses have spherical or cylindrical surfaces. Spherical lenses focus light in two dimensions - bringing a circular beam down to a point. Cylindrical lenses focus in one dimension - bringing a circular beam down to a line. The lenses are classified as either positive or negative, where positive lenses bend rays so they converge and negative lenses bend rays so they diverge [5].

Positive (Converging) Lenses



Double Convex



Plano-Convex

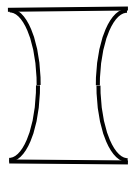


Positive Meniscus

[5]

Positive lenses are thicker in the middle than on the edges, with the middle of the lens retarding an incoming wave more than the edge. Positive lenses bend the wave in front of an incident optical signal. The incident plane wave will emerge so the wave surfaces converge to a point behind the lens.

Negative (Diverging) Lenses



Double Concave



Plano-Concave

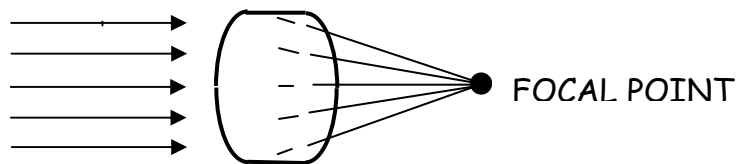


Negative Meniscus

[5]

Negative lenses are thicker at the edges than in the middle. A negative lens bends an incident plane wave such that the wave surfaces are diverging from a point in front of the lens.

The focusing power of a lens is measured by examining its focal length, the distance from the center of a thin lens to the focal point. The focal length will depend on the curvature of the lens and the refractive index of the lens material. The focal point of a positive lens is the point where the rays of light initially parallel to the axis all come to a point as shown by the following:

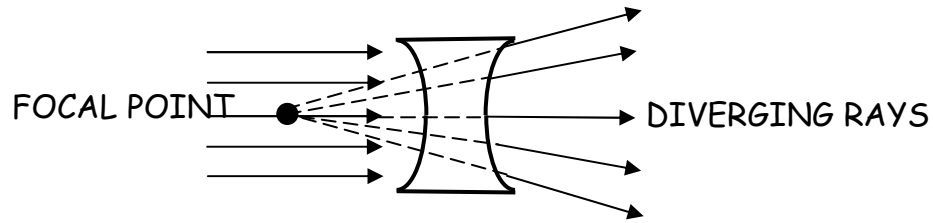


PARALLEL RAYS

POSITIVE LENS

[5]

The focal point of a negative lens is the point behind the lens from which rays of light appear to diverge as seen below:



PARALLEL RAYS NEGATIVE LENS

[5]

The focal length is an important property to measure since it can be used to determine optical characteristics with relatively simple calculations.

The position of an image formed by a lens can be found by using the Thin Lens Equation:

$$1/f = 1/S_1 + 1/S_2 \quad (4)$$

where f = focal length, S_1 = distance from object to lens, and S_2 = distance from image to lens.

(ii) Laser Safety

Laser safety is classified by the wavelength of the emitted light and either the average power output in Watts for continuous wave lasers, or the total energy per pulse measured in Joules for pulsed lasers. The following table taken directly from Goldwasser's "Laser Safety Classifications" [8], demonstrates the classifications of laser safety.

Laser Safety Class Type	Safety Guidelines
Class I lasers	Lasers that are not hazardous for continuous viewing or are designed in such a way that prevent human access to laser radiation. These consist of low power lasers or higher power embedded lasers (i.e., laser printers). Maximum power less than 0.4 μ W
Class II visible lasers (400 to 700 nm)	Lasers emitting visible light which because of normal human aversion responses, do not normally present a hazard, but would, if viewed directly for extended periods of time. This is like many conventional high intensity light sources. Maximum power less than 1 mW for He-Ne laser.
Class IIa visible lasers (400 to 700 nm)	Lasers emitting visible light not intended for viewing and under normal operating conditions would not produce a injury to the eye if viewed directly for less than 1,000 seconds (i.e. bar code scanners). Maximum power between .40 and 1 mW for He-Ne laser.
Class IIIa lasers	Lasers that normally would not cause injury to the eye if viewed momentarily but would present a hazard if viewed using collecting optics (fiber optics loupe or telescope). He-Ne laser power 1.0 to 5.0 mW.
Class IIIb lasers	Lasers that present an eye and skin hazard if viewed directly. This includes both intrabeam viewing and specular reflections. Class IIIb lasers do not produce a hazardous diffuse reflection except when viewed at close proximity. Visible Argon laser power 5.0 mW to 500 mW.
Class IV lasers	Lasers that present an eye hazard from direct, specular and diffuse reflections. In addition such lasers may be fire hazards and produce skin burns. Maximum power greater than 500mW

Table 2 – Summary of Laser Safety Guidelines [8].

(ii) Interferometers*

* Taken from Antonelli, L., Desjardins, C., Soares, E., "A remote and non-contact method for obtaining the blood-pulse waveform with a laser Doppler vibrometer" submitted to the proceedings SPIE Photonics West: BiOS, January 2007.

One method to optically detect a small displacement or movement of an object is by means of interferometry. The principle of laser Doppler vibrometer (LDV) operation is based on the interference of two beams of light. The two laser (reference and measurement) beams arrive at the photodetector surface after one has undergone an optical path change and Doppler frequency shift. The measurement beam illuminates a surface and undergoes an optical path length change as the surface moves along the direction of the laser beam. This optical path difference is caused primarily by the vibration of the skin. The phase difference between the two beams inside the interferometer is represented by their beat frequency at the photodetector.

In our work, we used a Polytec PI model OFV-353 LDV to obtain initial measurements of the blood pulse waveform by non-contact means at the subject's skin over the carotid artery. The system works on the basic principle of laser interferometry for Doppler shift velocity detection. Red light from a He-Ne laser source is divided evenly by a beam splitter (BS1) into a reference beam and a measurement beam. The frequency of the reference beam is shifted using an acousto-optic modulator (Bragg cell) to introduce a 40 MHz signal. The modulation of the reference beam is desired in order to discern the direction (along the axis of the laser beam) of the movement obtained from Doppler shift of the returned signal. The measurement signal goes through the polarizing beam splitter (BS2) and Quarter Wave Plate (QWP), which behaves as a directional coupler. The light output from the vibrometer goes straight to the object under test, and the reflected beam is redirected to beam splitter (BS3). The reference beam and the return

beam from the object are detected by detectors D1 and D2 and are subsequently combined and demodulated to obtain velocity and displacement information. Figure 4 shows a block representation of such a system, which is based on a Mach-Zehnder interferometer [25].

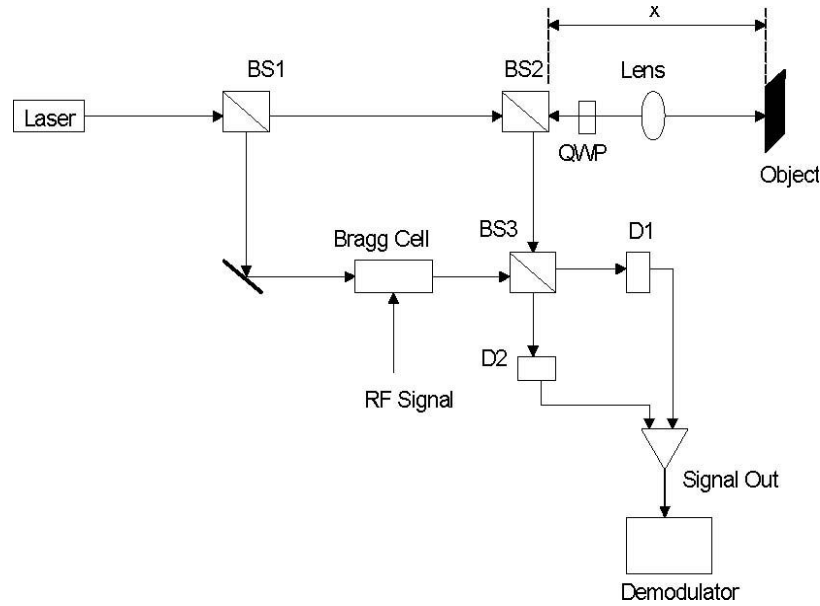


Figure 4 - Modified Mach-Zehnder heterodyned interferometer configuration used in the Polytec Laser Doppler Vibrometer [25]

The equations to follow give a mathematical representation of the system operation. The laser output beam into the first beam splitter is represented by the electric field equation

$$E = E_0 e^{i(\omega t - kx)} \quad (5)$$

where $E = \sqrt{I}$ is the original field amplitude and I is the field intensity, ω is the angular frequency and k is the wave number of the optical wave, x is the laser beam propagation distance, and t is time.

Each of the two light beams will undergo a phase shift determined by the distance it has traveled. When the light reach detectors D1 and D2 its amplitude will be reduced by half due to the BS1 and BS2 beamsplitters. The two field amplitudes interfering on the surface of D2 can be described by:

$$E_1 = \frac{E_0}{2} e^{i(\omega t - k_1 x_1)} \quad (6)$$

$$E_2 = \frac{E_0}{2} e^{i(\omega t - k_2 x_2)} \quad (7)$$

The phase shift $k_i x_i = 2\pi l_i / \lambda$ is related to the optical path traveled by the beams. The quantity λ is the wavelength of the light source emitted by the laser Doppler vibrometer. The total field amplitude at D1 is the combination of E_1 and E_2 from (1) and (2).

$$E_{total} = \frac{E_0}{2} e^{i(\omega t - k_1 x_1)} + \frac{E_0}{2} e^{i(\omega t - k_2 x_2)} \quad (8)$$

The photodetector detects the intensity of the light, which is calculated from the field amplitude E_{total} by multiplication with its complex. The total intensity at the photodetectors D1 and D2 are:

$$I_1 = \frac{E_0^2}{2} - \frac{E_0^2}{2} \cos(k_2 x_2 - k_1 x_1) \quad (9)$$

$$I_2 = \frac{E_0^2}{2} + \frac{E_0^2}{2} \cos(k_2 x_2 - k_1 x_1) \quad (10)$$

Given that the interferometer has been accurately and symmetrically aligned, the optical

phase difference $\Delta\theta$

$$\Delta\theta = k(x_2 - x_1) = 2\pi \left(\frac{x_2 - x_1}{\lambda} \right) = 2\pi \frac{\Delta x}{\lambda} = \frac{2\pi}{\lambda} 2x \quad (11)$$

between the reference and measurement beams, is determined by the external distance that the light travels from BS2 to the object (skin surface) and back to the sensor. The change in the path length modulates the phase of the laser due to the lateral movement of the target, (motion along the axis of the laser beam) in this case the pulsatile motion (velocity) of the skin.

The distance, $x = vt$ can be expressed in terms of the velocity, v that the target moves towards or away from sensor head along the axis of the laser beam in a given time, t . Therefore, the time-dependent phase difference becomes:

$$\Delta\theta = 2\pi \frac{2v}{\lambda} t = 2\pi f_D t \quad (12)$$

where f_D is the Doppler frequency. However, this does not show the direction of the object motion. Equations 5 and 6 can then be written showing Doppler information as:

$$I = \frac{E_0^2}{2} + \frac{E_0^2}{2} \cos(2\pi f_D t) \quad (13)$$

The direction of movement of the target is obtained modulating the reference beam with Radio Frequency (RF) signal. The photodetector detects the signal with a frequency given by:

$$f_{out} = f_m + f_D \quad (14)$$

where f_m is the modulation frequency. The frequency modulation principle denotes the heterodyne interferometer system design approach [26] used here to detect the Doppler and direction of its movement. The skin motion causes a change on the optical path length from the laser to the skin surface and back to the detector. The LDV is assumed to be stationary while measuring the skin motion.

b) Lasers in Medicine

i) Laser-Tissue Interactions*

* Taken from Antonelli, L., Desjardins, C., Soares, E., "A remote and non-contact method for obtaining the blood-pulse waveform with a laser Doppler vibrometer" submitted to the proceedings SPIE Photonics West: BiOS, January 2007.

The optical properties of skin tissue influence all biological signal measurements that employ light energy. Models that predict reflection and transmission of light by tissue have been developed. However the accuracy of these models depends on how well the optical properties of tissues are known. Optical parameters are obtained by converting measurements of observable quantities like reflection into parameters that characterize light propagation in tissue. Such conversion processes are based on a particular theory of light transport in tissue [13]. The theory of light transport in tissue is preferred in tissue optics instead of analytical approaches using Maxwell equations because of the inhomogeneity of biological tissue.

The reflectance from the skin is dependent upon the optical properties of the skin structure including the blood-free epidermis, as well as dermis layers as shown in Figure 5. The thickness of the epidermis including the stratum corneum is 10-150 μm . The dermis layer is approximately 1-4 mm thick and contains elastic collagen fibers and blood vessels of different sizes. The epidermal layer contributes about 6% to the total reflectance at wavelengths over the range from 400 to 800 nm [14]. This is a specular reflectance at the air-stratum corneum interface, which suggests that minimal scattering occurs in the epidermis, so that it acts primarily as an absorptive medium. Van Gemert *et al* [15] found that for wavelengths between about 300nm and 1000nm, light scattering from nonpigmented tissues dominates absorption. And for wavelengths between 240nm

and 633nm skin layers are strongly forward scattering media, meaning that the greatest scattering happens at the zero degree to the incident light.

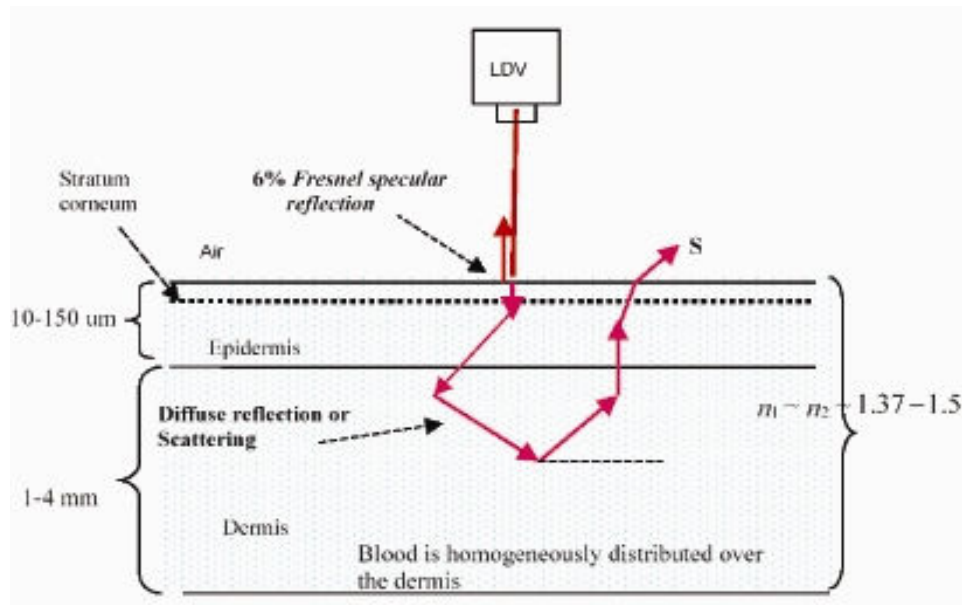


Figure 5 - Simplified model of the skin with plane parallel epidermal and dermal layers¹⁵.

Light penetration through tissue is important because the skin tissue is composed of several layers, which in turn can be broken down into sub-layers. Radiation at some wavelengths penetrates deeper than others and the absorption and scattering of such wavelengths in a tissue varies. Such scattered light once detected and demodulated provides information on the lateral displacement and velocity of the vessels and therefore the necessary information to show an arterial blood pulse waveform.

Measurements done during this study used an LDV to probe the surface area of the skin directly above the carotid artery on the neck of a person. Little skin preparation was needed, especially since this is an area with minimal hair growth. Any hair follicles that exist buried within the skin tissue layers will contribute to some extent to the absorption and scattering of the light and to the physiological noise present in the tissue.

Such characteristics of light as it travels in a tissue should be accounted for and explained by the diffusion of light in tissue theory. Optional optical equipment can be used at some instances to enhance the intensity of the reflected light at the detector, while preventing optical transmission into the skin layers. As described in the Experimental Setup section, retro-reflective tape was used throughout the project in order to enhance the signal.

(ii) Medical Applications of Lasers

The following section is a summary of Essue, Paul, David P. Beach, and Allen Shotwell. Applications of Lasers and Laser Systems [7] and Niemz, Markolf H. Laser-Tissue Interactions [13]. Lasers have found their way into many fields of medicine, including Ophthalmology, Dermatology, Dentistry, Gynecology, Urology, Cardiology/Angioplasty, Neurosurgery, Orthopedics, Gastroenterology, Otorhinolaryngology, and Pulmology [9]. In 1961, just one year after the invention of the laser, the first experimental studies were conducted in ophthalmology. By 1963, patients were already being treated for retinal detachment with a ruby laser. Also by 1963, the first surgical application of lasers was documented to have removed a growth on the vocal chords of a three-year-old boy [9]. The most significant advances have been recently made in medical laser surgery. Most lasers today are used in minimally invasive surgery (MIS), non-contact, and bloodless surgical procedures. Lasers have been nicknamed "the bloodless scalpel" and have earned the title as the universal scalpel and treatment aid [5].

There is still much potential left for lasers in the medical field and that this technology has seen only its beginning stages in the medical world. There is a demanding need for research in biostimulation for therapeutic purposes with extremely low-powered lasers. There are so many possibilities for applications if successful results occur. Biostimulation is believed to be a photochemical interaction occurring at very low irradiances, so that the temperature of the target tissue does not rise above normal body temperature. The understanding of the science behind biostimulation is something that is

still unknown and needs to be improved. There have not been many patients in the studies and clinical protocols were never established, especially between research groups. There has also been difficulty examining the placebo effect since half of the time the patients claimed to be spontaneously cured without treatment [9]. The following table demonstrates the ambiguity of the research that has taken place in biostimulation.

Observation	Target	Laser Type	Reference
Hair Growth	Skin	Ruby	Mester <i>et al.</i> 1968
Wound Healing	Skin	Ruby He-Ne	Mester <i>et al.</i> 1969, 1971 Brunner <i>et al.</i> 1984 Lyons <i>et al.</i> 1987
No Wound Healing	Skin	He-Ne Argon Ion	Hunter <i>et al.</i> 1984 Strube <i>et al.</i> 1988 Jongsma <i>et al.</i> 1983 McCaughan <i>et al.</i> 1985
Stimulated Collagen Synthesis	Fibroblasts	Nd:YAG He-Ne	Castro <i>et al.</i> 1983 Kubasova <i>et al.</i> 1984 Boulton <i>et al.</i> 1986
Suppressed Collagen Synthesis	Fibroblasts	Nd:YAG	Abergel <i>et al.</i> 1984
Increased Growth	Cells	Diode	Dyson and Young 1986
Suppressed Growth	Cells	He-Cd He-Ne	Lin and Chan 1984 Quickenden <i>et al.</i> 1993
Vascularization	Oral Soft Tissue	Diode	Kovacs <i>et al.</i> 1974 Cho and Cho 1986
Pain Relief	Teeth	He-Ne Diode	Carrilo <i>et al.</i> 1990 Taube <i>et al.</i> 1990
No Pain Relief	Teeth	He-Ne Diode	Lundenberg <i>et al.</i> 1987 Roynesdal <i>et al.</i> 1993

Table 3 - Biostimulative Effects [9]

The contradictory evidence given in Table 3 implies that further research is needed, since for just about every desired effect, there are contradictory results. These discrepancies need to be resolved, and the only way to do so is by continuing basic research in this area. When the proper research has been done, these biostimulation effects could have tremendous effects in the medical field, especially in the cases of increased growth in

cells and wound healing. Biostimulation could be the answer to some of medicine's most troubling issues.

Before investigating all of the medical applications of lasers, it was important to first understand the reaction of biological tissues with lasers. There are mainly five interactions of laser light with biological tissue: photochemical interactions, thermal interactions, photoablation, plasma-induced ablation, and photodisruption [9].

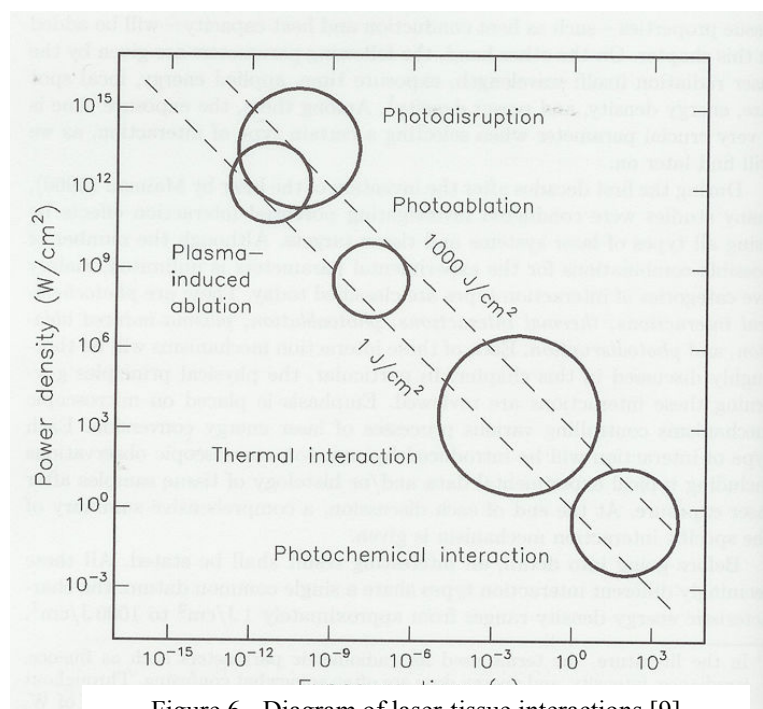


Figure 6 - Diagram of laser-tissue interactions [9]

Photochemical Interactions:

The study of photochemical interactions of lasers with tissue arose from the observation that light can induce chemical effects and reactions with macromolecules and tissues. The most obvious example is the process of photosynthesis in plants.

Photochemical interactions take place at very low power intensities and long exposure times ranging from seconds to long continuous waves. Selection of the laser parameters

is determined by the scattering in the target tissue. For the most part, wavelengths in the visible range are chosen, such as rhodamine dye lasers at 630 nm, because of their efficiency and high optical penetration depths. Although it has not yet been proven, biostimulation has been attributed to photochemical effects. Photochemical interaction mechanisms are the most important in photodynamic therapy (PDT) [9].

PDT is a method used in hospitals today to get rid of unwanted cells. During PDT, special chromophores are injected into the body and monochromatic irradiation triggers very selective photochemical reactions that result in biological transformations. Since the early 1900's, certain dyes have been known to induce photosensitizing effects. In 1942, it was found that certain porphyrins have a long clearance period in tumor cells and in 1976 the first application of a photosensitizer was used in the case of human bladder carcinoma [9].

PDT is a major pillar for the treatment of cancer, but research is also being done to try to use its powers to eliminate bacteria. So far, photosensitizers have been used on streptococcus sanguis, a bacterium of dental plaques. Photosensitizers may also be used to diagnose tumors since it takes so much longer for the tumor cells to get rid of the photosensitizers [9].

A chromophore capable of light-induced reactions in other non-absorbing molecules is called a photosensitizer. Photosensitizers are mostly organic dyes and are characteristic for remaining inactive until irradiated. After excitation by irradiation, the photosensitizer performs simultaneous/sequential decays which result in intramolecular transfer reactions. Towards the end of the reactions, highly cytotoxic reactions occur and cause irreversible oxidation of essential cell structures [9].

A typical PDT procedure would consist of the following steps:

1. Inject the photosensitizer into a vein of the patient
2. Within a certain known time frame, the photosensitizer is distributed throughout the body to all of the soft tissues excluding the brain.
3. After a known time frame, most of the photosensitizer is cleared from the healthy tissue and will remain in the tumor cells.
4. Laser irradiation is applied for as long as needed and selective necrosis of the tumor cells is enabled.

Thermal Interactions:

The major parameter change of thermal interactions is an increase in temperature and can be caused by either pulsed or continuous-wave (CW) laser radiation. The different effects that may be observed in biological tissue are coagulation, carbonization, melting, and vaporization depending on the duration and peak temperature of the application [9].

Temperature	Biological Effect
37°C	Normal
45°C	Hyperthermia
50°C	Reduction in enzyme activity, cell immobility
60°C	Denaturation of proteins and collagen, coagulation
80°C	Permeabilization of membranes
100°C	Vaporization, thermal decomposition (ablation)
>100°C	Carbonization
>300°C	Melting

Table 4 - Thermal Effects of laser irradiation [9]

The location of these thermal effects in the tissue is diagrammed below:

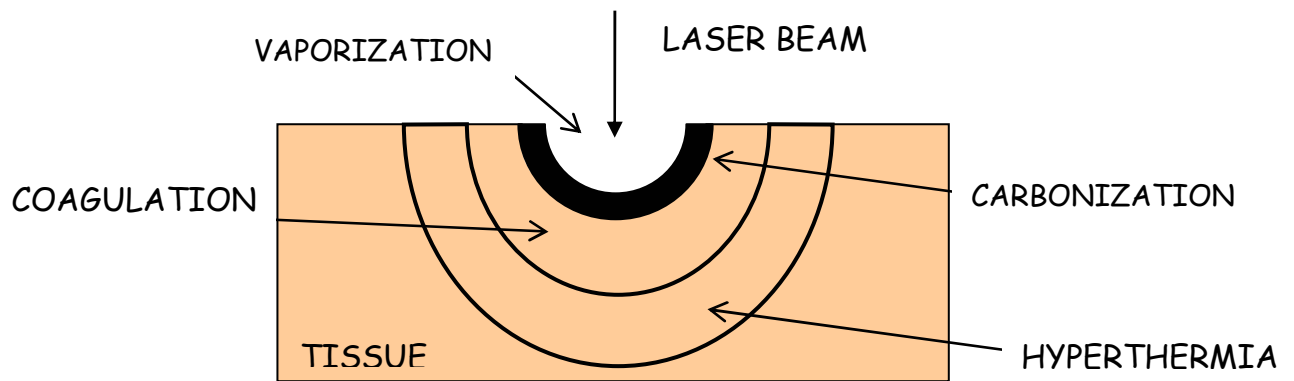


Figure 7 - Location of thermal effects in tissue [9]

Coagulation is the process of changing from liquid to a thickened mass, like blood clotting. During coagulation, temperatures reach up to about 60°C (about 140°F) and the tissue becomes necrotic, or dead.

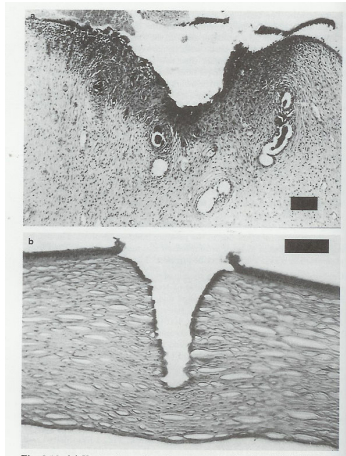


Figure 8
 (a) Uterine tissue of a rat coagulated with a CW Nd:YAG laser
 (b) Human cornea coagulated with 120 pulses from an Er:YAG laser [9]

Vaporization is the conversion of a solid or liquid into a vapor and is also known as a thermomechanical effect because of the pressure build-up which occurs. The resulting ablation is called thermal decomposition [9].

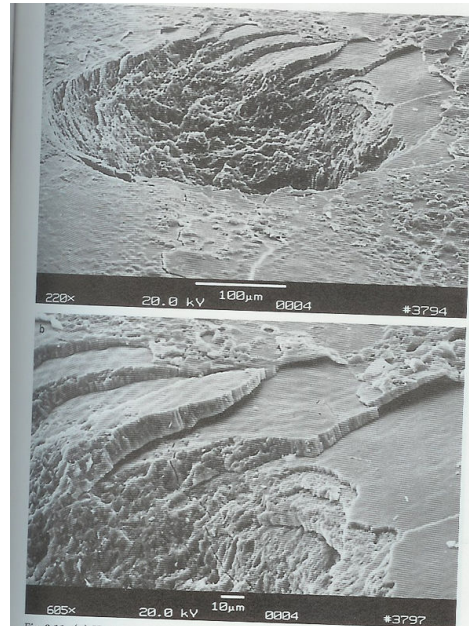


Figure 9
 (a) Human tooth vaporized with 20 pulses from an Er:YAG laser
 (b) Enlargement [9]

Carbonization is actually an unwanted process that can occur if too much energy is applied to the target tissue. When temperatures reach above 100°C, the tissue carbonizes, or releases carbon, which turns the tissue black. Carbonization only makes surgery more difficult since it is now harder to see with blackened tissue.

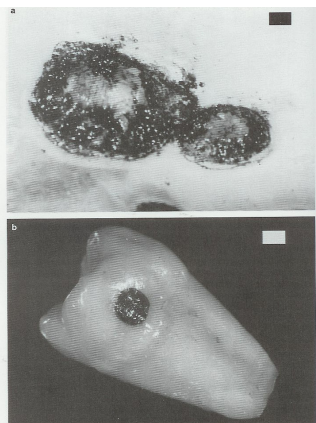


Figure 10
 (a) Tumor metastases on human skin carbonized with a CW CO₂ laser
 (b) Human tooth carbonized with a CW CO₂ laser [9]

Melting is the process of changing from a solid to a liquid state and will occur above 300°C [9].

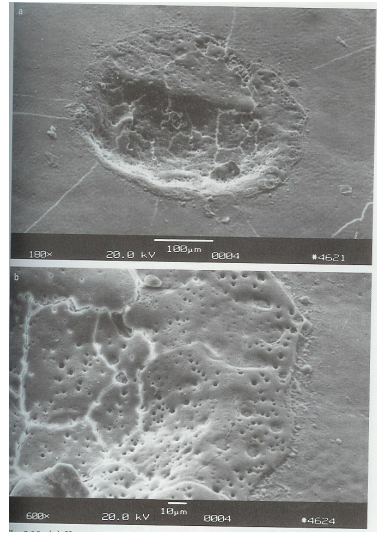


Figure 11
(a) Human tooth melted with 100 pulses from a Ho:YAG laser
(b) Enlargement [9]

Like photochemical reactions, thermal interactions can be applied towards the treatment of tumor cells. Laser-Induced Interstitial Thermotherapy (LITT) has recently been introduced to treat various tumors of the body including the retina, brain, prostate, liver, or the uterus. Gynecology and urology have the most significant uses of LITT to treat malignant tumors in the uterus as well as treating benign prostatic hyperplasia (BPH). The main idea of LITT is to position a laser applicator inside the tissue to be treated (like a tumor), and achieve necrosis by heating the cells above 60°C so that coagulation may occur [9].

Photoablation:

Photoablation is an ultra-violet light induced ablation which precisely "etches" tissue. Photoablation is also known as ablative photodecomposition since the material is decomposed when exposed to high intense laser irradiation. Overall, the UV light excites the chemical bonds of the target material, thus changing the molecules from an attractive to a repulsive state. This will also change the volume that each molecule now occupies,

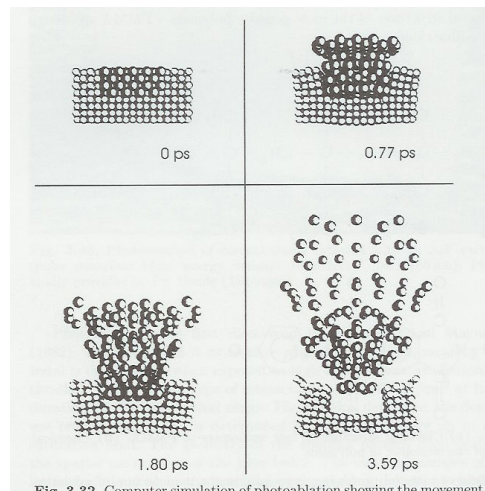


Fig. 3.32. Computer simulation of photoablation showing the movement of

Figure 12 - Computer simulation of photoablation [9]

therefore changing their momentum, and the result is ablation [9]. It is important to note that once the target molecules have disassociated, there is an ejection of that section and necrosis does not occur, as shown by Figure 12. It is also important to distinguish the difference between thermal interactions and photoablation. During photoablation, the energy of the UV photons is high enough to dissociate the molecules completely. Thermal interactions, however, have lower photon energy which does not reach the energy of repulsive states; it only promotes the molecules to vibrate within only a few energy levels of its ground state. The absorbed energy then dissipates to heat as the molecules return back to their ground state [9]. Thus, the main difference between photoablation and thermal interactions is the photon energy, or the laser wavelength.

The depth of tissue removal is determined by the energy up to a certain saturation limit. The geometry of the etching is established by the spatial parameters of the laser being used. The great advantages of photoablation are its precise etching, predictability, and lack of thermal damage to the surrounding tissue [9].

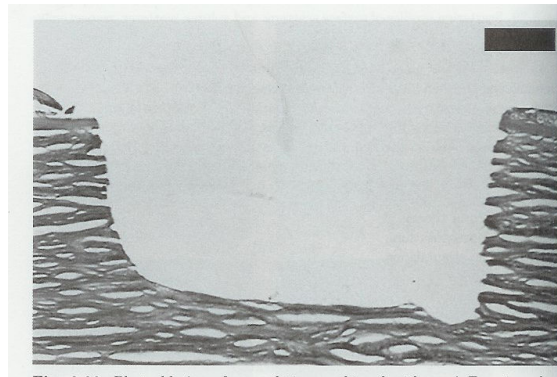


Figure 13 - Photoablation of corneal tissue with an ArF excimer laser [9]

Plasma-Induced Ablation:

We can achieve ablation of tissue by ionizing plasma formation. When exceeding power densities on the order of 10^{11} W/cm² in solids and fluids, optical breakdown occurs and a bright plasma spark forms pointing towards the laser source. By choosing the appropriate laser parameters, a very well defined and clean removal of tissue is accomplished without thermal or mechanical damage [9].

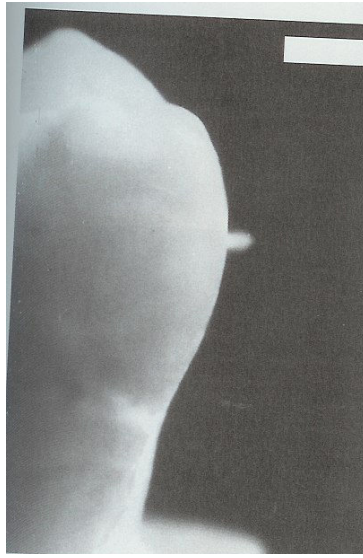


Figure 14 - Laser-induced plasma sparking on a tooth surface with a single pulse from a Nd:YLF laser [9]

Photodisruption:

Besides plasma formation, shock wave generation can occur from optical breakdown at higher pulse energies. If breakdown occurs in soft tissues or liquids, cavitations and jet formations can take place. Cavitations occur when the laser beam is focused into the tissue rather than on the tissue surface. Photodisruption has become extremely useful for minimally invasive surgery. Photodisruption splits the tissue by mechanical forces; however its effects are spread to adjacent tissue, unlike plasma-induced ablation. For nanosecond pulse durations, however, these effects are on the order of millimeters [9].

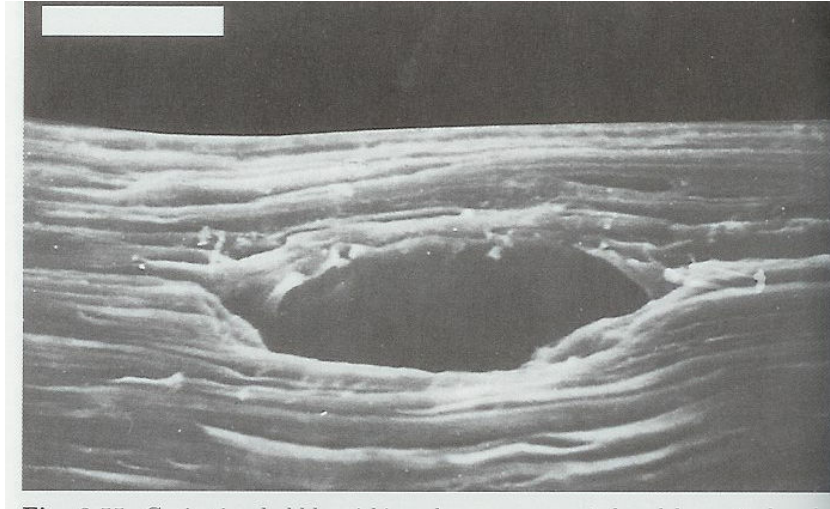


Figure 15 - Cavitation bubble with a human cornea induced by a single pulse from a Nd:YLF laser [9]

c) Cardiology

i) The Heart and How it Functions

The circulatory system is an extremely important component for living organisms since it provides rapid mass transport. Circulation provides transport of gases, solutes and heat, as well as the transmission of force [17]. The heart functions as the pump for the circulatory system by using a system of muscles which contract and shorten. For mammals, circulation is closed, which ensures that the blood returns to the heart without leaving the blood vessels (arteries, capillaries, and veins). The mammalian, and thus the human, heart consists of a four-chambered pump with contractile walls and valves to prevent the backflow of blood.

The right side of the heart functions to collect oxygen deficient blood from the body and pump it to the lungs to pick up oxygen and release carbon dioxide, thus it is conventionally color-coded as blue. The left side of the heart takes this oxygenated blood and pumps it to the rest of the body, so it is color-coded as red.

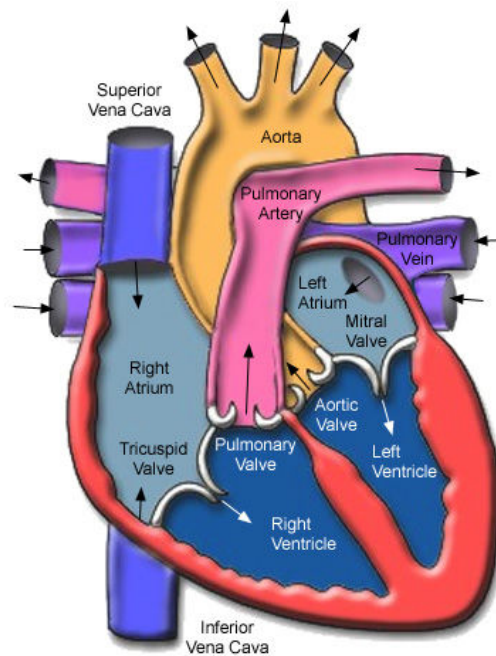


Figure 16– Figure of the human heart
<http://www.texasheartinstitute.org/HIC/Anatomy/anatomy2.cfm>

The easiest way to understand the function of the heart is to first describe the flow of blood through the heart. De-oxygenated blood coming from the superior and inferior vena cava enters the heart at the right atrium. Blood flows through the tricuspid valve into the right ventricle. From here, the blood flows through the pulmonary artery to the lungs, where gas exchange takes place. The oxygenated blood then flows back to the heart through the pulmonary veins and enters the left atrium. The blood passes through the bicuspid (or mitral) valve and flows through the left ventricle. The blood is now pumped through the aortic valve and oxygenated blood is distributed throughout the body as it leaves the heart through the aorta.

(ii) Blood Pressure

The blood pressure is the force of the blood against the walls of the arteries as it is traveling throughout the body [17]. The valves of the heart function as one-way exits for the blood to leave each chamber without flowing backwards. When a chamber contracts, the valve opens, and when the chamber relaxes the valve will close. The tricuspid valve is the exit of the right atrium and the pulmonary valve is the exit for the right ventricle. The mitral valve is the exit for the left atrium and the aortic valve is the exit for the left ventricle [17].

There are two phases which describe the performance of the heart; systole and diastole. During the systole period, the heart beats/contracts to pump blood out of the heart. First the right atrium contracts to pump blood to the right ventricle which contracts to pump blood to the lungs. Then the left atrium contracts and pumps blood to the left ventricle which then contracts to pump the blood out of the heart and to the body. During diastole, the heart relaxes before the next beat to allow blood to fill back up into the heart [17]. When taking blood pressure measurements, it is during these two periods that readings are taken of the force of blood against the walls of the arteries. The first reading corresponds to the systolic pressure and the second is the diastolic pressure. The reading is usually announced as, "systolic over diastolic". The average blood pressure for a healthy adult is 120/80 mmHg [4].

(iii) Cardiac Parameters

The efficiency of a circulatory system is highly depends on the capacity of the blood to carry O_2 , since the volume of blood pumped can be reduced if the blood has a high capacity [17]. The amount of O_2 carried is simply the product of the blood volume and the O_2 content in the blood. Mammalian circulation also ensures that the rate of blood flow through the lungs is equal to the blood flow through the rest of the body. The blood leaving from the mammalian heart equals the entire ejected blood volume taken up by the changes in the volume of blood vessels since both halves of the heart contract simultaneously [17]. Birds and mammals are unique in that their systemic and pulmonary circulations are separate, thus there can be a difference in pressure in each circulation. The pressure in the pulmonary system is significantly smaller than that in the systemic. The pulmonary system may have pressures lower than 20 mm Hg and the systemic may have pressures greater than 100 mm Hg, which can benefit the animal since there does not need to be equal amounts of blood in the pulmonary and systemic circulations to fit the needs of blood-gas diffusion [17].

The pulse rate, or heart frequency, is defined as the number of heartbeats per minute (bpm). The average pulse rate of an adult human at rest is approximately 70 bpm [17]. Heart rate is inversely related to the body size of the mammal: the smaller the animal, the higher the pulse rate. To demonstrate this inverse relationship, consider the resting heart rate of an elephant at 25 bpm, and of a small shrew at 600 bpm [17]. Heart rate increases with physical activity. Pulse rates as high as 1200 bpm (the heart

completes 20 cycles per second) have been observed in hummingbirds and small bats in flight [17].

Another useful measurable quantity is the cardiac output, the volume of blood pumped by the heart per unit time.

$$\text{Cardiac Output} = \text{Heart Rate} \times \text{Stroke Volume} \quad (15)$$

An increase in the venous return of blood will result in the increase of the cardiac output. The major organs to receive blood are the kidneys, liver, heart and brain [4].

Controlled by nerve impulses and hormones, the pacemaker, or sinus node, is located where the vena cava enters the right atrium and thus controls the start of contraction through the atria. In between the atria and ventricles is the atrioventricular bundle, which conducts the impulse to the ventricles [4].

Blood vessels have elastic walls with layers of smooth muscle within the walls to let them change diameter. The arteries have heavy, thick walls with strong layers of elastic fibers and smooth muscle [4]. As the arteries branch off, their walls become thinner as they lead into capillaries. The capillaries are the smallest of the blood vessels consisting of only a single layer of cells. It is in the capillaries that the exchange of substances takes place since the high amount of branching provides such a large cross-sectional area [4]. The capillaries lead into the veins, which are thinner but still contain elastic fibers and smooth muscle.

d) Relevant Mathematics

(i) First Derivative Test

It is necessary to present some basic mathematical concepts in order to describe some of the analysis performed in the project. It is assumed that the reader has an understanding of derivatives and integrals, however, the reader may refer to Stewart's Single Variable Calculus: Concepts & Contexts found the references cited for the proper definitions. As will be discussed in the Methods and Results section, mathematically computing peak locations of the blood pulse waveform is desired. Using the First Derivative Test is one method to locate peaks of a signal. The First Derivative Test states:

Suppose that c is a critical number of a continuous function f :

- a) If f' changes from positive to negative at c , then f has a local maximum at c**
- b) If f' changes from negative to positive at c , then f has a local minimum at c**
- c) If f' does not change sign at c , then f has no local maximum or minimum at c**

The critical number, c , is defined such that the derivative of f at c equals zero. Thus,

$$f'(c) = 0. \tag{16}$$

Therefore, local maxima may be located on the blood pulse waveform by first calculating all critical points (where the skin velocity waveform equals zero), and then using the First Derivative Test to determine which critical points are local maxima.

(ii) Fundamental Theorem of Calculus

The Fundamental Theorem of Calculus (FTC) was another important concept used in the creation of the blood pulse waveform. The FTC states:

Suppose f is continuous on $[a, b]$:

a) If $g(x) = \int_a^x f(t)dt$, then $g'(x) = f(x)$. (17)

b) $\int_a^b f(x)dx = F(b) - F(a)$, (18)

where F is any antiderivative of f , that is, $F' = f$.

From Part (a) we can conclude that if f is integrated and the result is then differentiated, the original function f is the outcome. In other words, one can view differentiation and integration as inverse processes. Thus, integration of a velocity signal will yield its displacement, and the derivative of the displacement signal is the velocity signal.

(iii) Fourier Transform and Filtering

Lastly, the Fourier Transform (FT) is an extremely important component in the processing analysis of the blood pulse waveform. A time signal, $f(t)$, may be viewed in a different format by means of the FT. Similar to the Taylor series expressing a function as a power series, the FT expresses a function as a sum of complex exponential functions, which are sine and cosine functions of varying amplitudes and frequencies. It is sometimes easier to work with the FT of a function than the actual time function itself. The FT is implemented in the following manner:

Let $f(t)$ be a function of time t . Define its one-dimensional Fourier Transform (FT) as

$$F(\omega) = \int_{-\infty}^{\infty} f(t)e^{-2\pi i\omega t} dt \text{ and its inverse as } f(t) = \int_{-\infty}^{\infty} F(\omega)e^{2\pi i\omega t} d\omega. \quad (19)$$

The filtering of $f(t)$ with a linear, shift invariant filter can be done with the process of convolution. The Convolution Theorem states:

$$\text{If } f_1(t) \leftrightarrow F_1(\omega) \text{ and } f_2(t) \leftrightarrow F_2(\omega), \text{ then } f_1(t) * f_2(t) \leftrightarrow F_1(\omega)F_2(\omega). \quad (20)$$

Thus, to convolve two functions, we take the FT of each function, multiply their respective FT's, and then take the inverse FT to obtain the desired result. A proof of the Convolution Theorem can be found in Papoulis' Signal Analysis found in the references cited. Using this theorem and the convolution equation, we obtain the filtered time signal $g(t)$ by the following:

$$g(t) = f(t) * h(t) = \int_{-\infty}^{\infty} f(\tau)h(t-\tau)d\tau, \quad (21)$$

where $g(t)$ is the filtered time signal, $f(t)$ is the input time signal, and $h(t)$ is the filter.

Expressing $g(t)$ in the Fourier domain we obtain,

$$G(\omega) = \int_{-\infty}^{\infty} g(t)e^{-2\pi i\omega t} dt. \quad (22)$$

Substituting in the expression for $g(t)$ found from Equation 21,

$$G(\omega) = \int_{-\infty}^{\infty} (f(\tau)h(t-\tau)d\tau)e^{-2\pi i\omega t} dt . \quad (23)$$

$$\text{Set } t = \tau + s \quad \Rightarrow \frac{dt}{ds} = 1 \quad \Rightarrow ds = dt , \text{ which yields}$$

$$G(\omega) = \int_{-\infty}^{\infty} \int_{-\infty}^{\infty} f(\tau)h(s)e^{-2\pi i\omega(\tau+s)} d\tau ds \quad (24)$$

$$= \int_{-\infty}^{\infty} \int_{-\infty}^{\infty} f(\tau)h(s)e^{-2\pi i\omega\tau} e^{-2\pi i\omega s} d\tau ds \quad (25)$$

$$= \left(\int_{-\infty}^{\infty} f(\tau)e^{-2\pi i\omega\tau} d\tau \right) \left(\int_{-\infty}^{\infty} h(s)e^{-2\pi i\omega s} ds \right) \quad (26)$$

$$= F(\omega)H(\omega). \quad (27)$$

Thus, $G(\omega) = F(\omega)H(\omega)$, and the time domain convolution is equivalent to multiplication in the Fourier domain. We can therefore choose to filter out any part of the obtained time signal $f(t)$ by simply multiplying its Fourier Transform with the appropriate filter, $H(\omega)$.

IV. Method and Results

a) Experimental Set-up

A Class II Polytec PDV-100 He-Ne Laser Doppler Vibrometer was used to measure the skin velocity of human subjects. The laser was mounted on an optical table for stability and freedom of rotation, or a tri-pod was used for portability. Different methods for data acquisition were investigated during the study. Initially the data was stored on a computer's sound card using the free online program Audacity[®], however we determined the method to be faulty due to internal filtering and scaling from the software. As an alternative, a National Instruments[®] 4-channel Hi-Speed USB Carrier (NI USB-9162) box was used with the associated software, *Measurement and Automation*, to digitize and store the data as text files. Additionally, the incoming data was observed in real-time either using an oscilloscope or was visualized by connecting the LDV to the laptop via USB cables and using the *Vibsoft* software manufactured by Polytec. The device and data acquisition system can be seen below in Figure 17.



Figure 17 – Photograph of device and data acquisition system.

Once the equipment is in place, a piece of optional retro-reflective tape is placed on the target artery to enhance the reflected beam back to the LDV. As shown in Figure 18, the retro-reflective tape is placed on the carotid artery and the subject used a mirror to navigate the laser beam directly onto the target.

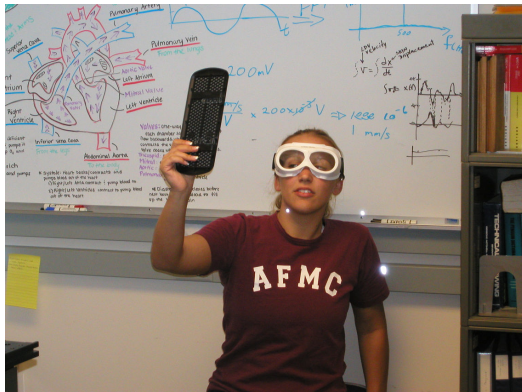


Figure 18 (a) Picture of a skin velocity waveform measurement of the carotid artery on a female subject.



Figure 18 (b) Picture of a skin velocity waveform measurement of the carotid artery on a male subject.

There were eight major arteries in the body that were measured; the facial, carotid, brachial, radial, femoral, popliteal, posterior tibial, and pedal arteries. These arteries were chosen based on the fact that they come up very close to the skin surface and a pulse can be easily located in each spot [11]. Figure 19 identifies the eight arteries measured in the body. The subject should be placed in a comfortable position so to remain still for the data acquisition. The subject may be sitting, standing, or in the supine position and the laser may be rotated to accommodate their position. Data acquisition can take place for any specified time interval, however it was found that approximately one to five minutes was sufficient to acquire an accurate waveform.

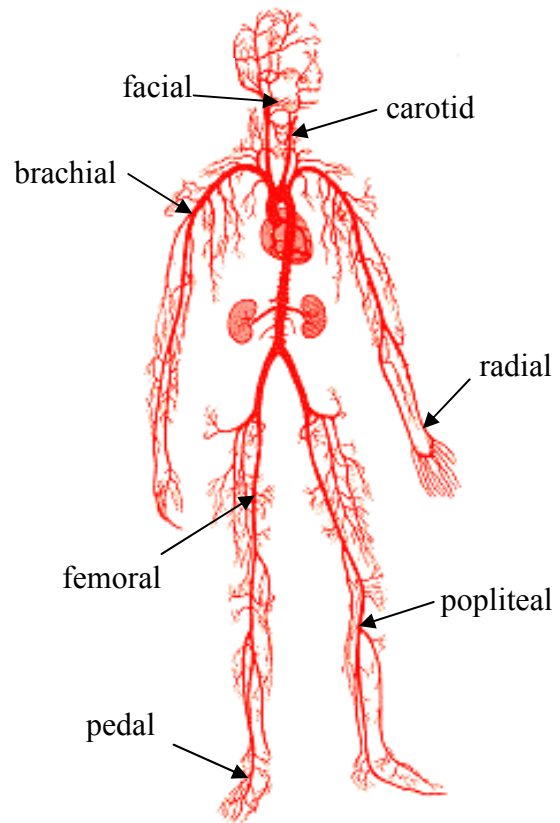


Figure 19 - Diagram of the human body arteriole system along with the target arteries labeled [10].

b) Data and Analysis

The velocity waveforms collected from each part of the body were all unique and identifiable. The waveforms below show the differences in the shapes, sizes, and cleanliness due to the different arteries measured.

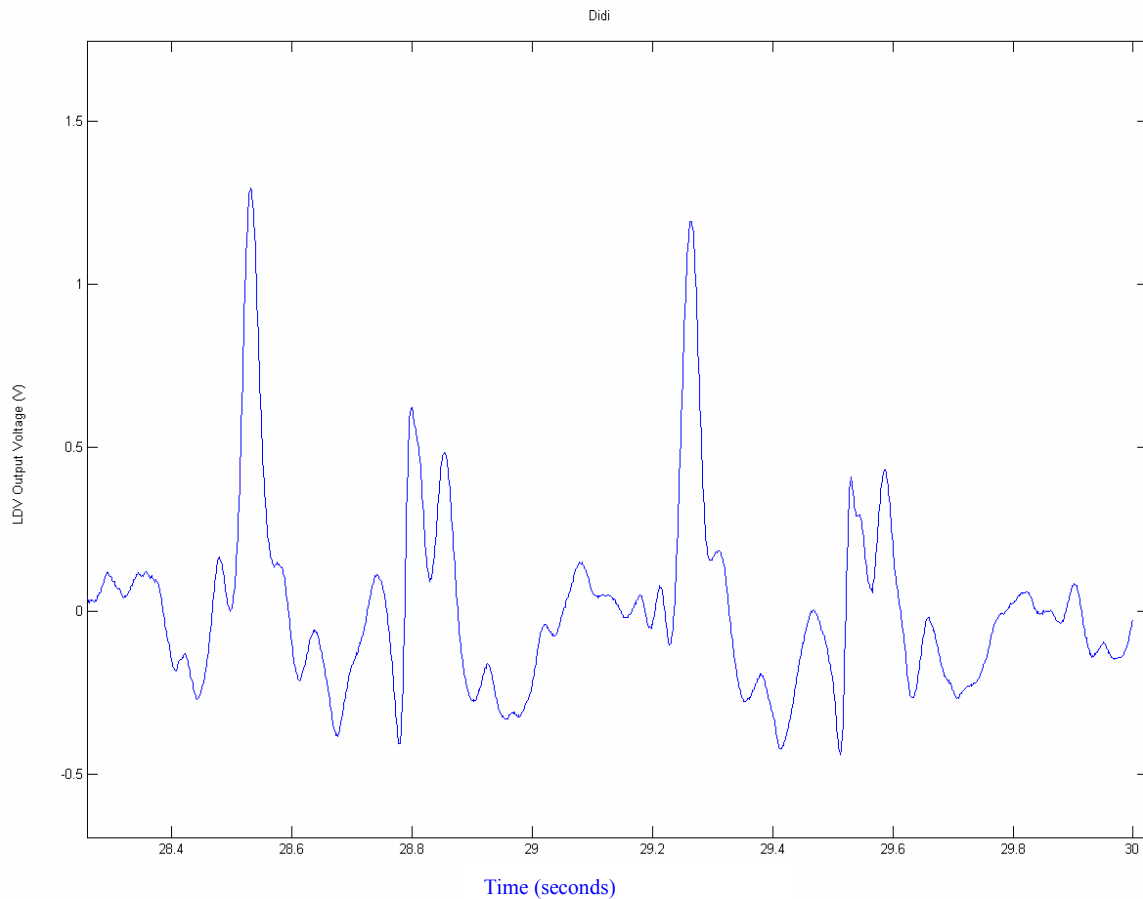


Figure 20 (a) - Carotid artery skin velocity measurement on a female subject.

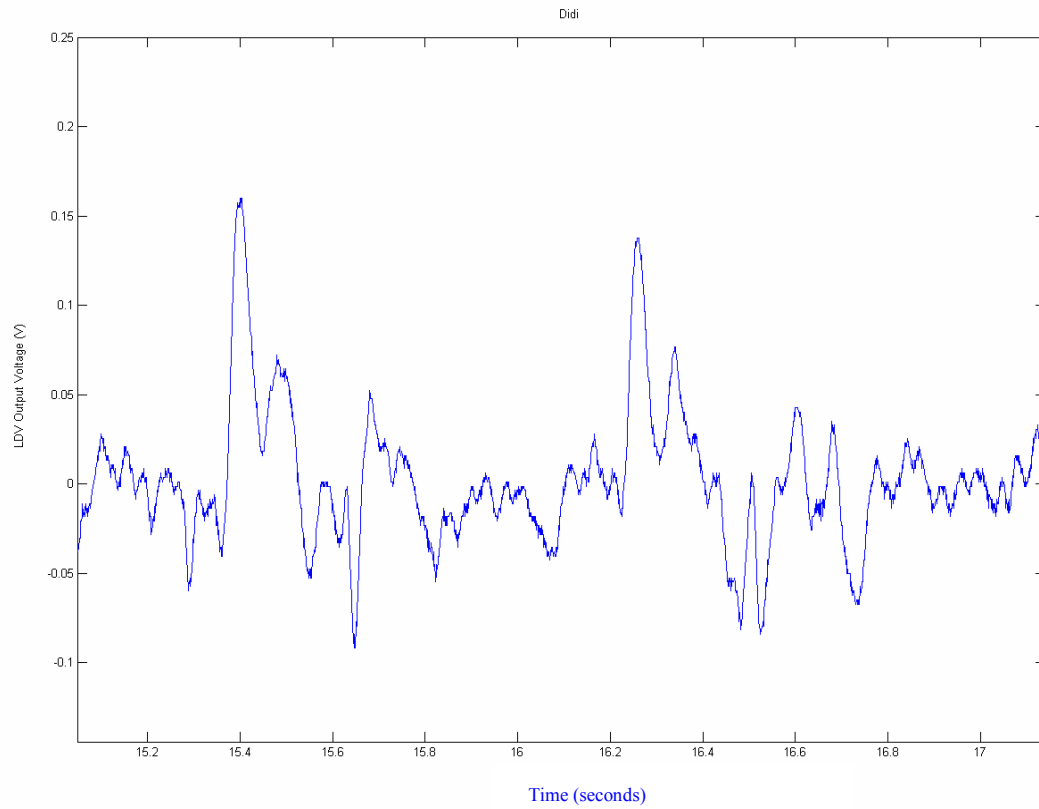


Figure 20 (b) - Facial artery skin velocity measurement on a female subject.

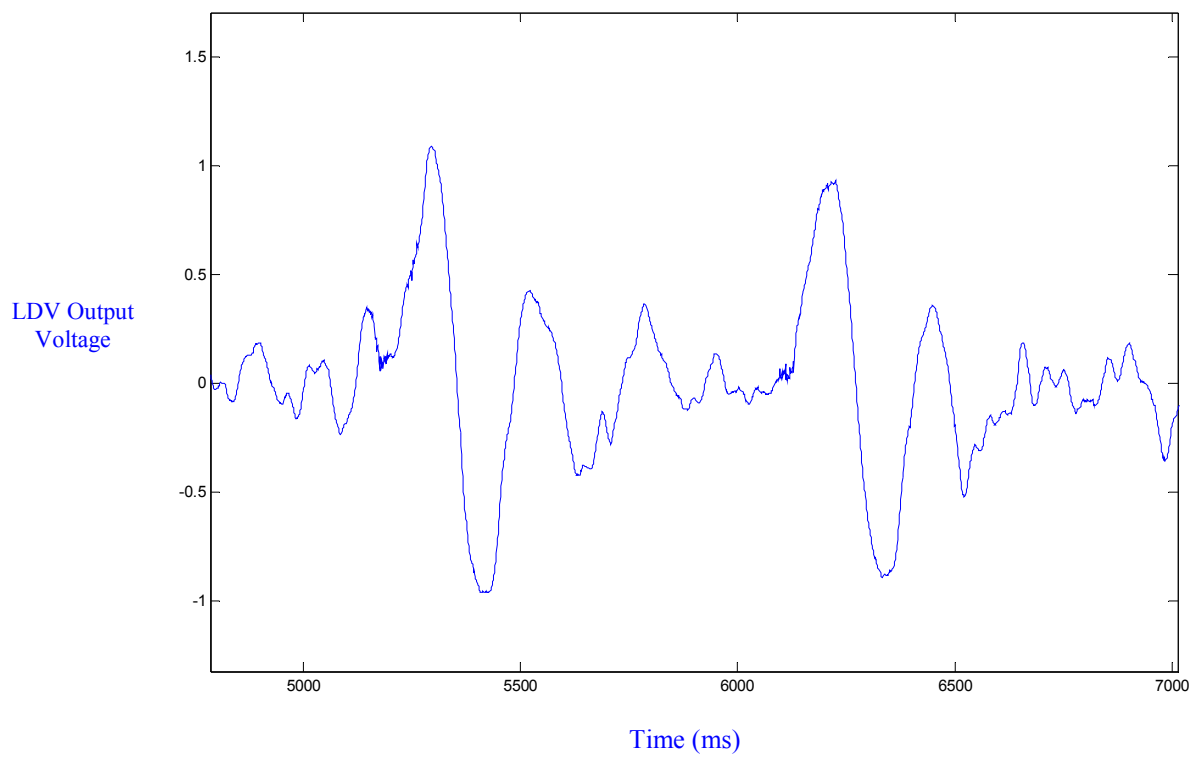


Figure 20 (c) - Brachial artery skin velocity measurement on a male subject.

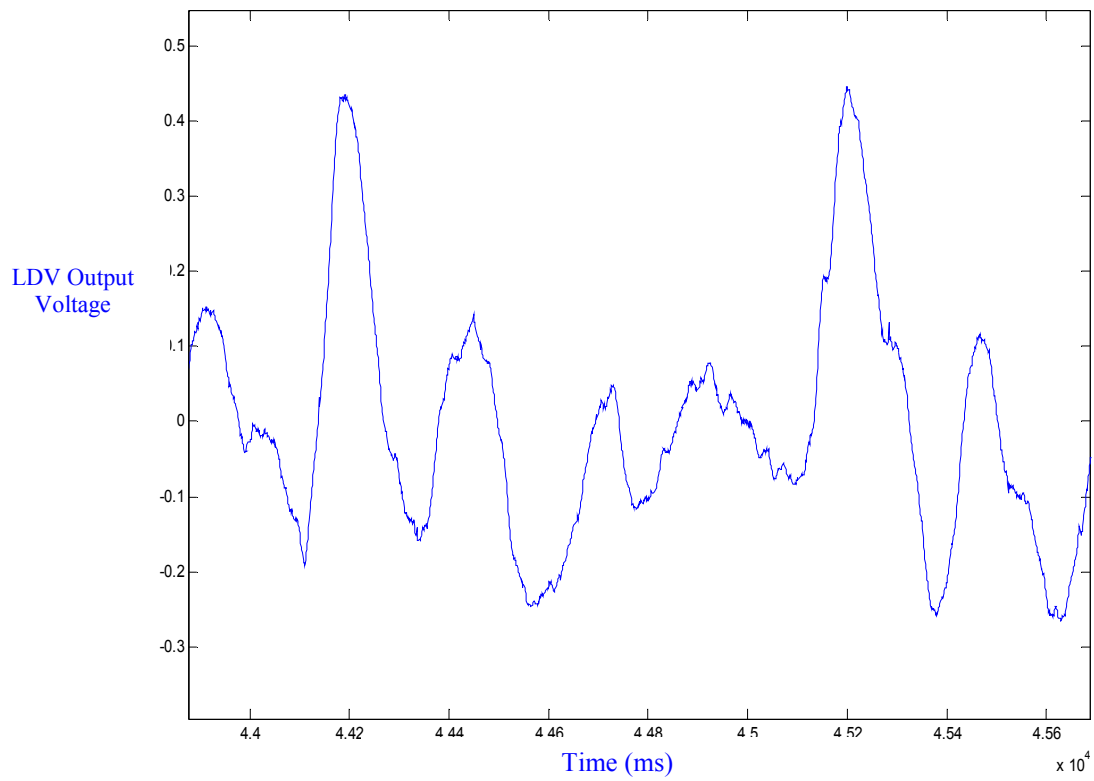


Figure 20 (d) – Radial artery skin velocity measurement on a male subject

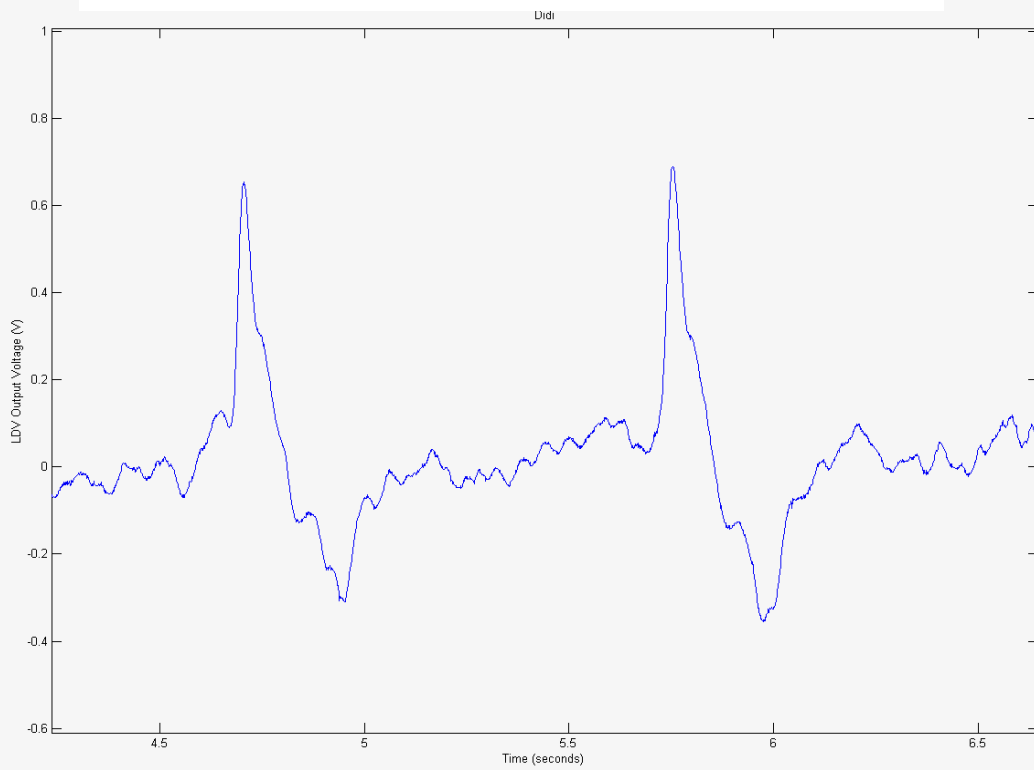


Figure 20 (e) - Femoral artery skin velocity measurement on a female subject.

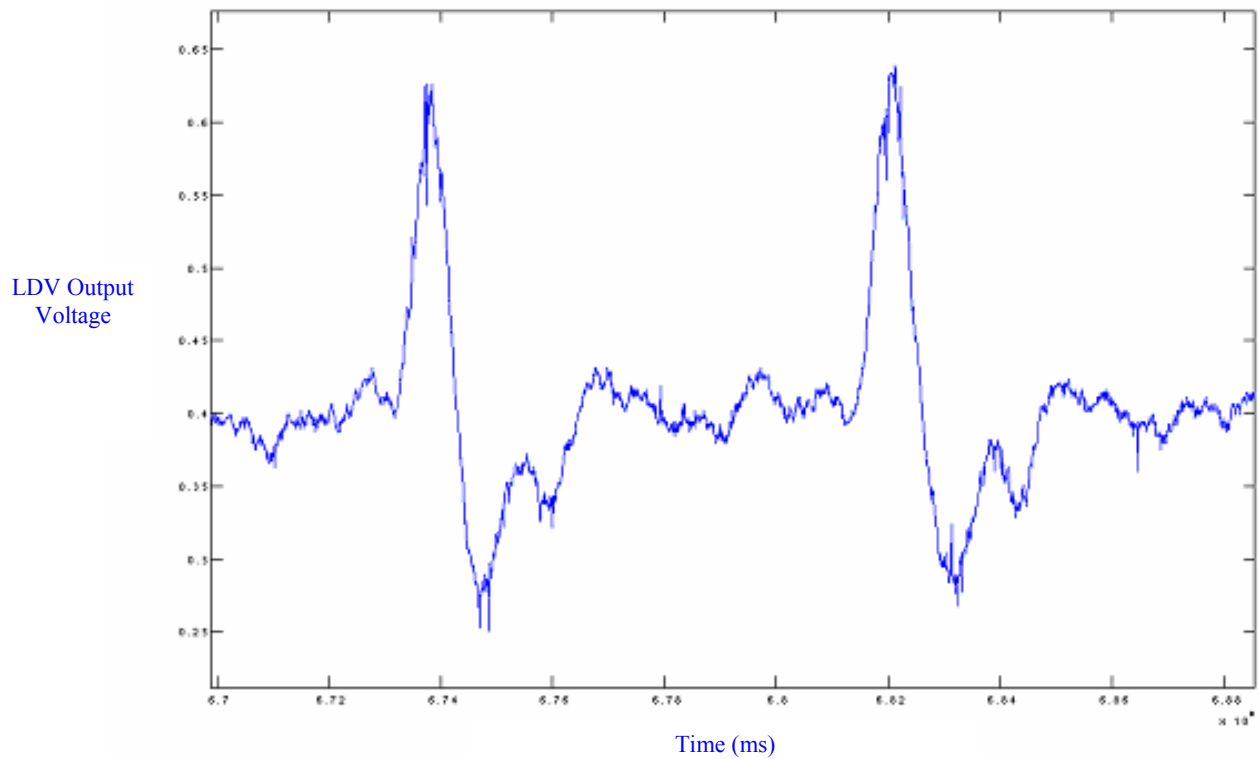


Figure 20 (g) - Posterior tibial artery skin velocity measurement on a female subject.

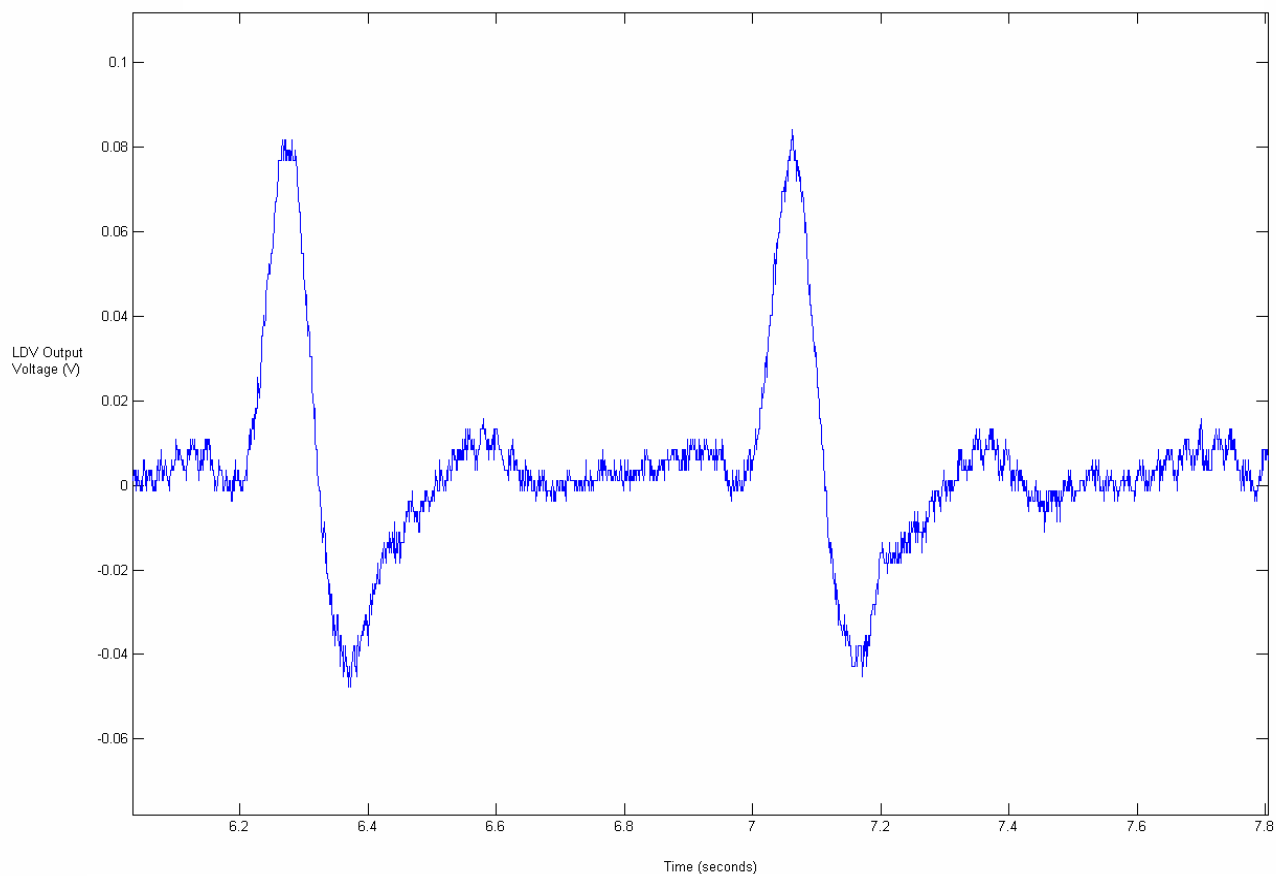


Figure 20 (f) - Pedal artery skin velocity measurement on a female subject.

What is consistent with each waveform is that a distinguished higher peak is present. The difference between each measurement location is in the shape of this peak, as well as the values in between the larger peaks, and the overall cleanliness of the signal (how much variation is present). Of all the figures presented, the pedal artery yields the simplest and cleanest waveform, while the radial and facial arteries produce waveforms with the most variation. It is hypothesized that the proximity of the radial and facial arteries to bone is affecting the quality of the skin velocity waveform; however, it is something that needs to be further investigated.

There are several things to keep in mind when analyzing the skin velocity waveforms obtained. It is important to recognize what the waveform actually tells us and to distinguish it from the blood pressure waveform. The waveform obtained represents the velocity of the pulsatile motion of the skin due to the blood's force acting upon it. Integrating the waveform will yield the displacement of the skin, and thus what we are classifying as the blood pulse waveform (BPU).

The Matlab[®] software package was used for all signal processing needs during the project. A method by which Matlab integrates a signal is with the cumulative trapezoidal (*cumtrapz*) command, which is their implementation of the Fundamental Theorem of Calculus using the trapezoidal rule. The *cumtrapz* command approximates the cumulative integral of the velocity signal by the trapezoidal sum method with unit spacing. If the raw, unfiltered skin velocity data was integrated, a shallow slope was observed as shown in Figure 21 below. The slope is due to a DC offset (dy) inherent in the LDV measurement system. To account for this, there are two procedures that may be done to eliminate the effect of this slope. The first method would take each point and

subtract out the dy value so that the resulting waveform would be straight as shown in Figure 21. The dy slope values would be manually calculated by examining $\Delta y/\Delta x$. The difficulty with this method is that the slope, or dy , must be calculated for each specific case.

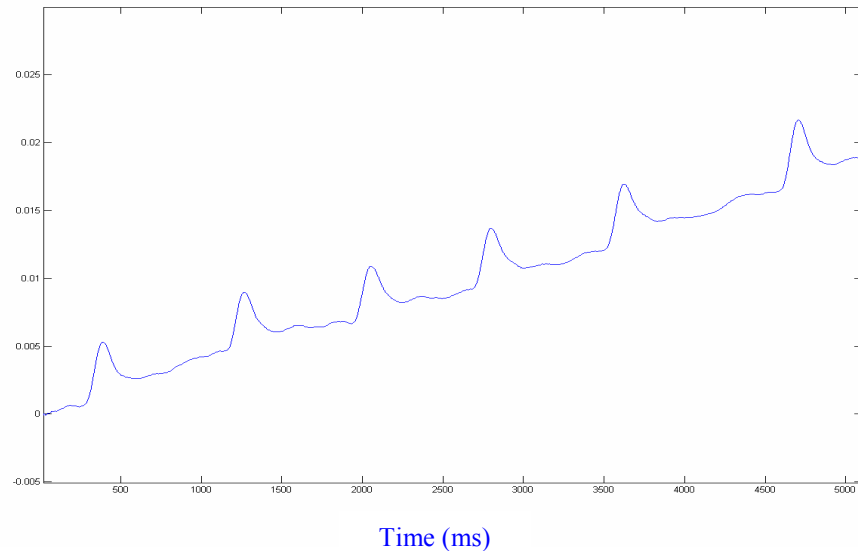


Figure 21 - Integration of raw data from the pedal artery of a female subject.

The alternate method filters out this DC component of the data using a third order, high-pass Butterworth filter having a cutoff frequency at one Hz. Shown below is the raw data along with the filtered data. Once the data is filtered, the integration may be done without an interfering slope as seen by Figure 22(a).

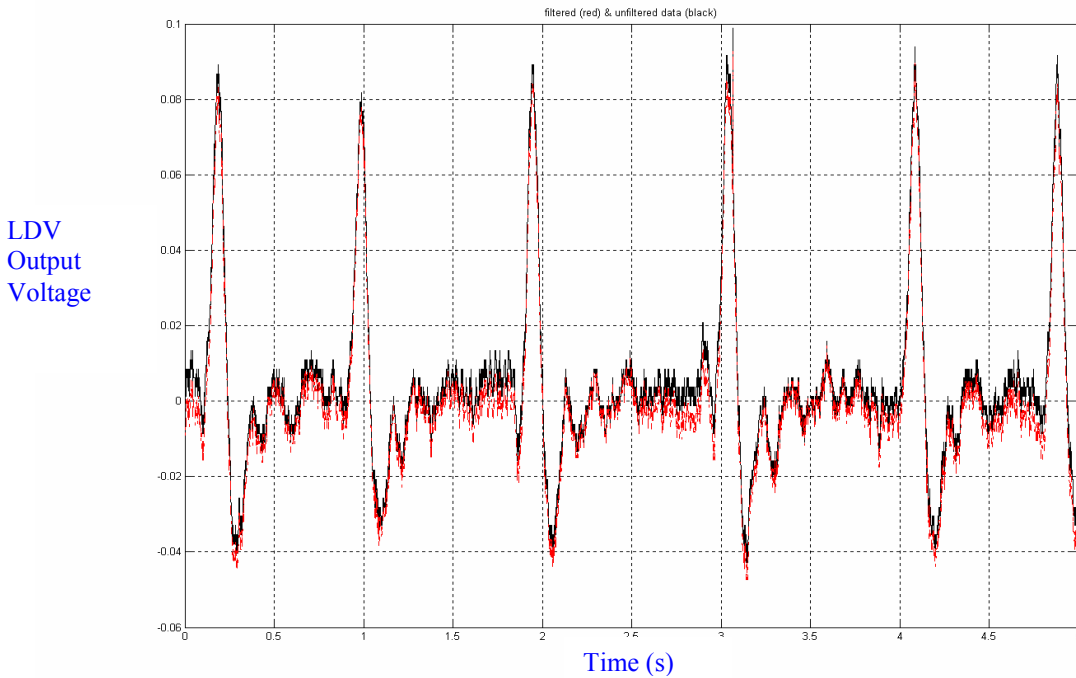


Figure 22(a) - Raw data from the pedal artery (black) and the filtered data (red).

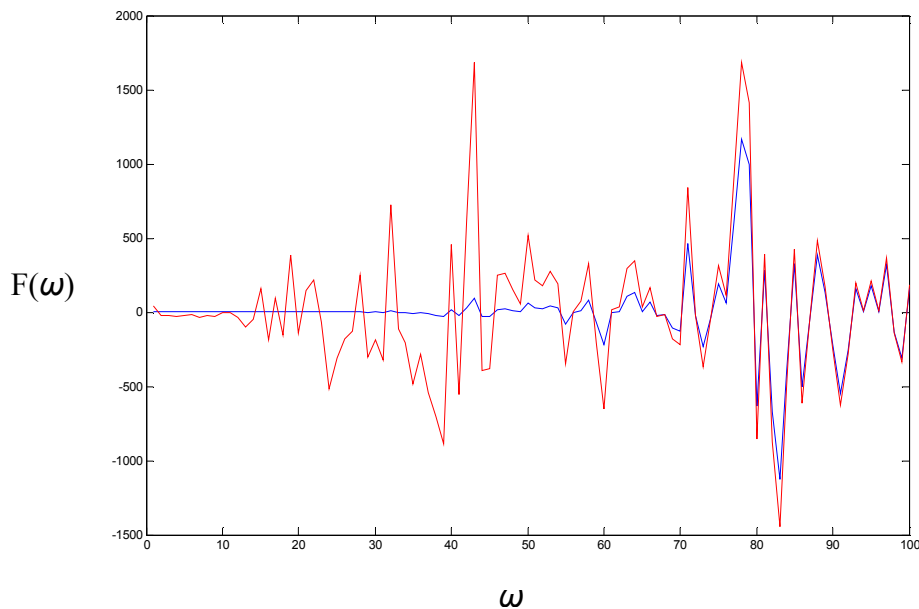


Figure 22(b) – Frequency spectrum of the unfiltered data (red) and filtered data (blue).

The hi-pass filter used attenuates the frequencies at the very low end of the frequency spectrum, which can be seen in Figure 22(b) above. The filtered velocity signal and the integrated filtered data are presented in Figure 23.

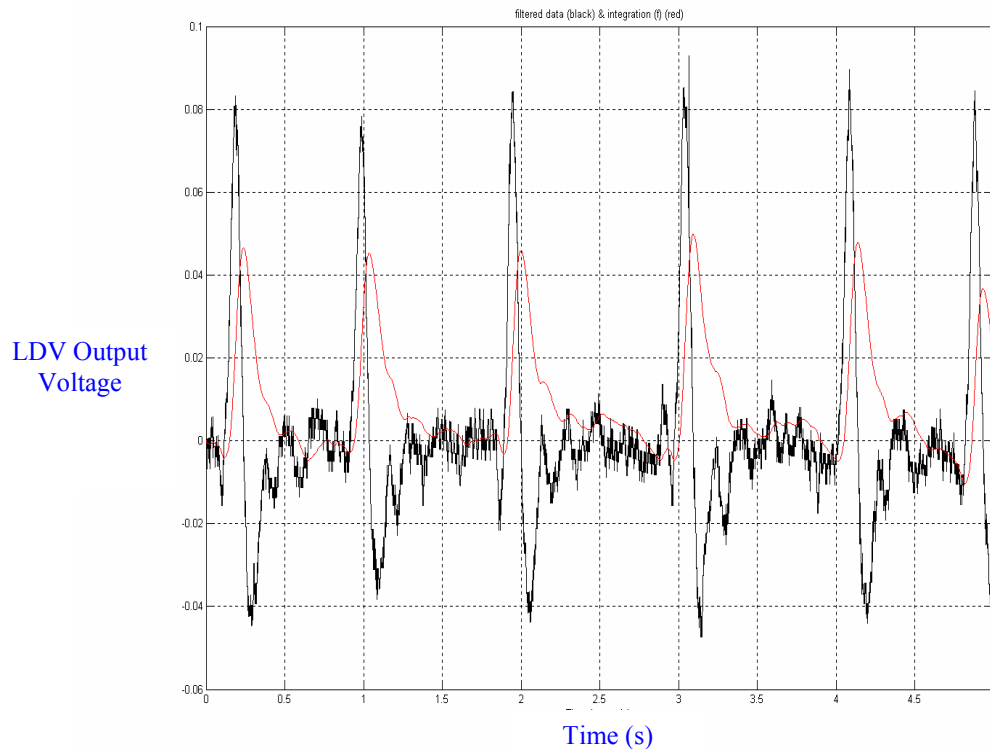


Figure 23 - Filtered data from the pedal artery (black) and the integrated filtered data (red)

When comparing the two methods, a very similar integration waveform is obtained as seen in Figure 24. There is a slight vertical shift between the two signals at several points; however the shapes of the graphs are nearly identical. Thus, the decision to use the filtered data throughout the project was based on the fact that it was more accurate. With the patient-independent filtering method, the same Matlab[®] programming could be used for multiple waveforms from different target arteries.

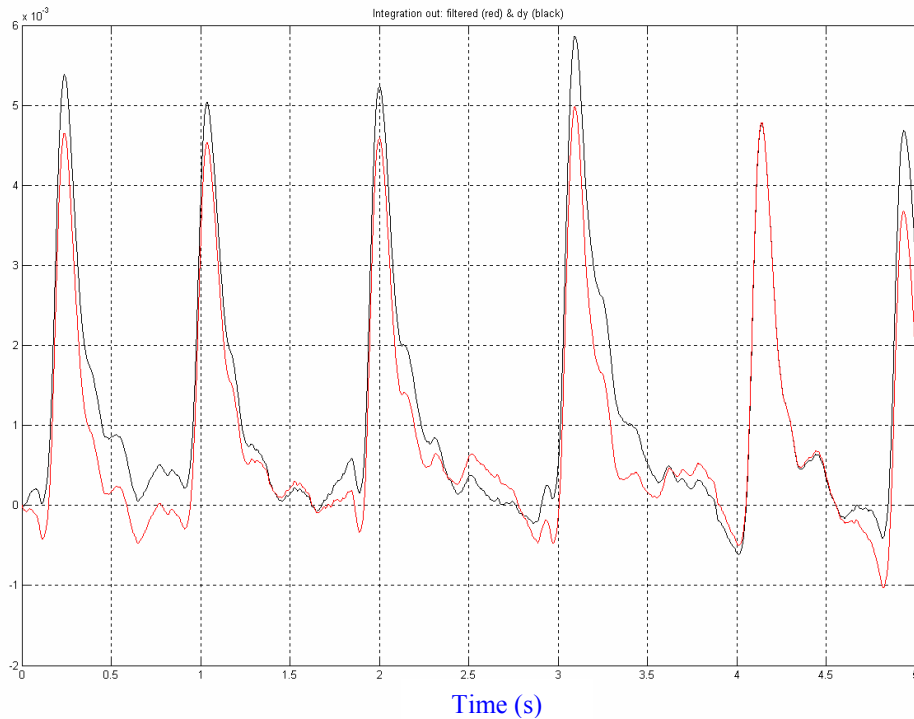


Figure 24 - Integration of the filtered data (red) and the integration of the raw data using the dy method (black).

During the analysis of the skin velocity waveforms from different body locations, a hypothesized breathing effect was observed in the carotid artery measurements. For these measurements, we believe there is movement detected by the LDV due to the subject's breathing motion, since the trachea lies next to the carotid artery. As shown in Figure 25 below, the changes in the amplitudes of the peaks of the carotid artery skin velocity measurement correspond to the breathing motion. If, however, one examines a waveform from the pedal artery, the amplitudes are all approximately the same since there would be no breathing effect from the foot.

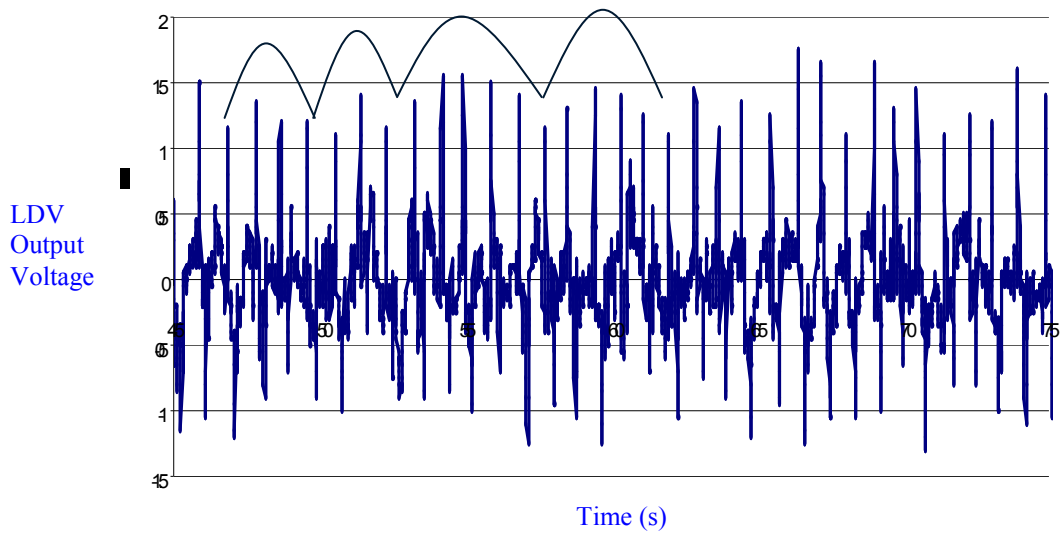


Figure 25 - Measurement of the carotid artery on a female subject showing the breathing effects drawn above.

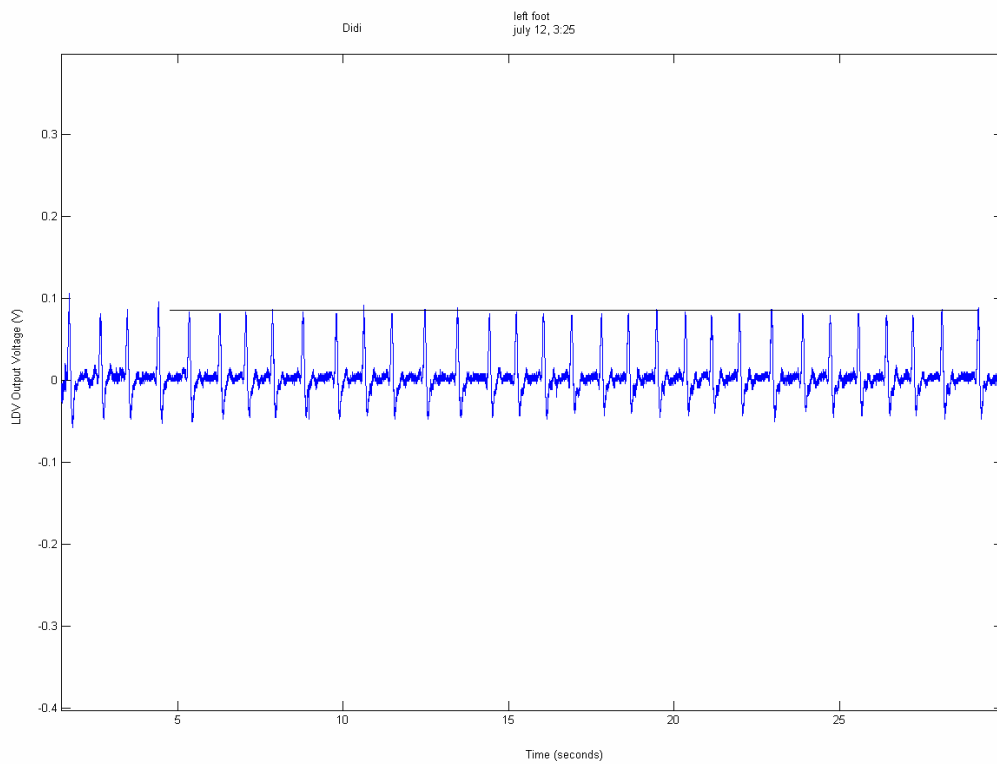


Figure 26 - Measurement of the pedal artery on a female subject showing the similar amplitudes as drawn above.

One use of the filtered velocity waveform is to determine the subject's heart rate. For any time interval, the heart rate will correspond with the number of peaks per time interval. Take for example the waveform below. There are eleven peaks per ten seconds, thus:

$$\frac{11 \text{ beats}}{10 \text{ seconds}} * \frac{60 \text{ seconds}}{1 \text{ minute}} = 66 \text{ bpm}$$

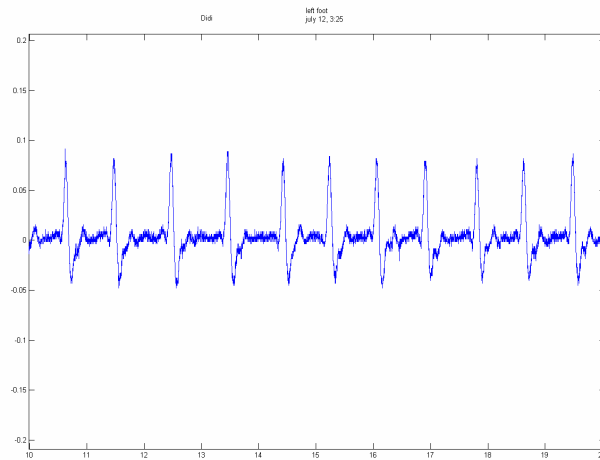


Figure 27 – Calculation of the heart rate on a pedal artery skin velocity waveform

The heart rate in humans can range from 40 to 200 beats per minute (BPM), depending on the age, size, and health of the subject [2]. The average resting heart rate for a healthy adult is 73 BPM.

This technology has tremendous potential for use as a diagnostic tool. In fact, I have personally benefited from using this system. During the summer of 2006, I attended a routine check-up with my physician and an arrhythmia was detected. An arrhythmia is a slight variation in the cycling of the sinus rhythm, therefore the heart rate is not a constant. An appointment was scheduled with a cardiologist later that month, but being naturally curious, I wanted to investigate what this irregularity actually was before

meeting with the physician. My carotid artery skin velocity waveform is presented in Figure 28 below with arrows illustrating the distance between peaks. It can be seen that the distance between peaks is not constant. A sinus arrhythmia fluctuates with the respiratory cycle, thus when the patient inhales the heart rate increases and decreases when the patient exhales.

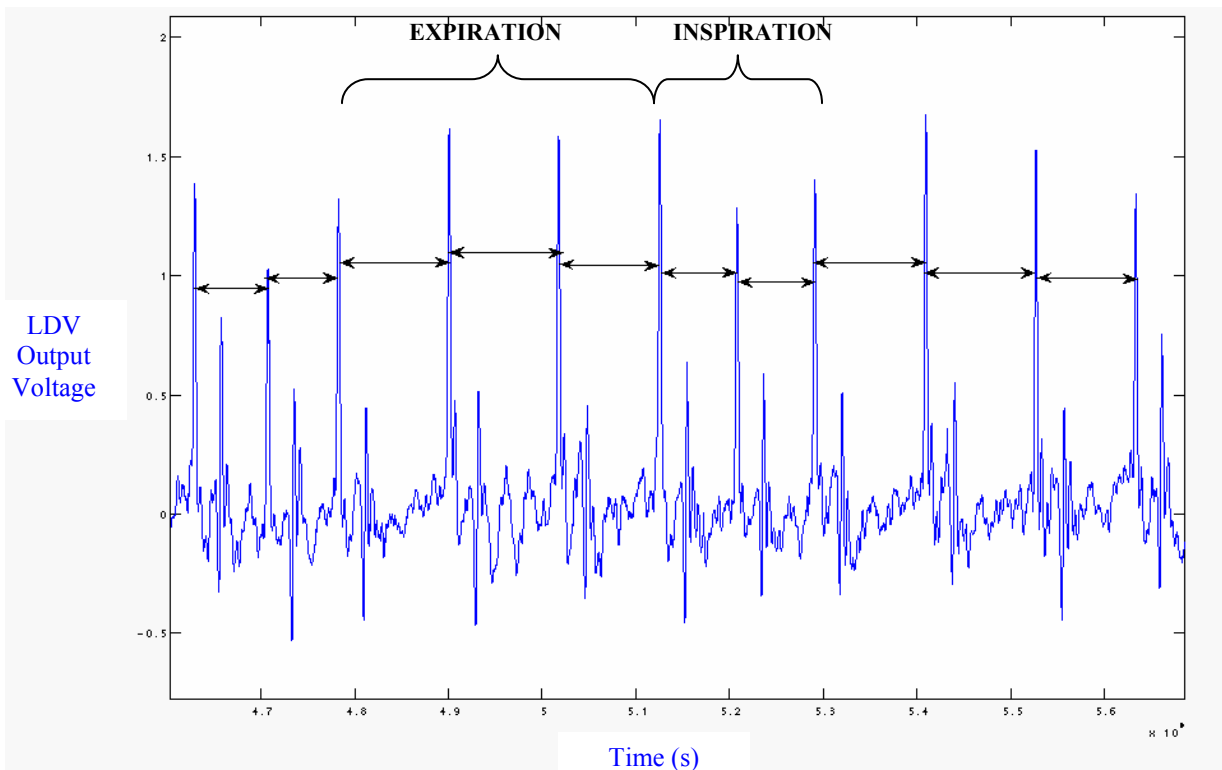


Figure 28 – Two breathing cycles of a carotid artery skin velocity measurement demonstrating a sinus arrhythmia.

During analysis of the data, it may be possible to locate the dicrotic notch. The dicrotic notch is the sudden drop in pressure after systolic contraction caused by the back flow of blood as the aortic valve is closing [2]. Determining the location of the dicrotic notch is a significant tool since it signifies the end of the systolic phase and the

beginning of the diastolic phase. Using this fact, it is possible to trace back to the velocity waveform and determine where the dirotic notch would typically be located.

I also investigated the effect of not using the retro-reflective tape on the target artery. Thus far, all the data shown has had retro-reflective tape used in order to enhance the incoming signal. The skin velocity waveform in Figure 29 below was obtained without the use of the retro-reflective tape.

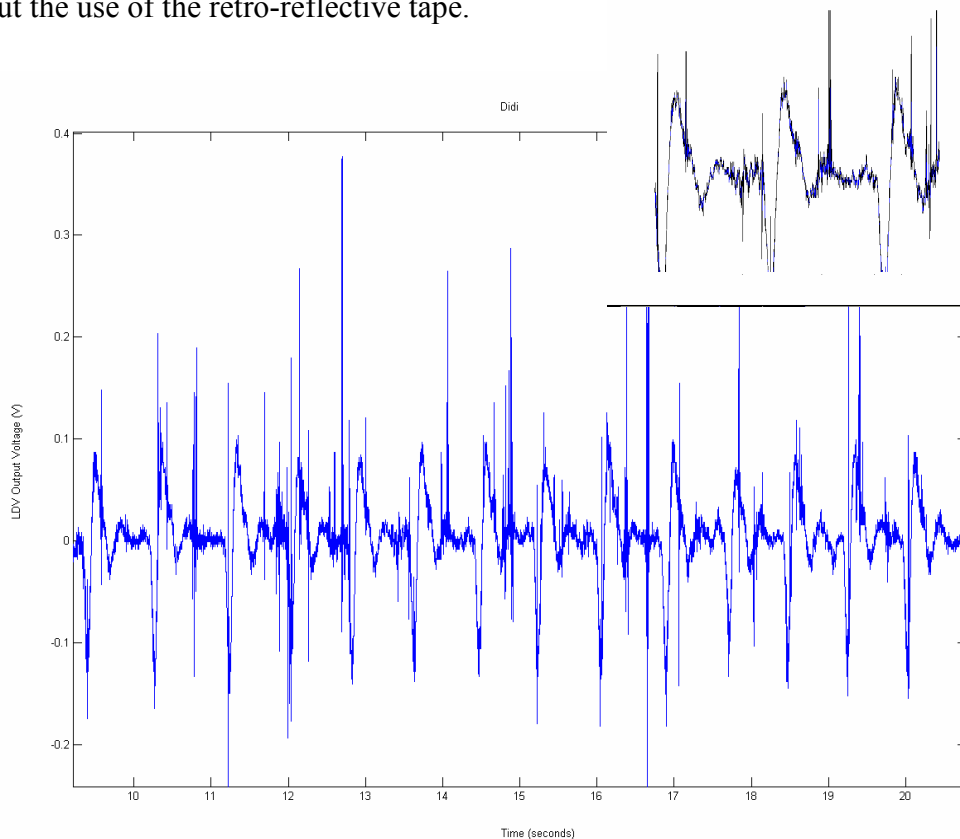


Figure 29 - Measurement of the pedal artery on a female subject without using the retro-reflective tape.

It is still easy to see the skin velocity waveform, but it is not as clean as those obtained with the use of the retro-reflective tape and there is a significant amount of signal drop-out. It is useful to know that if there is a situation where retro-reflective cannot be used, a

velocity, and thus a blood pulse waveform can still be detected. The effect that the tape has on the skin stiffness also needs to be investigated further.

c) Human Subject Trials

After obtaining approval from the College of the Holy Cross' Human Subjects Committee, I was able to begin human volunteer trials on campus. I recruited student, faculty, and staff volunteers via campus-wide emails, fliers, and by word of mouth in order to obtain a population of subjects varying in age, sex, and weight. I measured the skin velocity waveforms of eighty-three volunteers during the fall semester using the Audacity[®] program described in the previous section. Due to the aforementioned errors involved in the recording of the data, I was unable to include these data points in the analysis that follows. I was fortunate enough to measure the waveforms of another one hundred volunteers during the spring semester with the National Instruments[®] 4-channel Hi-Speed USB Carrier, which is the basis of the results contained herein. Volunteers were given a consent form and health questionnaire, which are both found in the Appendix, and the protocol described in the previous section was used on each volunteer. The distribution of the subjects according to each feature collected is demonstrated in Figure 30 below.

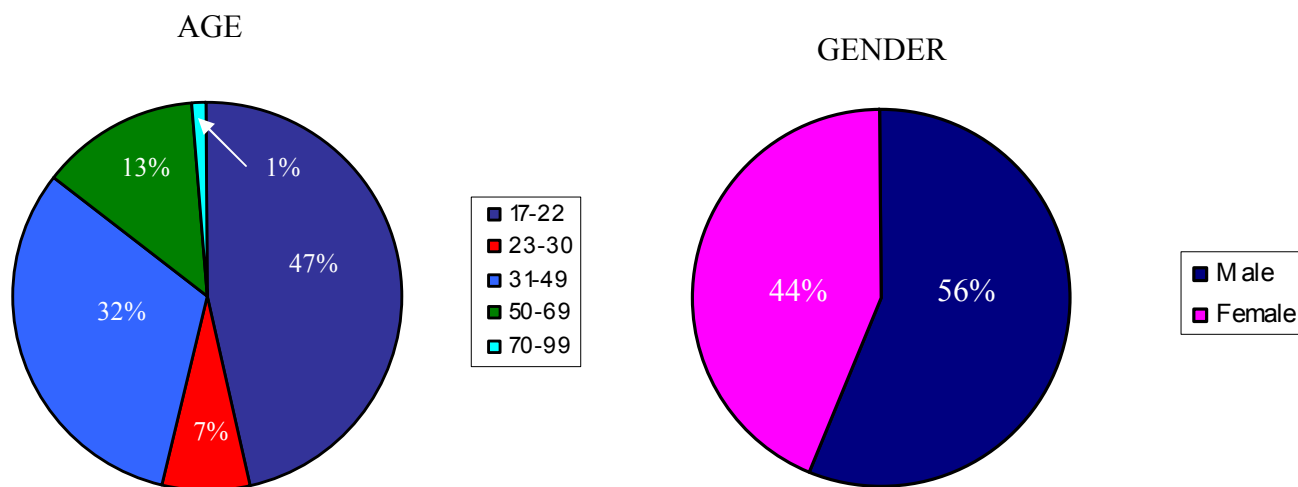


Figure 30 – Distribution of age and gender in the human subject trials

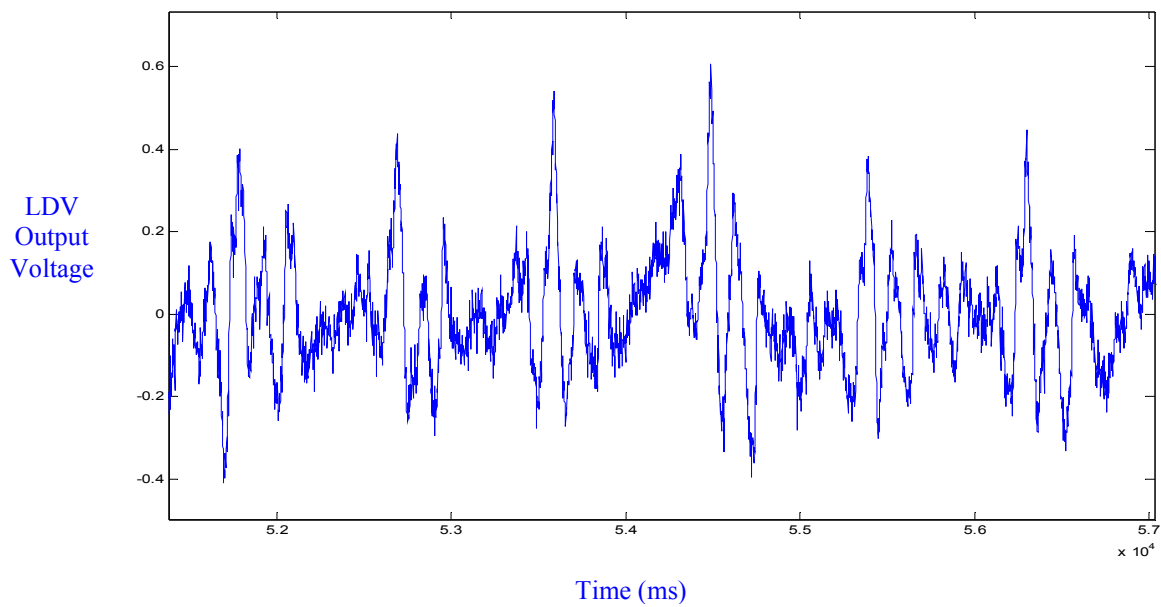


Figure 31 (a) - Carotid artery skin velocity waveform of an 87 year old female subject.

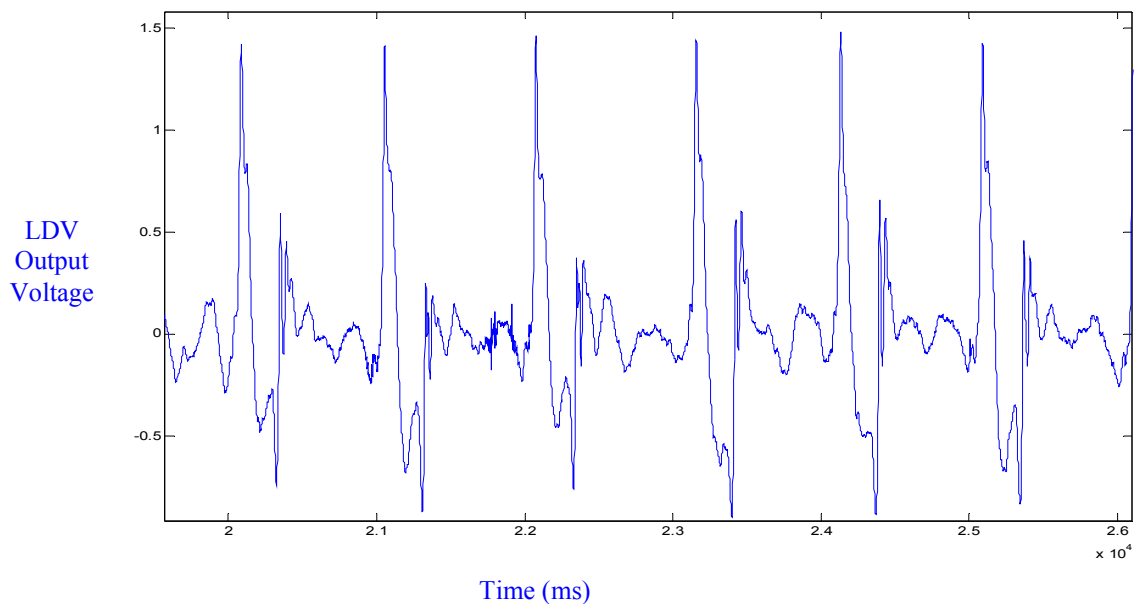


Figure 31 (b) - Carotid artery skin velocity waveform of an 18 year old male subject.

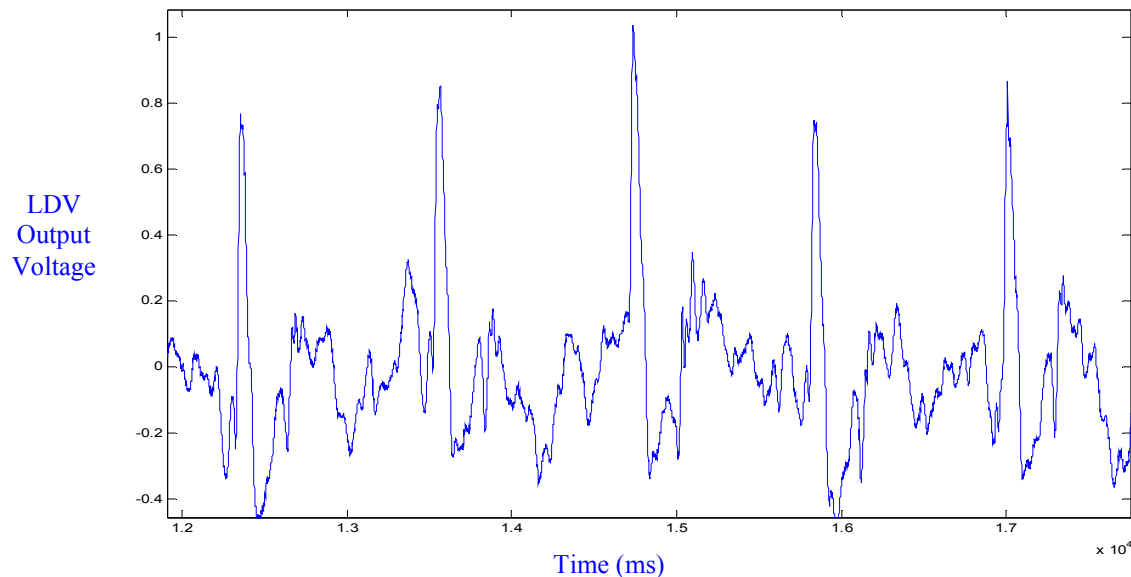


Figure 31 (c) - Carotid artery skin velocity waveform of a 44 year old female subject.

It is clear from Figure 31 (a) that the skin velocity waveform from the oldest subject is not as clean as the waveforms from Figure 31 (b) and (c) of the younger subjects, which may be due to several factors. One factor may be the quality of the subject's skin. Elderly patients tend to have loose and less elastic skin, so their skin velocity waveforms may not be as precise as a younger patient with tighter, elastic skin. Similarly, the patient's arterial health may have an effect on the skin velocity waveform. As the patient grows older, their arteries can stiffen (atherosclerosis) and/or blockages may form, which could affect the resulting skin velocity since the blood flow is restricted. Another factor may be due the fact that elderly patients are not able to remain as still as younger patients, and a movement artifact may be found in the skin velocity waveforms of older subjects.

Besides age and gender, a diverse distribution in body mass index (BMI) was also desired. The BMI measurement is considered a reliable indicator of body fatness for the general population and according to the Center for Disease Control, research has shown

that BMI correlates to direct measures of body fat, such as underwater weighing. The formula for calculating one's BMI is show below:

$$\text{BMI} = (\text{weight (lb)} / \text{height (in)}^2) * 703 \quad (27)$$

The distribution of BMI's obtained from the Holy Cross Human Subject trials in shown in Figure 32 below.

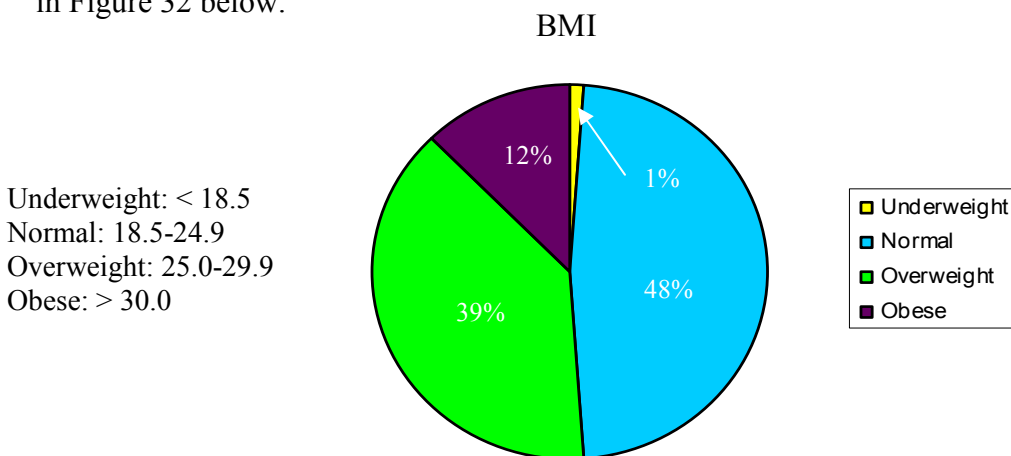


Figure 32 – Distribution of BMI's from Holy Cross subjects

An underweight and an obese patient's skin velocity waveforms are presented in Figures 33 (a) and Figure 33 (b), respectively. There was concern at the start of the project that the skin velocity waveforms of obese patients would not be able to be obtained due to the amount of tissue on top of their carotid artery. By inspection of Figure 33 (b), however, obesity does not seem to play a major role in the obtainment of the skin velocity waveform. Throughout the human subject trials, I did not have any issue obtaining waveforms from obese patients; however, more data is needed to verify this hypothesis, specifically for the morbidly obese patients.

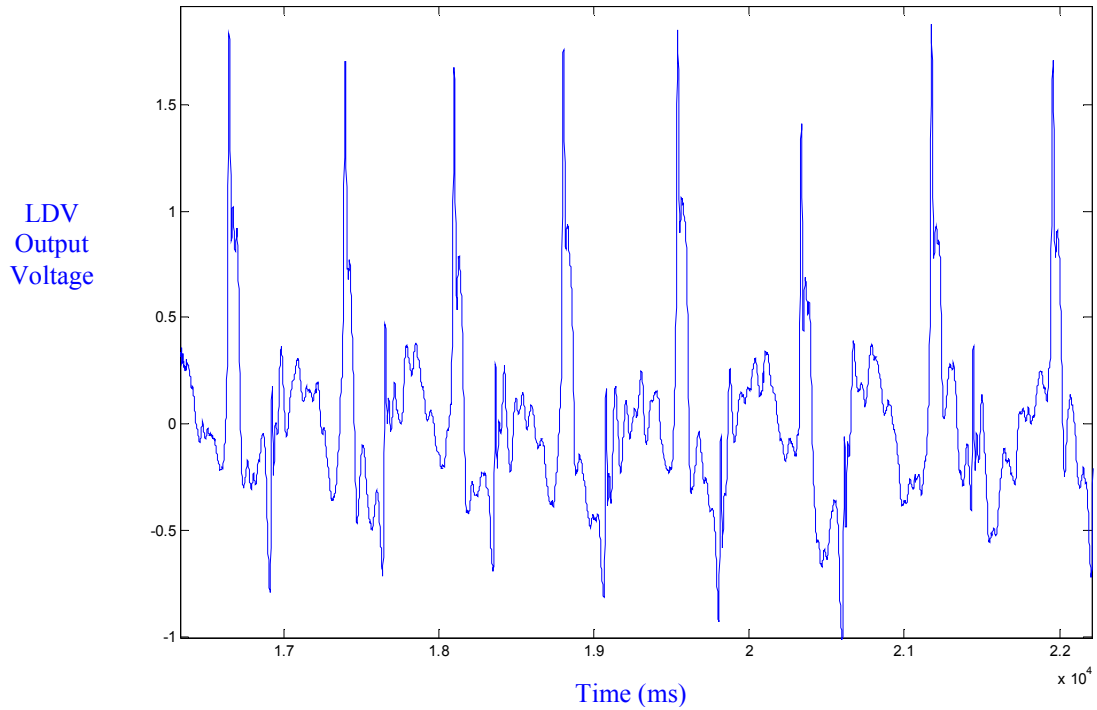


Figure 33 (a) - Carotid artery skin velocity measurement of an underweight male subject

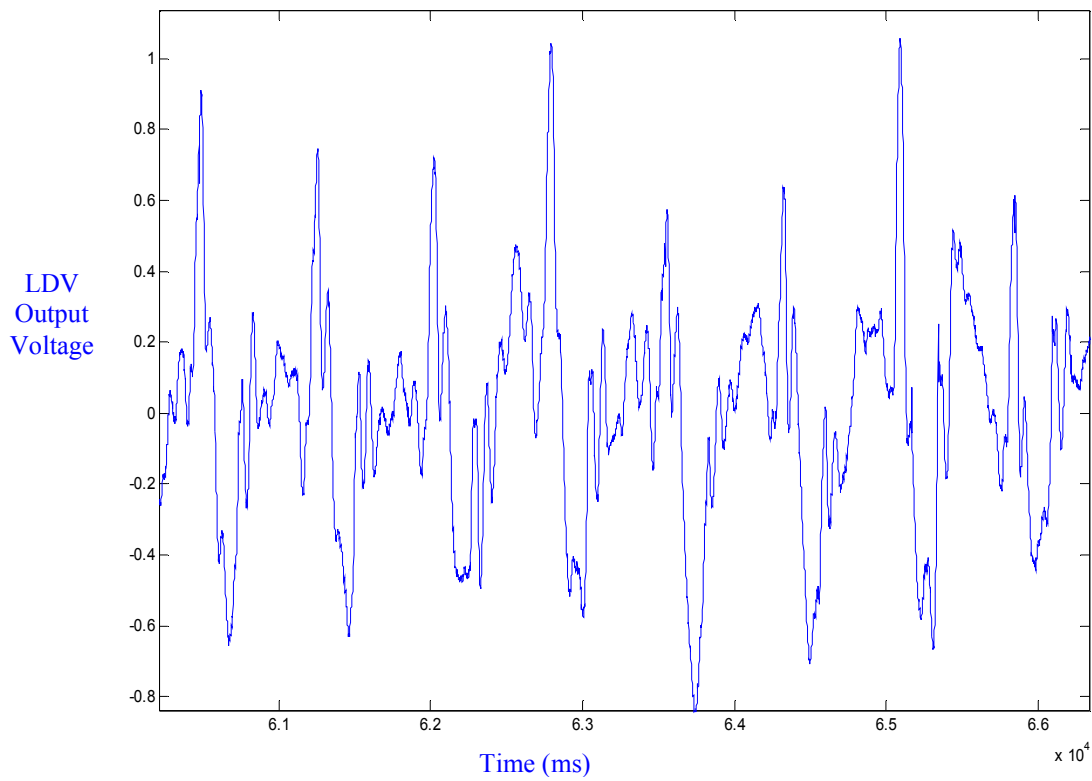


Figure 33 (b) - Carotid artery skin velocity measurement of an obese male subject

Along with the calculated BMI, the skin caliper readings were taken for each subject in the trial. The skin caliper reading represents the amount of tissue present on top of the target artery. In Figures 33 (c) and (d) on the following page, the skin velocity waveforms are presented with the minimum and maximum skin caliper readings from the trial, respectively. Once again, the larger amount of tissue on top of the artery does not seem to present an issue in terms of obtaining a clean waveform.

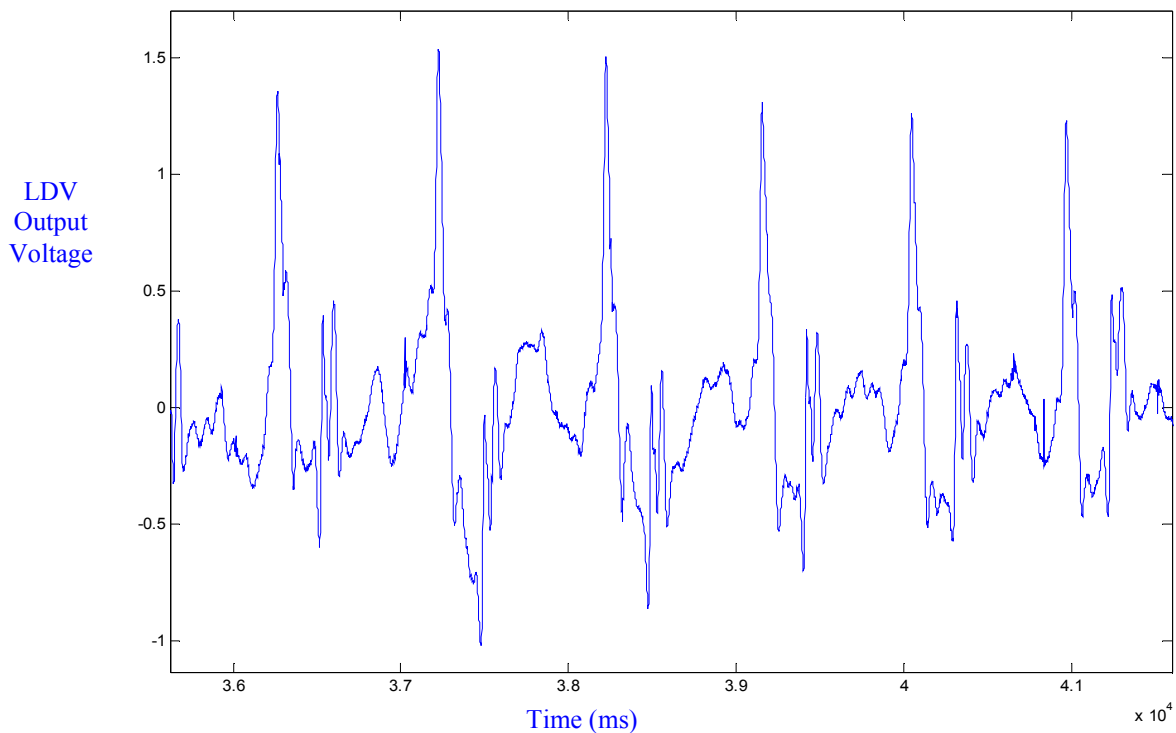


Figure 33 (c) - Carotid artery skin velocity measurement of a male subject with skin caliper reading of 6mm.

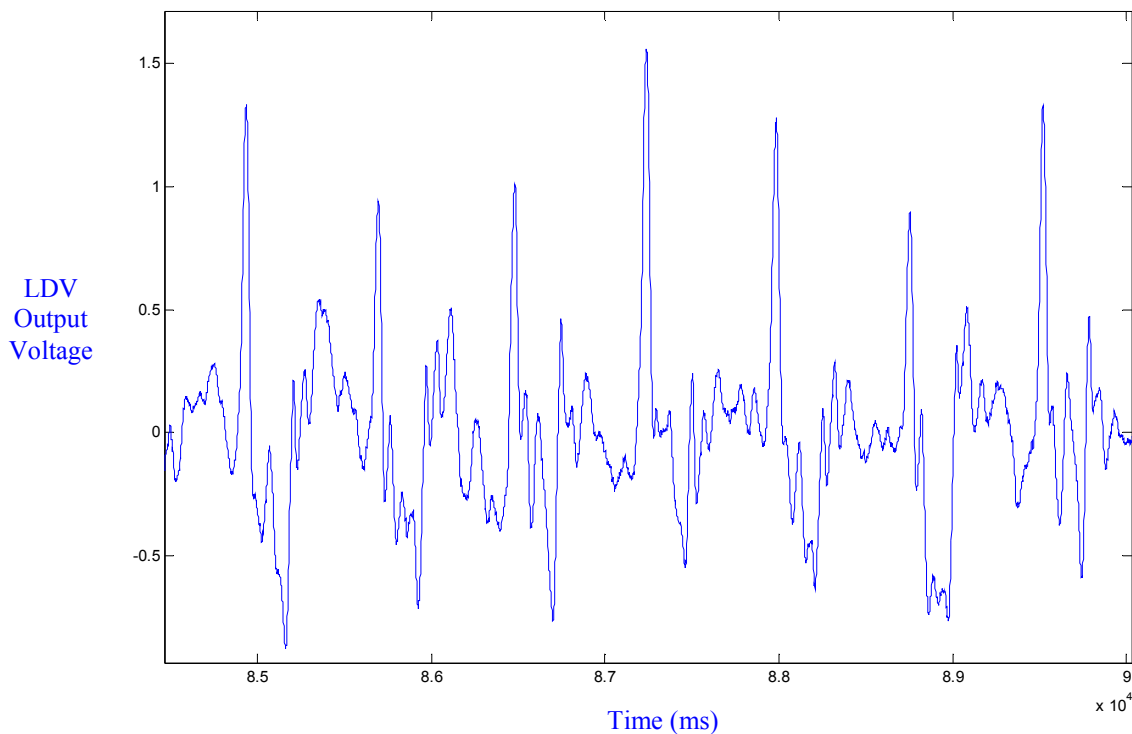


Figure 33 (d) - Carotid artery skin velocity measurement of a female subject with skin caliper reading of 16mm.

The blood pressure and heart rate was measured with an Omron HEM-780 *Intelli-sense* blood pressure cuff monitor. Figures 33 (e) and (f) demonstrate the skin velocity waveforms of subjects with the minimal and maximal blood pressure readings, respectively. Similarly, Figures 33 (g) and (h) show the skin velocity waveforms of the patients with lower and higher measured heart rates, respectively. When examining Figures 33 (e) and (f), one notices that maxima and minima of the waveform from the patient with the higher blood pressure are greater and less, respectively, than those from the patient with the lower blood pressure. The amplitude values correspond to the voltage output from the LDV. More research needs to be done as to the significance of

these voltage values, and whether the measured blood-pulse waveforms correspond to the blood pressure waveform.

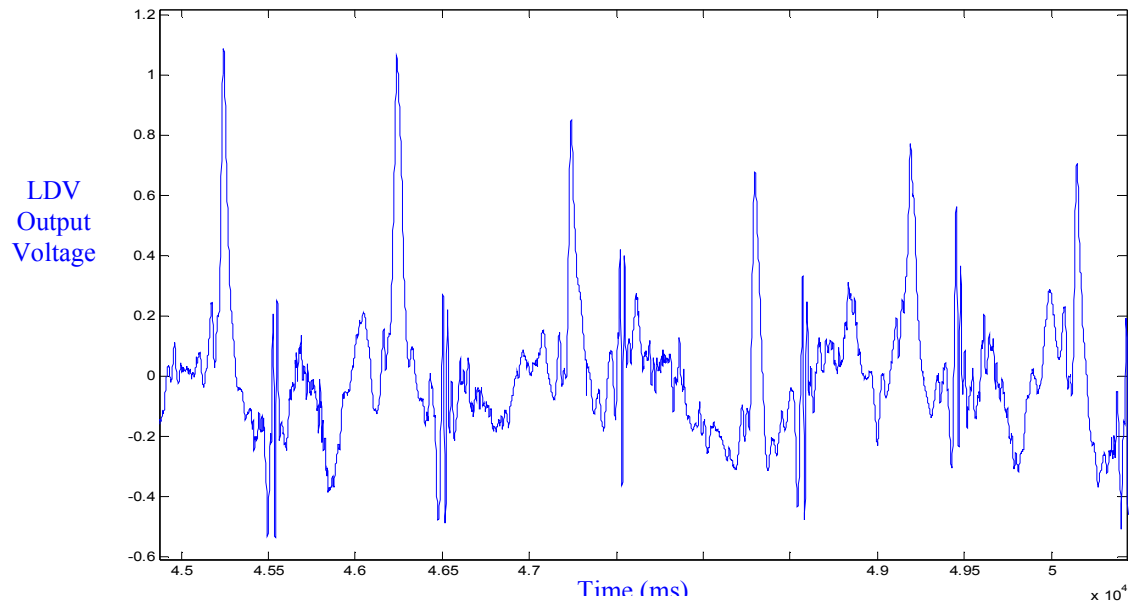


Figure 33 (e) - Carotid artery skin velocity measurement of a female subject with cuff reading of 81/64 mmHg.

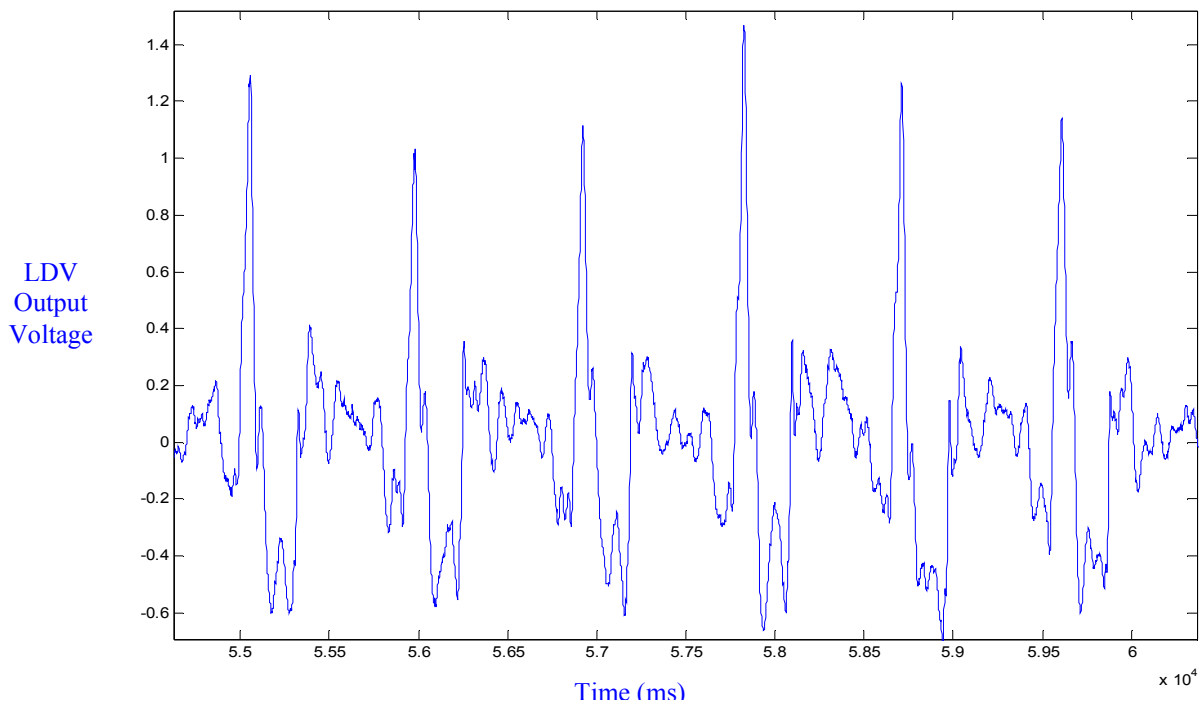


Figure 33 (f) - Carotid artery skin velocity measurement of a male subject with cuff reading of 176/113 mmHg.

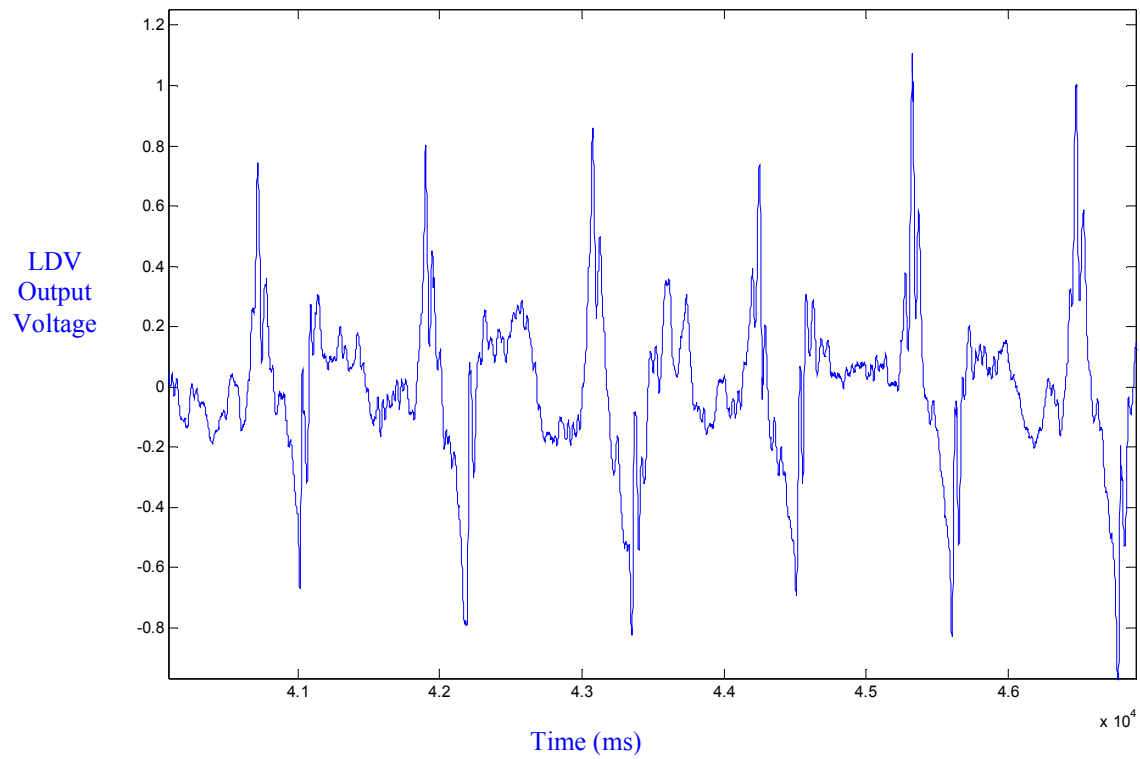


Figure 33 (g) - Carotid artery skin velocity measurement of a female subject with a heart rate of 60 bpm.

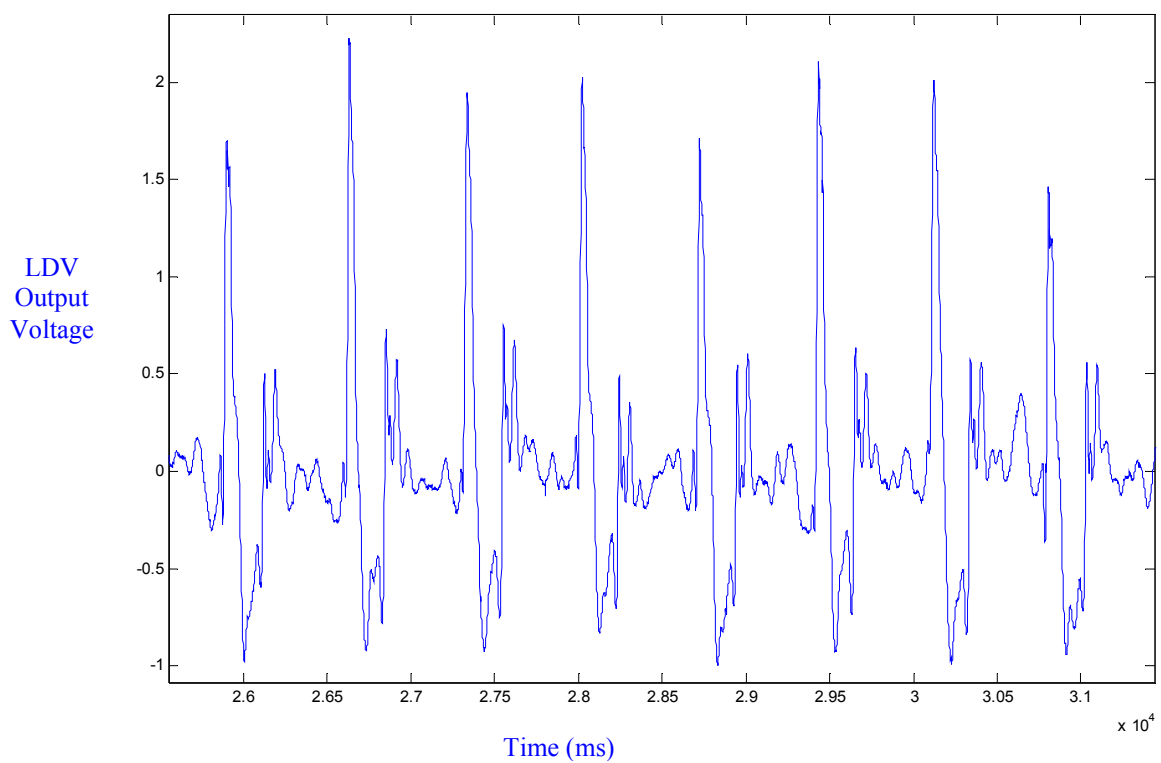


Figure 33 (h) - Carotid artery skin velocity measurement of a male subject with a heart rate of 96 bpm.

d) University of Massachusetts Medical School Clinical Trials

The most exciting part of this project has undoubtedly been the chance to begin clinical trials at the University of Massachusetts Memorial Medical Center in Worcester, Massachusetts. After much effort, Dr. Antonelli, Dr. Soares, and I obtained Institutional Review Board approval from the University of Massachusetts Medical School Committee for the Protection of Human Subjects in Research in mid April. This approval was needed for the obtainment of the blood pulse waveform of patients using our laser Doppler vibrometer (LDV). I began the testing of our LDV system on anesthetized cardiac ablation patients on April 20th, and will continue the trials until the end of the summer.

I spend approximately four to five hours per patient study in the Electrophysiology (EP) Lab with Dr. Lawrence Rosenthal and the nursing staff, who are all kind enough to continually inform me of the procedures taking place. After Karen Rofino, Dr. Rosenthal's assistant, obtains patient consent, I set up the optical and data analysis equipment in the EP Lab. The LDV is set up on a tri-pod approximately one foot away from the patient table and a piece of retro-reflective tape is placed on the patient's carotid artery. In Figure 34 below, I am shown aiming the LDV at Dr. Soares in the EP lab.



Figure 34 – LDV system being used on a subject in the Electrophysiology Lab at UMASS Memorial Hospital.

Since the patient is typically anesthetized, their eyelids are taped shut and laser goggles are not needed. Two BNC cables are connected to the LDV for two types of data acquisition, the first being the National Instruments USB system described in the **Experimental Set-Up** section. Both the electrocardiogram and blood pressure waveform signals are taken from the *Analog Out* channels on General Electric's *Prouca*[®] computer system, which controls the data acquisition system in the EP lab. Thus, all three signals are simultaneously obtained with the USB box on a laptop computer and are saved as text files.

The second method is to channel in the LDV analog signal into the *Prouca* system. The LDV skin velocity signal is displayed in real time on all monitors in the lab along with the electrocardiogram and arterial blood pressure waveforms. The three simultaneous waveforms are then extracted and saved as text files. Both methods have proved to be sufficient, however, the latter method is much more convenient due to the real time monitoring, as well as the fact that there is less wiring required.

Once an arterial catheter is inserted in the patient (either in the radial or femoral artery), I obtain the skin velocity waveform from the patient with our LDV apparatus for approximately five to ten minutes along with the electrocardiogram and arterial blood pressure waveform. In the Figures 35 a-c below, data from a male patient is shown.

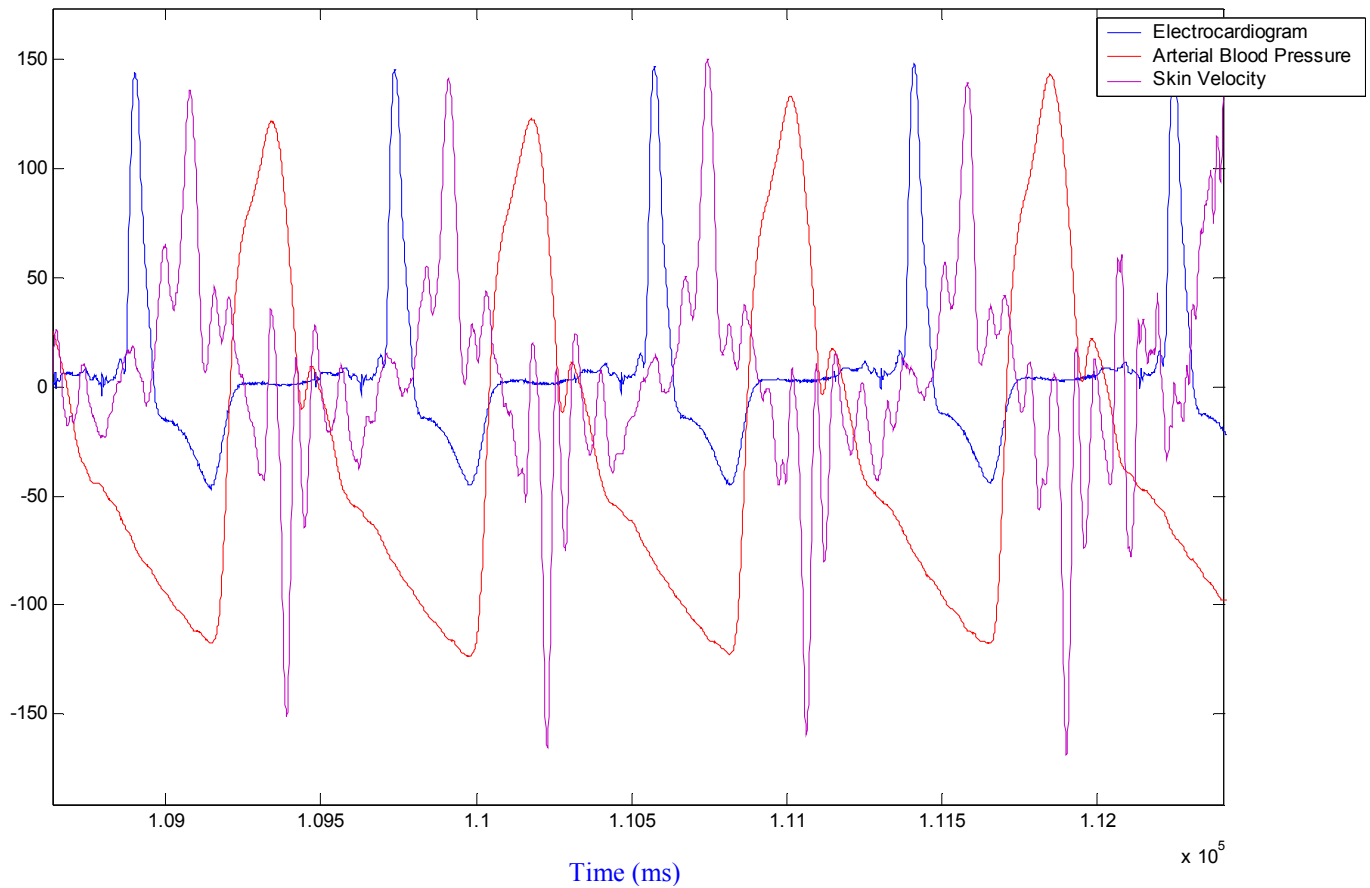


Figure 35 (a) – Electrocardiogram (blue), Radial Arterial Blood Pressure Waveform, and the Carotid Artery Skin Velocity Waveform of a male subject.

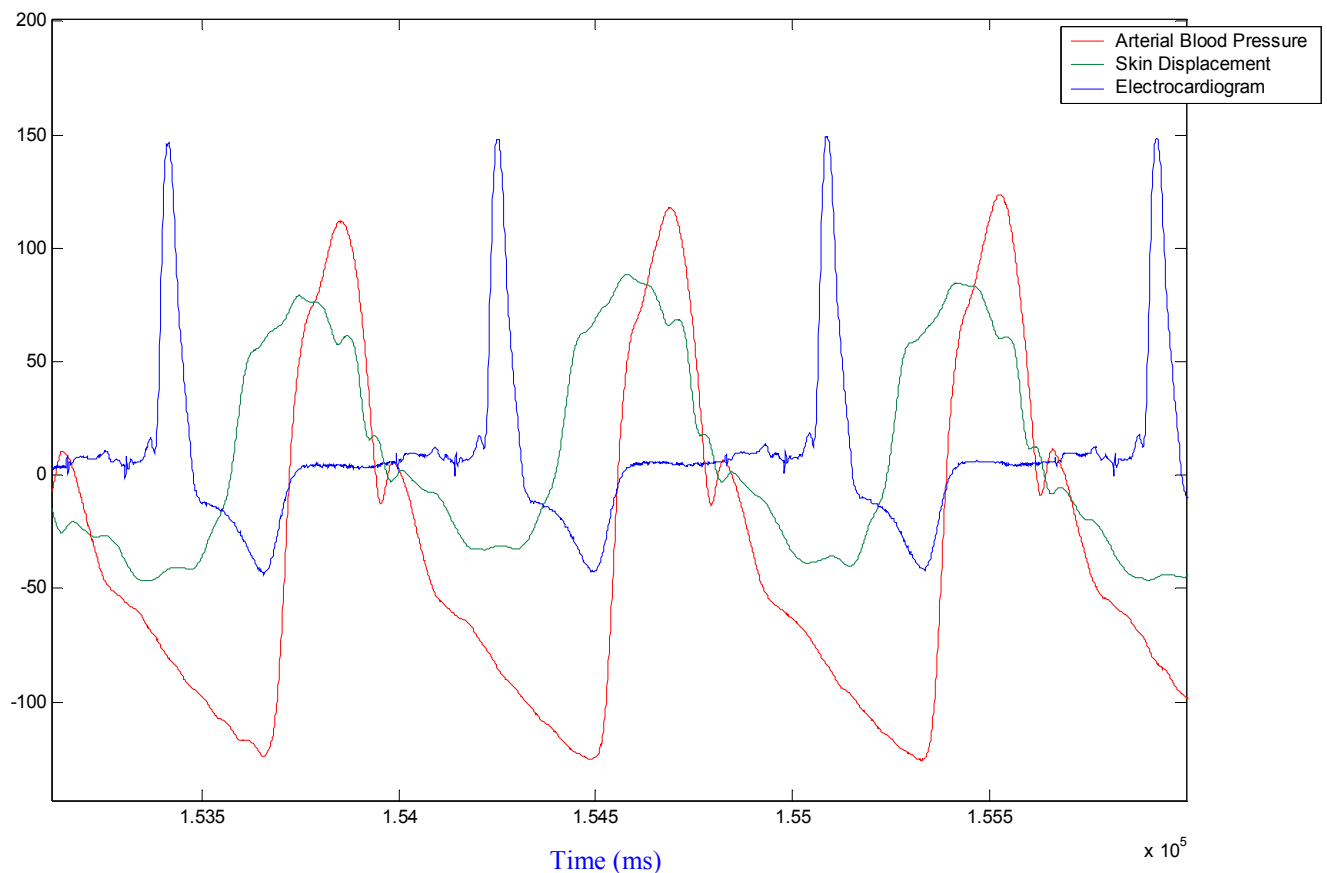


Figure 35 (b) – Electrocardiogram (blue), Radial Arterial Blood Pressure Waveform (red), and the Carotid Artery Blood Pulse Waveform (green) of a male subject.

It must be noted at this point that each waveform in both figures was scaled and shifted so the y-axis is not relevant. The waveforms were manually shifted and scaled in order to view them all on the same axis to observe any relationships between the waveforms. It is apparent from both figures that all waveforms are consistent and are related to each other. More work needs to be done, particularly with a cardiac physiologist, in order to establish all relationships between both the skin velocity and blood pulse waveforms with the electrocardiogram and arterial blood pressure waveforms. It is essential that these relationships are established and verified since both the electrocardiogram and arterial blood pressure waveforms are valuable and well known parameters.

In Figure 35 (c) below, the electrocardiogram, arterial blood pressure, skin velocity, and blood pulse waveforms are all presented on the same graph.

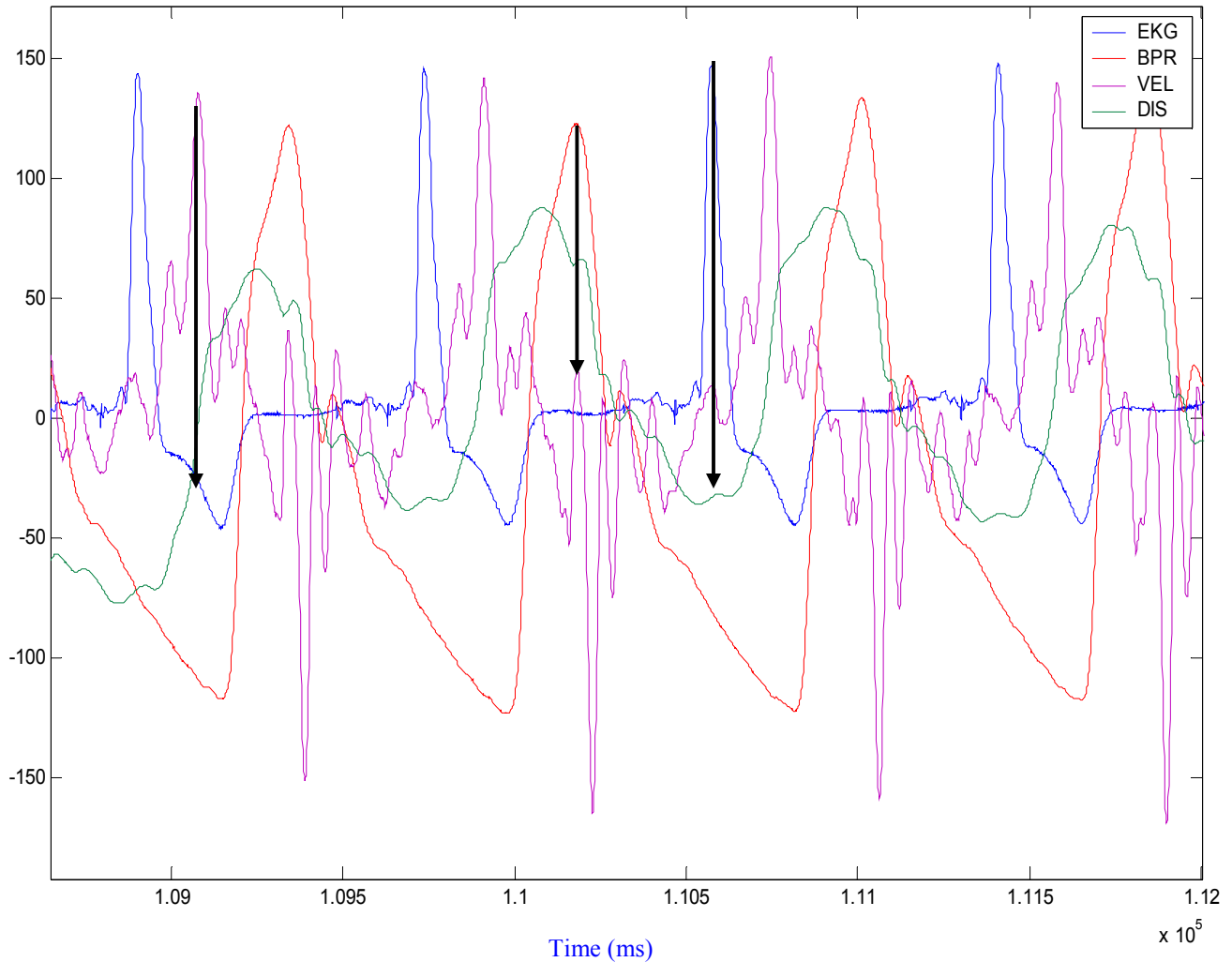


Figure 35 (c) – Electrocardiogram (blue), Radial Arterial Blood Pressure Waveform (red), the Carotid Artery Skin Velocity Waveform and the Carotid Artery Blood Pulse Waveform (green) of a male subject with arrows drawn to demonstrate some of the relationships between the waveforms.

In the figure above, arrows are drawn on the graph to demonstrate just a few of the noticeable relationships between peaks and inflection points of the various waveforms. It can be noted that these relationships are replicated over each cardiac cycle. The underlying physiology must be determined to fully understand these relationships and

their significance, particularly for diagnostic purposes. When examining the relationship between the radial arterial blood pressure and carotid artery blood pulse waveforms, one notices that the peak of the blood pulse waveform occurs slightly before that of the blood pressure waveform. This may be due to the fact that the carotid artery is located closer to the heart than the radial artery.

It has truly been an exciting experience to take real patient data, and I am always very enthusiastic to receive an early morning phone call from Karen Rofino at UMass to let me know that an ablation patient has consented to take part in our research. I was certainly pleased to expand my Fenwick project with these patient trials, as well as investigate and understand other cardiac procedures.

e) Principal Component Analysis

One of the main goals of this project was to determine the diagnostic usefulness of the data that we obtained. Many patients have similar skin velocity and blood pulse waveforms. A natural question that came up during our analysis of the data was how to distinguish between the waveforms of patients with similar waveforms but different physiological health states. Not only do I want to discover the underlying physiology behind both the skin velocity and blood pulse waveforms, but I also wish to determine if there are any features present in the waveforms that could indicate physiological abnormalities or other distinguishing health-related problems. Principal components analysis (PCA) may be able to allow us to discriminate between the different types of waveforms obtained from a population of patients with various health states.

In Figures 36 a-d, waveforms with various distinguishable characteristics are presented.

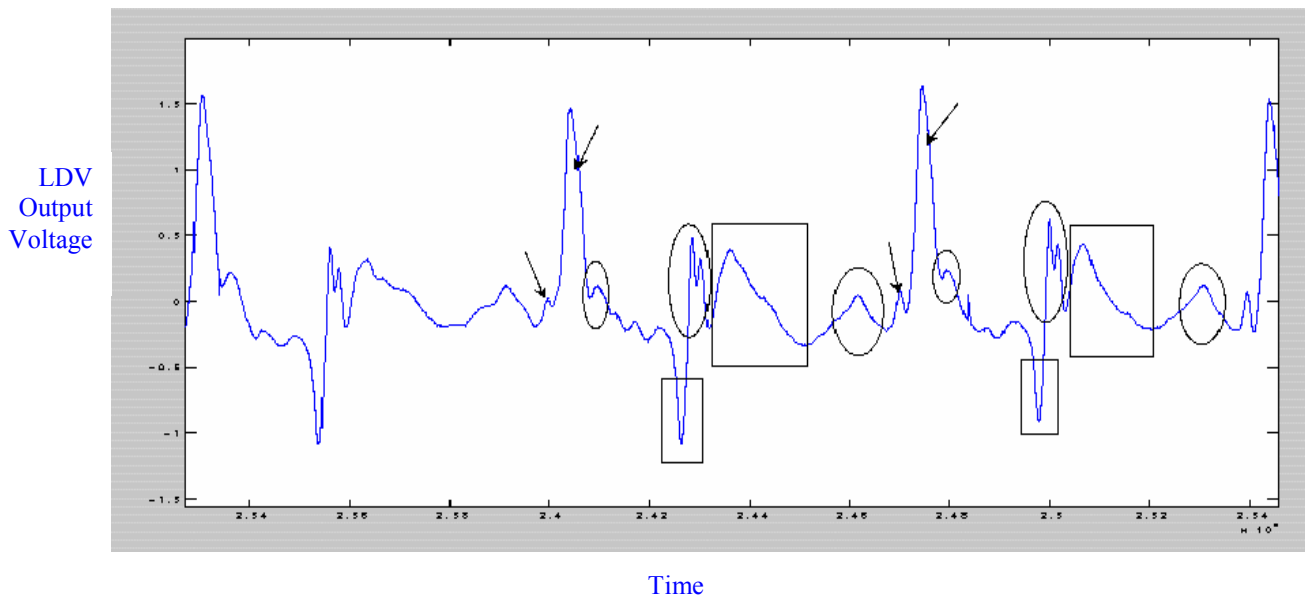


Figure 36 (a) – Carotid artery skin velocity waveform of a male subject with various distinguishable characteristics indicated.

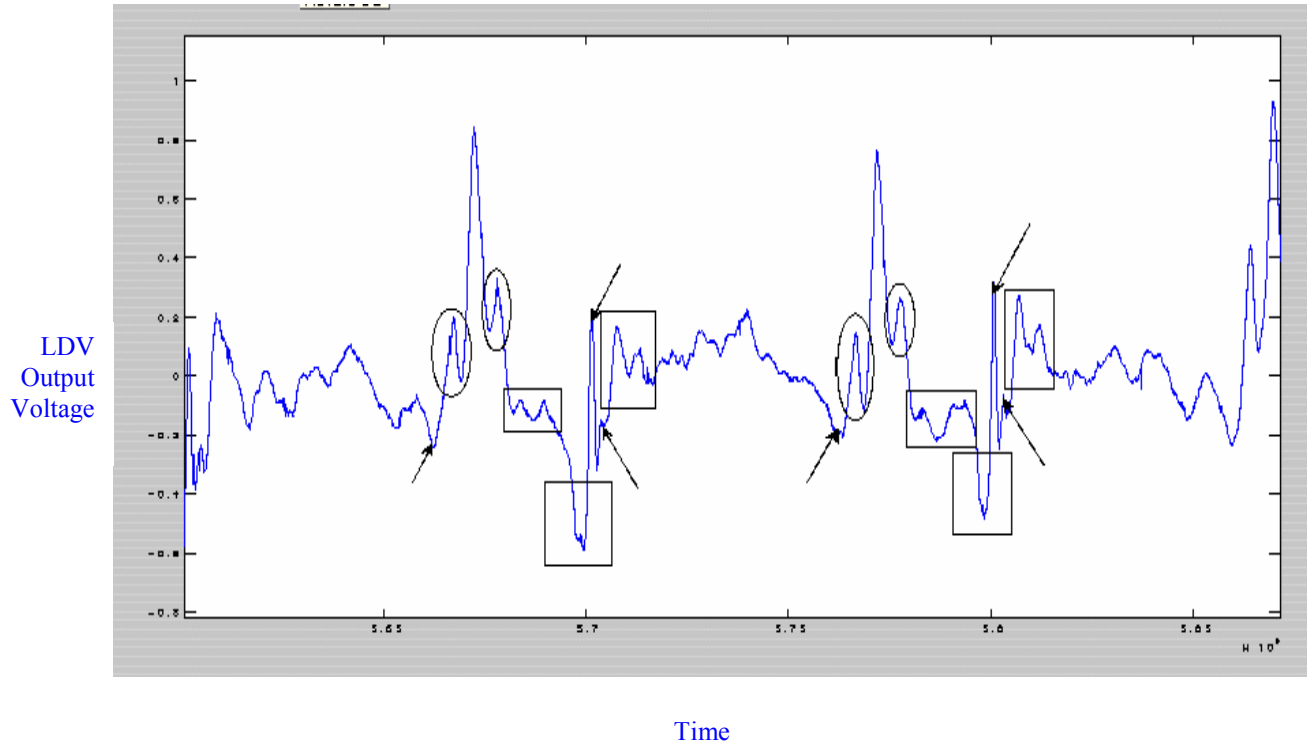


Figure 36 (b) – Carotid artery skin velocity waveform of a female subject with various distinguishable characteristics indicated.

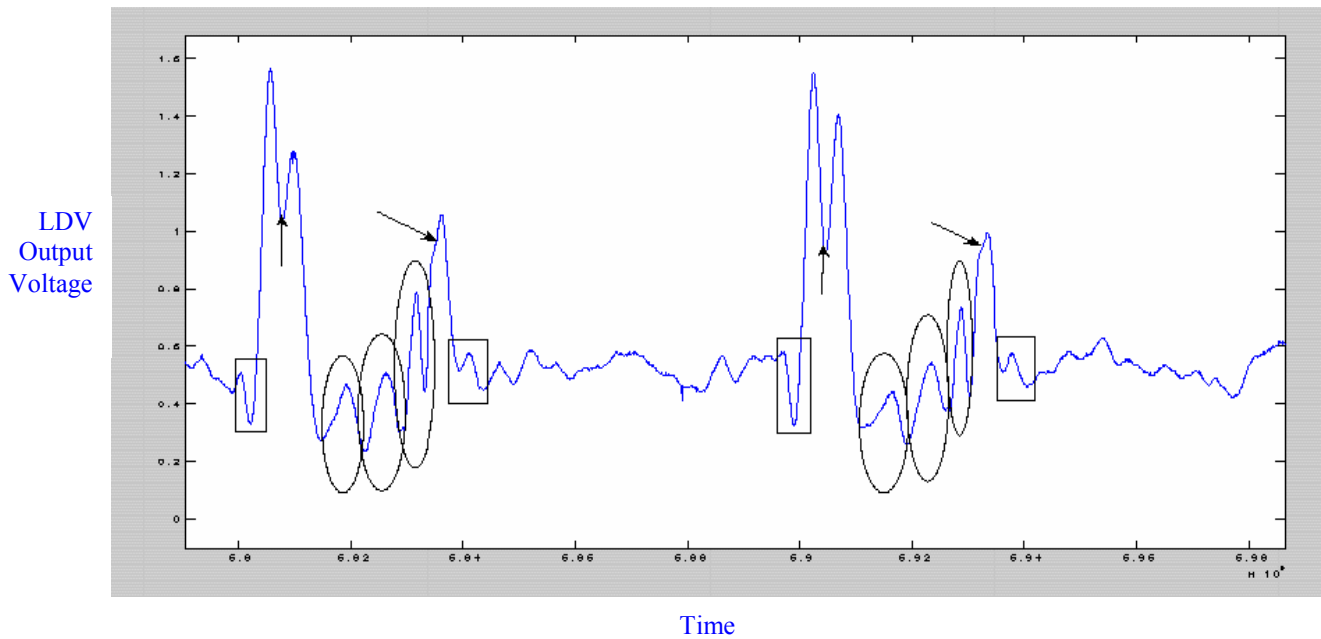


Figure 36 (c) – Carotid artery skin velocity waveform of a female subject with various distinguishable characteristics indicated.

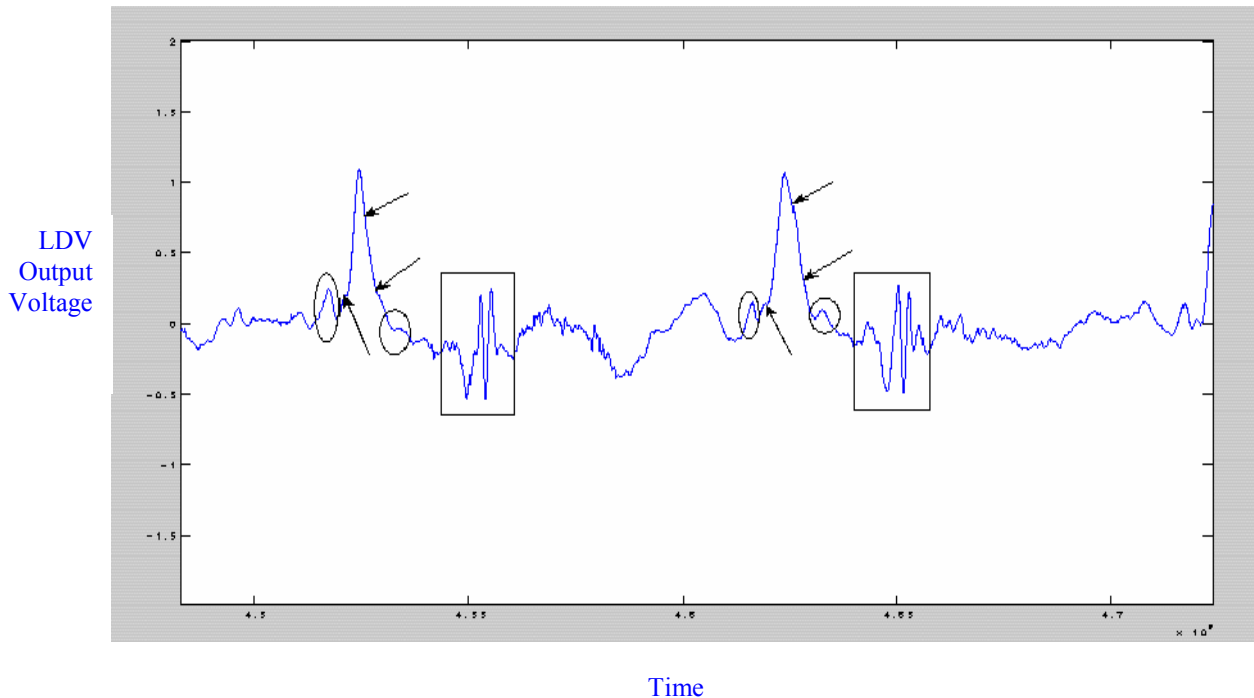


Figure 36 (d) – Carotid artery skin velocity waveform of a male subject with various distinguishable characteristics indicated.

It is clear that the waveforms above have a similar structure, but each has its own distinguishable features. For example, consider the large peaks present in each waveform. In Figures 36 (b) and (c), there are two distinctive maxima present, whereas in Figures 36 (a) and (d), a less noticeable inflection point is found. A discriminatory feature found in each of the four waveforms is the shape of the doublet (two adjacent maxima) found after the larger peak. The shape and timing of the doublets is different in each case, so it may be a characteristic of a patient's physiological condition. After examining the similarities and differences between waveforms, it is clear that an analysis must be made to discriminate between the waveforms of various patients.

In order to utilize principal component analysis, a single cycle of either the skin velocity or blood pulse waveform must be obtained for the $m = 1, 2, \dots, M$ total patients in the study. Thus, we will have a total of M waveforms, one for each patient in the analysis. When using PCA, each single-cycle waveform must be normalized to have the same length, as each patient has a different single-cycle time length. For simplicity, assume we can normalize each waveform over the interval, $[0, 1]$. Furthermore, assume the skin velocity, and thus the blood pulse waveforms are measured at $(T + 1)$ time points given by

$$t = 0, 1/T, 2/T, \dots, T/T = 1.$$

(since the time point $t = 0$ is included). Also, let $\Delta t = 1/T$ be the spacing between points. In Figure 37 below, a typical normalized blood pulse waveform is shown for a patient, keeping in mind that the single cycle is represented from peak tip to the next peak tip.

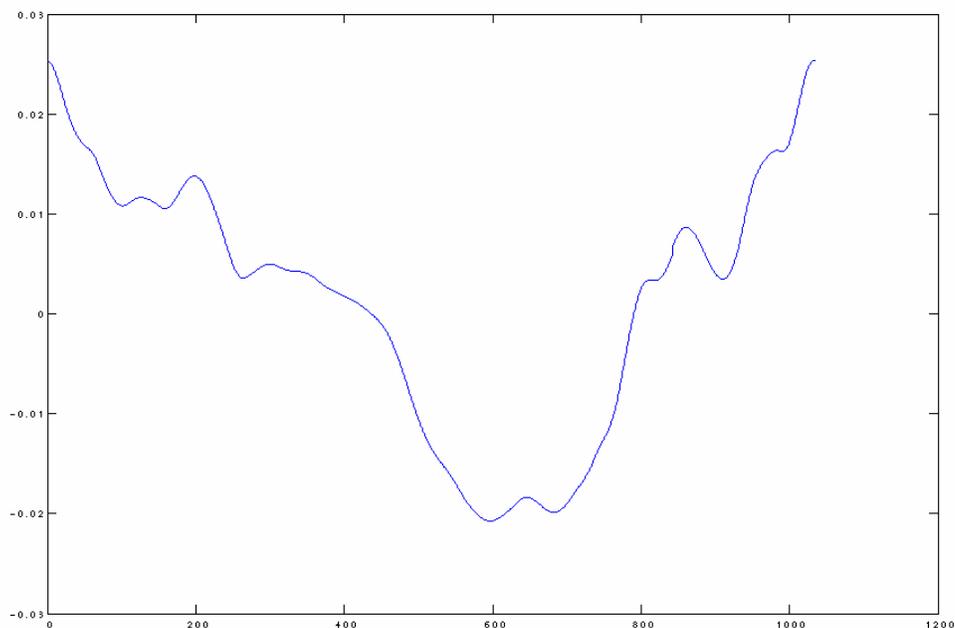


Figure 37 – A single cycle waveform for patient, m

The goal now is to create a feature vector, $\bar{x}^{(m)}$ for each of the M total patients in the study such that:

$$\bar{x}^{(m)} = \begin{pmatrix} x_0^{(m)} \\ x_1^{(m)} \\ \vdots \\ x_T^{(m)} \end{pmatrix} \quad (28)$$

where $x_i^{(m)}$ is the waveform measurement at time i/T for patient m . Thus, we obtain a set of M feature vectors $\{\bar{x}^{(m)}\}_{m=1}^M$. The mean vector is now computed for all M patients, producing a $(T + 1)$ by 1 matrix.

$$\bar{\bar{x}} = \frac{1}{M} \sum_{m=1}^M \bar{x}^{(m)} = \begin{pmatrix} \bar{\bar{x}}_0 \\ \bar{\bar{x}}_1 \\ \vdots \\ \bar{\bar{x}}_T \end{pmatrix} \quad (29)$$

From Equation (29) above, $\bar{\bar{x}}_i$ is the mean blood pulse signal of all patients at time i/T .

The next step is to compute the $(T + 1)$ by $(T + 1)$ covariance matrix as shown in

Equation 30 below:

$$S_{\bar{x}^{(m)}} = \frac{1}{M-1} \sum_{m=1}^M (\bar{x}^{(m)} - \bar{\bar{x}})(\bar{x}^{(m)} - \bar{\bar{x}})^t \quad (30)$$

$$= \frac{1}{M-1} \sum_{m=1}^M \begin{pmatrix} (x_0^{(m)} - \bar{\bar{x}}_0)^2 & (x_0^{(m)} - \bar{\bar{x}}_0)(x_1^{(m)} - \bar{\bar{x}}_1) & \cdots & (x_0^{(m)} - \bar{\bar{x}}_0)(x_T^{(m)} - \bar{\bar{x}}_T) \\ \vdots & (x_1^{(m)} - \bar{\bar{x}}_1)^2 & & \vdots \\ \vdots & & \ddots & \vdots \\ (x_T^{(m)} - \bar{\bar{x}}_T)(x_0^{(m)} - \bar{\bar{x}}_0) & \cdots & \cdots & (x_T^{(m)} - \bar{\bar{x}}_T)^2 \end{pmatrix}$$

$$= \begin{pmatrix} \sigma_0^2 & \sigma_{01} & \cdots & \sigma_{0T} \\ \sigma_{01} & \sigma_1^2 & \cdots & \sigma_{1T} \\ \vdots & \vdots & \ddots & \vdots \\ \sigma_{0T} & \sigma_{1T} & \cdots & \sigma_T^2 \end{pmatrix}.$$

The diagonal values σ_i^2 are the average squared deviations from the mean, or the variance in blood pulse measurement $x_i^{(m)}$ over all M patients at time i/T . The value σ_{ij} is the covariance in the blood pulse measurements $x_i^{(m)}$ and $x_j^{(m)}$ over all M patients between times i/T and j/T .

The next step is finding the eigenvectors of $S_{\bar{x}^{(m)}}$, and since it is a symmetric matrix, it is orthogonally diagonalizable by the Spectral Theorem. The proof of the Spectral Theorem may be found from Lay's Linear Algebra and Its Applications found in the references cited. We can find an orthogonal matrix P such that

$$S_{\bar{x}^{(m)}} = PDP^t \text{ or } D = P^t S_{\bar{x}^{(m)}} P \quad (31)$$

and $P = (\bar{P}_0 \bar{P}_1 \cdots \bar{P}_T)$ is the matrix whose columns are the eigenvectors and \bar{P}_i is the

eigenvector for time i/T . The diagonal matrix of eigenvalues, $D = \begin{pmatrix} \lambda_0 & & \mathbf{0} \\ & \ddots & \\ \mathbf{0} & & \lambda_T \end{pmatrix}$ is such

that $\lambda_0 \geq \lambda_1 \geq \cdots \geq \lambda_T$, where λ_i is the variance for the principal component i . The Principal Component transform can now be done on all blood pulse waveforms of the M patients, after subtracting the mean:

$$\bar{Y}^{(m)} = P^t (\bar{x}^{(m)} - \bar{\bar{x}}). \quad (32)$$

A set of M Principal Component transformed vectors is now obtained.

$$\bar{Y}^{(1)} = \begin{pmatrix} Y_0^1 \\ Y_1^1 \\ \vdots \\ Y_T^1 \end{pmatrix} \quad \bar{Y}^{(2)} = \begin{pmatrix} Y_0^2 \\ Y_1^2 \\ \vdots \\ Y_T^2 \end{pmatrix} \quad \cdots \quad \bar{Y}^{(M)} = \begin{pmatrix} Y_0^M \\ Y_1^M \\ \vdots \\ Y_T^M \end{pmatrix} \quad (33)$$

In general, one plots ordered pairs or ordered triples, $\{(Y_i^{(m)}, Y_j^{(m)}, Y_k^{(m)})\}_{m=1}^M$, as scattergrams to compare the now principal component transformed waveforms. If the

points cluster in some fashion, then we may be able to discriminate between different waveforms.

The principal component analysis is not yet complete due to a few challenges faced throughout the semester. As previously mentioned, a single cycle must be produced from all of the waveforms and these single cycles must be normalized over the same interval. The first challenge is finding a method to automate the obtainment of a clean single cycle waveform. Single cycle waveforms were acquired by using the First Derivative Test to locate peaks and then removing a single cycle from one peak to another. During this analysis, a peak threshold was defined so as not to include other local maxima. The problem with this method was that there were some waveforms with local maxima on the large peak with almost identical amplitudes so the peak threshold method was inefficient. Once an effective method is found to obtain single cycle waveforms, an accurate method to resample the data to a normalized interval must also be found. Whether compressing or stretching the single cycle, we must ensure that there are no re-sampling artifacts present.

f) Related Projects

In the summer of 2005, I visited Professor Yitzhak Mendelson of the Biomedical Engineering Department of Worcester Polytechnic Institute to discuss his project and compare it with ours. Dr. Mendelson and his team have developed tiny biosensors consisting of light emitting diodes (LEDs) and highly sensitive light detectors to determine a human's heart rate, skin temperature, and blood oxygenation for military use on the battlefield. The sensors may be placed on any soft tissue, and the light shines through the skin to detect how much blood occupies the area at any given moment. Thus, over a continuous time period, the pulse can be determined due to the increase and decrease of the blood flow [4]. For the entirety of the visit, the index finger was used for the WPI measurement, since it is the easiest, and provides the most reliable data. The carotid artery was used for the LDV measurements. The WPI data was used as a control to validate the LDV data. Using the setup as described, the velocity waveform was measured on both the pedal and the carotid artery simultaneously with the biosensor on the index finger of the subject.

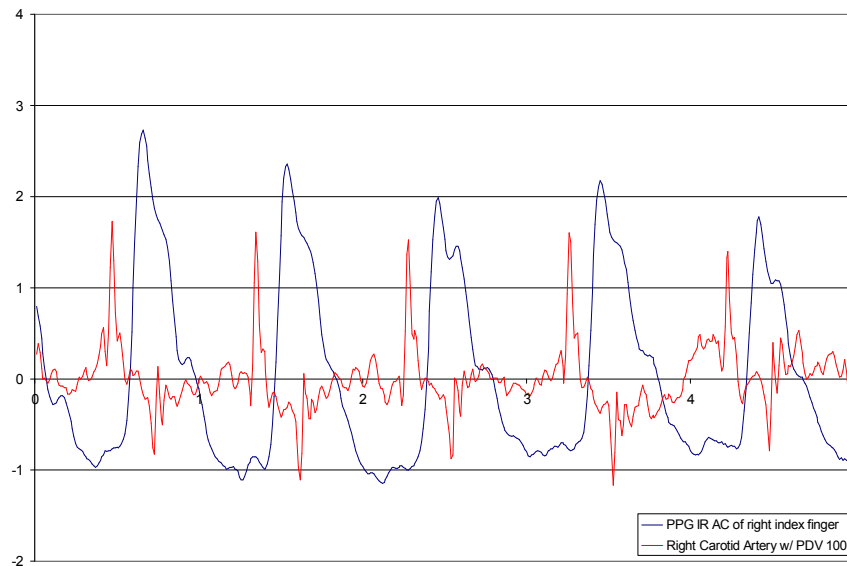


Figure 38 - Laser vibrometer velocity measurement on the carotid artery of a female subject (red) and the biosensor LED measurement on her right index finger.

The biosensor measurement is internal, while the laser measurement is external. Figure 38 shows the simultaneous measurement of the biosensor with the LDV collected waveform.

The WPI data is a displacement waveform, so its derivative would yield a velocity waveform. It was our goal to compare our LDV velocity waveform with the velocity waveform obtained from differentiating the WPI data. The graph below in Figure 39 is the derivative of the biosensor's data, along with the data from the LDV. From this, it can be seen that the peaks do look similar, but the biosensor velocity waveform is shifted slightly to the right of the LDV velocity waveform. This may be due to the fact that different parts of the body were measured simultaneously, and the time lag would be due to the different blood pressures throughout the body, as the blood must take more time to flow to parts of the body that are further away from the heart. It is important to note that the periods of the waves are approximately the same.

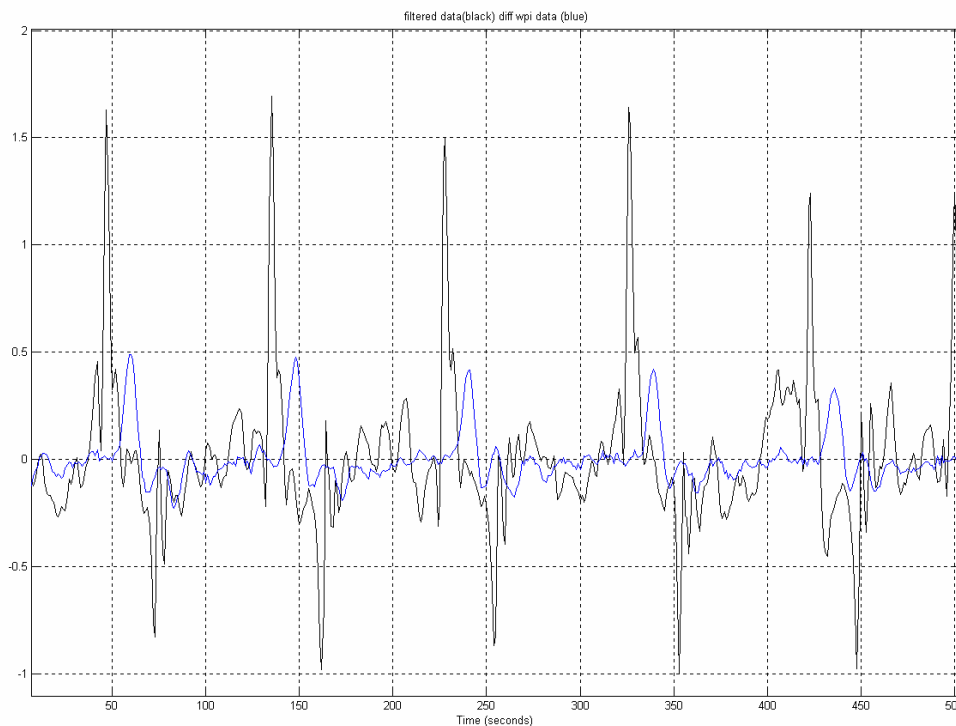


Figure 39 - Filtered data of the carotid artery measurement with the laser vibrometer (black) and the derivative of WPI biosensor measurement of the index finger (blue).

I then investigated the raw biosensor data with the filtered integrated (displacement) waveform previously discussed. Again, notice that the WPI data is shifted slightly towards the left in Figure 40, but the periods are approximately the same for both waveforms.

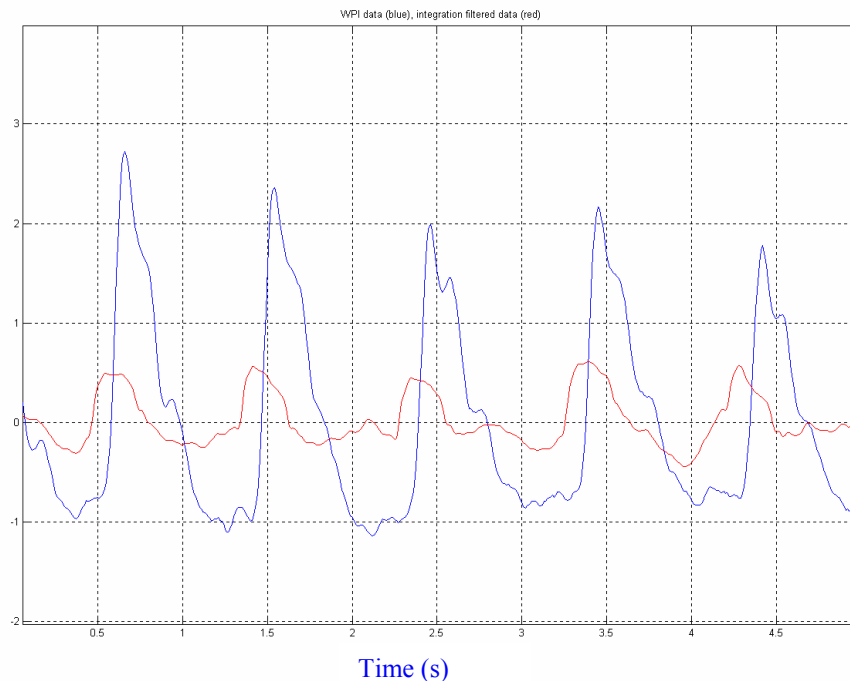


Figure 40 - WPI biosensor measurement of the index finger (blue) and the integration of the filtered laser vibrometer data from the carotid artery (red).

One goal of the project was to determine the location of the dicrotic notch, the sudden drop in pressure after systolic contraction caused by the backflow of blood as the aortic valve is closing, on either the skin velocity or blood pulse waveform obtained from the LDV. The location of the dicrotic notch has been verified on the biosensor waveform, so we hoped to determine a relationship between the biosensor and LDV data in order to hypothesize the location of the dicrotic notch on the LDV waveform. Using the fact that the dicrotic notch is definitely known in the biosensor data, we hoped

to find a relationship which could be applied to any velocity waveform to detect the dicrotic notch fairly easily.

The relationship between the dicrotic notch of the biosensor displacement data was found with its derivative waveform in Figure 41 below. As shown by the arrows, the dicrotic notch of the velocity waveform is located on the second, smaller peak. Using this fact, the filtered LDV velocity waveform was superimposed on the graph in Figure 42 with the integration for displacement. Once again, the arrows point to the dicrotic notch on the velocity waveform. It was not as easy to identify the location of the dicrotic, but using the biosensor data findings as a guide, the second peak was determined to be the dicrotic notch. Hopefully, data can be taken to verify the hypothesis that the dicrotic notch is located on the top of the second, smaller peak of the velocity waveform.

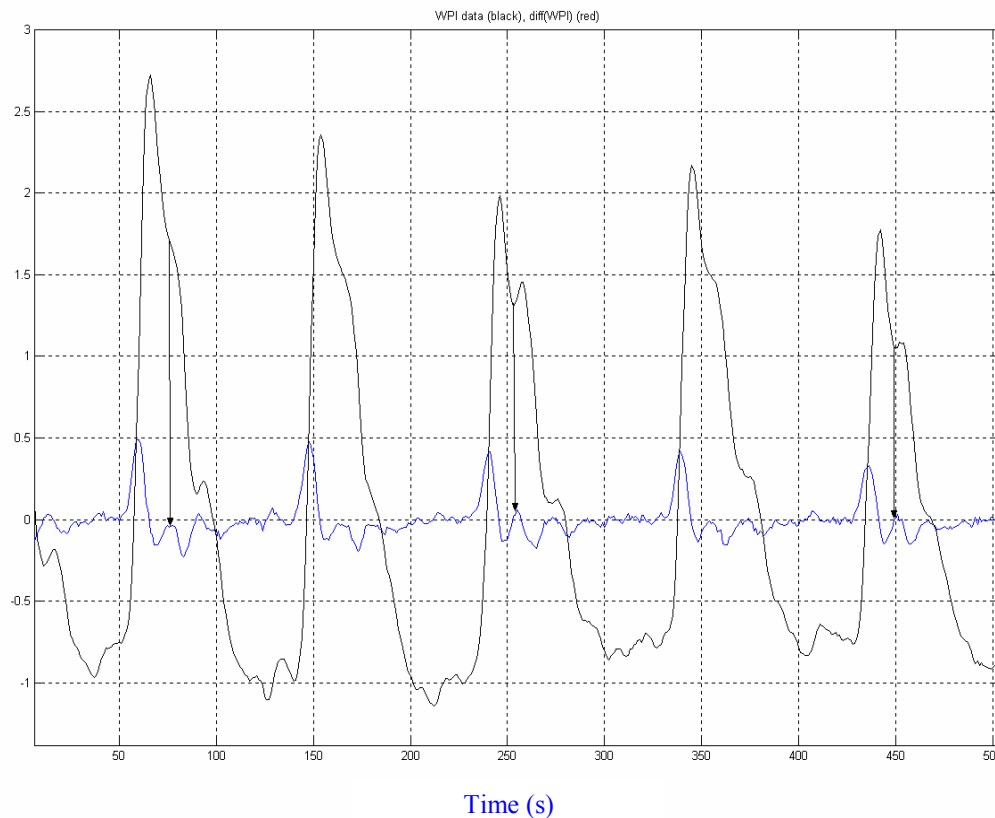


Figure 41 - Measurement from the WPI biosensor on the index finger (black) and the derivative of the biosensor data (blue). The dicrotic notch is labeled at several points with a black arrow from one waveform to another.

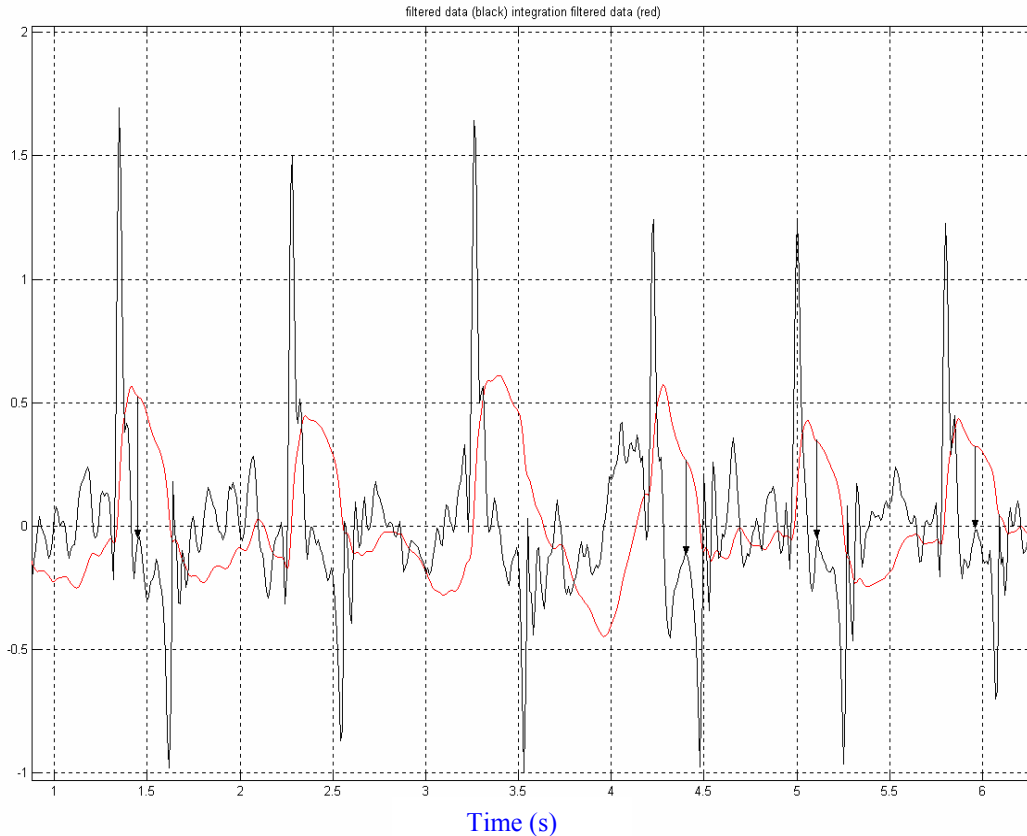


Figure 42 - Filtered data from the laser vibrometer of the carotid artery (black) and the integration of the filtered data (red) . The dicrotic notch is labeled at several points with a black arrow from one waveform to another.

My visit to WPI was quite informative. Not only was I able to get a better understanding of the location of the dicrotic notch by using their project as a control, but I also got a boost of confidence in our work. The similarity in the results obtained by the integration and differentiation of the appropriate waveforms verify that our project has great potential.

g) Applications

The LDV technology has the potential to be used in clinical medicine, especially in emergency room (ER) situations. The skin velocity waveform detection could be used in an ER for trauma or burn victims as a non-contact method of finding the heart rate and the blood pressure waveform if a relationship between the blood pulse and blood pressure waveforms can be found. The measurement itself could take as little as five seconds and the software can produce a waveform very quickly, which gives doctors a very fast reading of the parameters. Another great aspect of the technology is the versatility of the measurement area. Doctors may have the flexibility of choosing their target area depending on each specific case that comes in. Typically, there is a lot of commotion in the upper body area when a patient is brought into the ER, making the pedal artery measurement more highly desired. As previously shown, data can be collected without the retro-reflective tape if the injury or time constraints prevent its application to the skin.

The blood pulse waveform detection may also be useful in the operating room (OR) as another means of monitoring. As before, the multiple measurement areas provide an accommodation to the surgeon and the area of operation. A patient is most likely sedated if in the OR, so movement of the target area would not be an issue. Thus, a continuous measurement of the blood pulse waveform can be displayed and monitored to further ensure a patient's well being.

During my research in the summer of 2005, it occurred to me that none of my pets had ever had their blood pressure measured in a veterinary office. I began doing research of veterinary procedures for routine check-ups and common complications for a dog or cat's health. Secondary hypertension of dogs and cats is a major concern in the veterinary

field and high blood pressure is a major sign. As of now, the methods to find blood pressure in dogs and cats are limited [8]. As with humans, a catheter may be inserted into an artery to directly measure the pressure, but the animal must be sedated which will alter the heart rate. Alternatively, an inflatable cuff may be fit around the foreleg, foot, or tail of the animal, and as with humans, the cuff is inflated to occlude the blood flow in the artery. However, a stethoscope is not sensitive enough for animals, so an ultrasonic probe must be used instead. A disadvantage of this method is the fact that diastolic blood pressure cannot be measured, and only systolic pressure can be read [3]. It is also difficult to do this procedure on animals since they are already nervous and most of the time, several readings must be made and the vet will have to take an average of the readings [12]. It's also been found that the systolic readings in larger dogs are very inaccurate, even after the several readings [8].

It was apparent to me that applying the LDV to animals would be a considerable benefit to the veterinary field. The femoral artery in dogs is located where the hind leg meets their abdomen, and a pulse can be easily found [12]. It also a convenient place to measure since the groin area is relatively fur-less and the retro-reflective tape can be applied. If the animal is excessively furry, a small spot may be shaven to apply the tape in order to obtain a cleaner waveform. It is an ideal spot since it easy to hold the animal's two hind legs still while laying on their back and it also prevents the animal from staring directly into the laser beam. As mentioned before, the laser is only Class II, but if necessary, a lamp-shade collar may be placed around the animal's neck to further prevent them from trying to look into the beam.

My neighbors were kind enough to allow me to test my idea on their eight-year-old Wheaton Terrier, Murphy. I brought all of the equipment to their home and the only difference in the setup was that the laser was held rather than mounted, as shown below.



Figure 43 - Picture of the set-up used for velocity measurement of a dog.



Figure 44 - Additional picture of the set-up along with the placement of the retro-reflective tape for the target femoral artery.

Using our software, once the velocity waveform was obtained, a blood pulse signal was also calculated as seen in Figure 45. The signal was not as clean as previous experiments, possibly due to the fact that the laser was not mounted. It is quite likely that the person directing the laser toward the target did not have a perfectly steady grip on the laser for the entire thirty seconds and some of the noise in the data may be accounted for that motion.

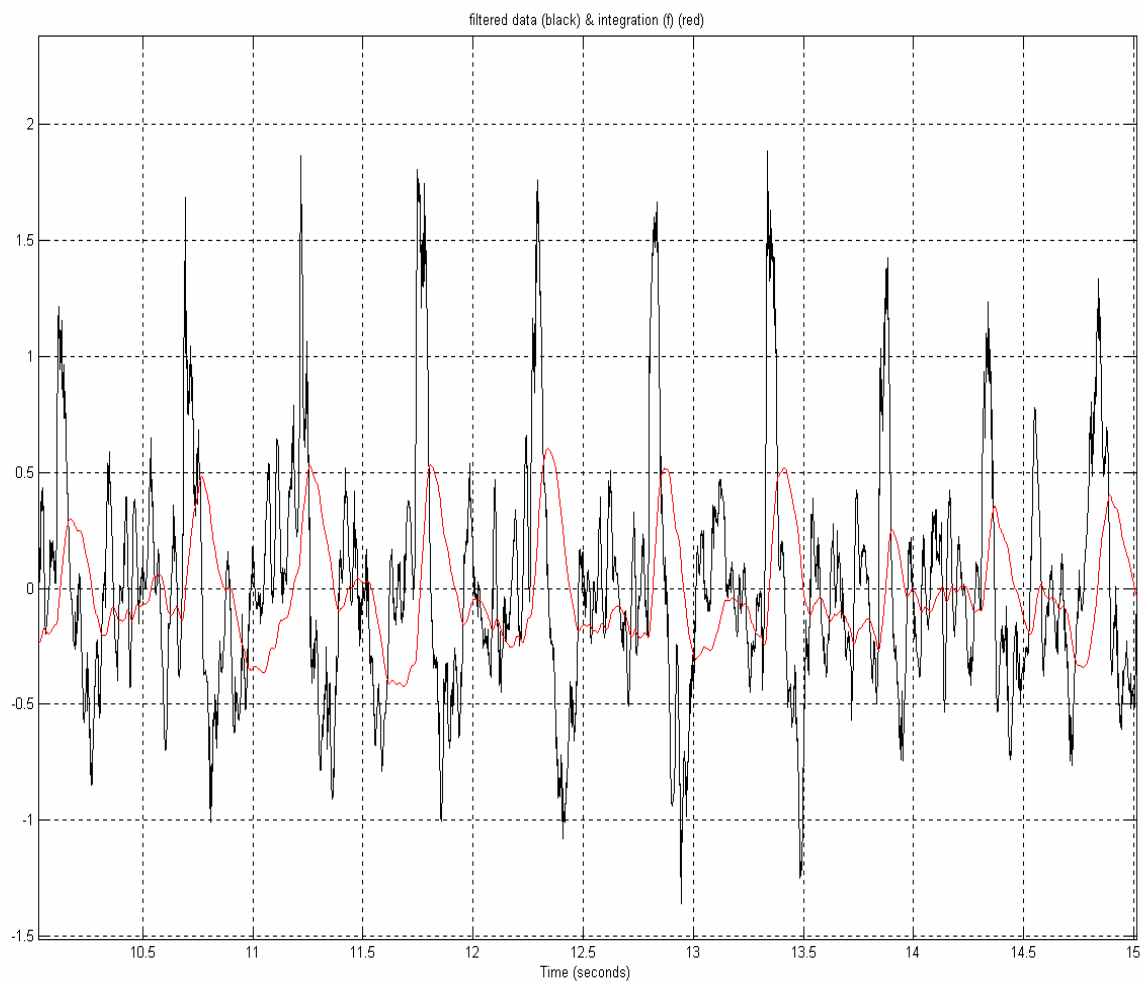


Figure 45 - Filtered data from the measurement of the femoral artery on a Wheaton Terrier (black) and the integration of the filtered data (red)

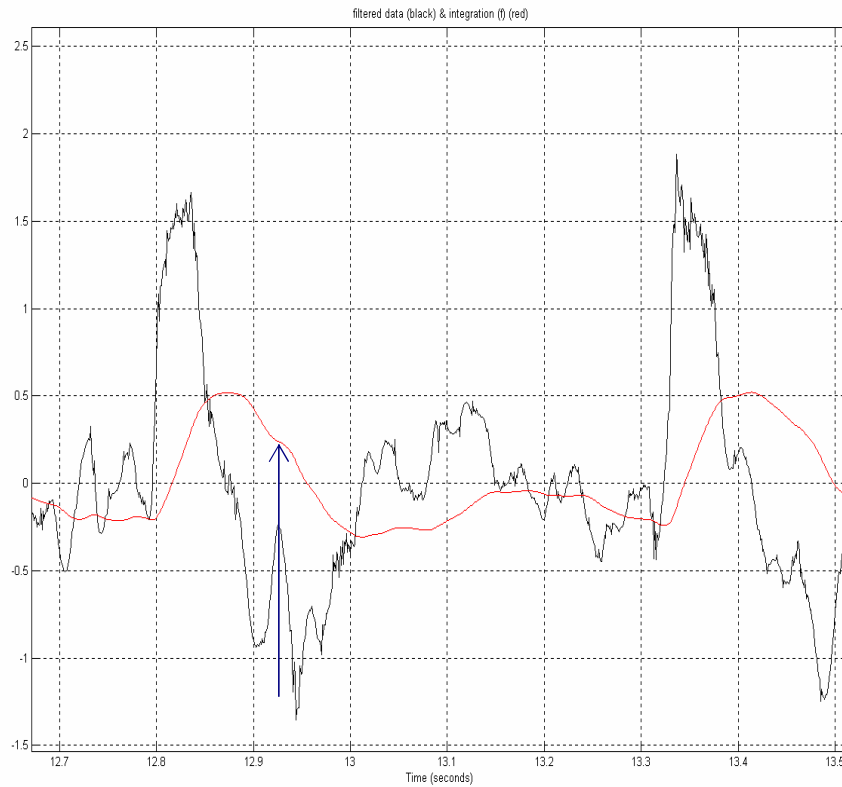


Figure 46 - Filtered data from the measurement of the femoral artery on a Wheaton Terrier (black) and the integration of the filtered data (red). The dicrotic notch is labeled with a black arrow from one waveform to another.

As previously observed, there are some hypothesized breathing effects on the amplitudes of the waveform. The femoral artery on the dog is located very close to the abdomen, and when laid on his back, his breathing motion could be seen. The breathing effects are shown in Figure 47 on the following page.

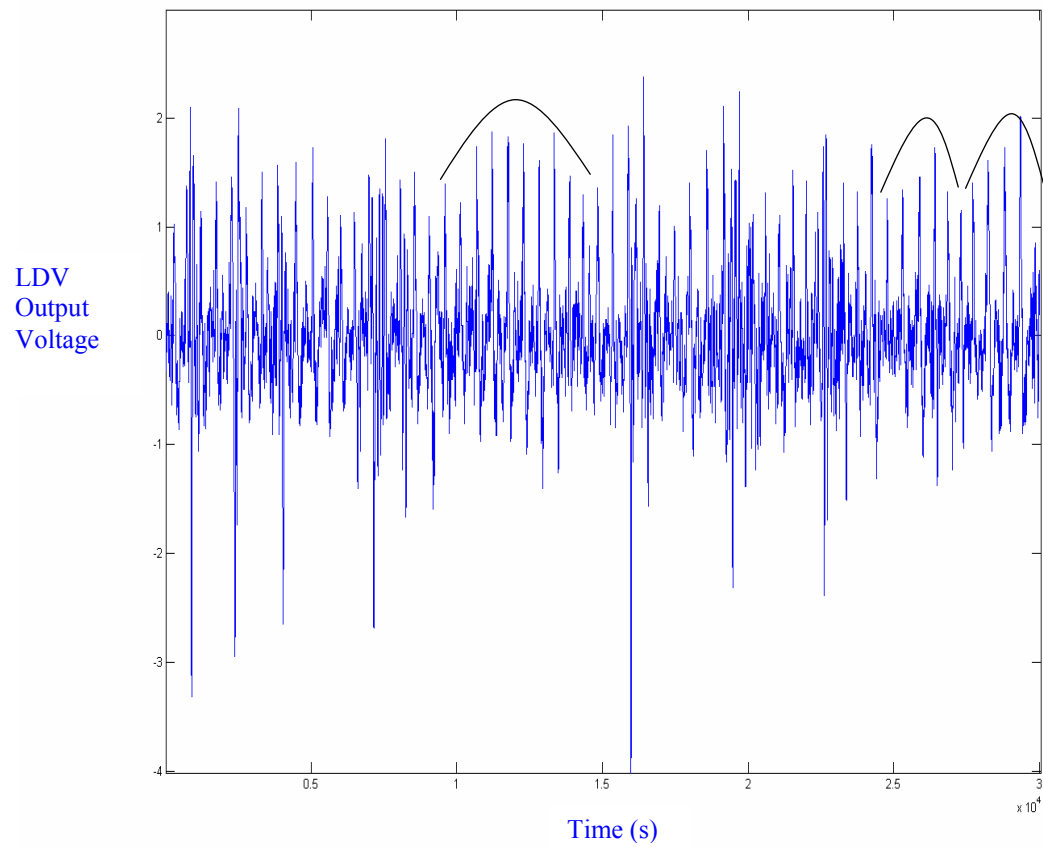


Figure 47 - Femoral artery measurement on a Wheaton Terrier with the breathing effects drawn above.

V. Future Work

Unfortunately the academic year has quickly come to an end and I will no longer be able to work on this amazing project. There are still several aspects of the project that I would have liked to continue to explore. First of all, I would have liked to take much more data. For some of the body parts, I was only able to obtain one or two waveforms in order to be time efficient. In the future, I think there should be several measurements made for each artery to achieve a precise and consistent waveform for replication purposes. On the same note, the position of measurement should also be investigated. For example, I was lucky enough to take a measurement from the radial artery, having experimented with seven or eight different positions, each yielding a waveform slightly different than the other. A protocol should be made for the position of measurement and exactly where to aim the laser beam for each target artery to produce the most precise data.

Once a protocol is made, data should be taken on numerous subjects of different ages, sizes, and health. Once enough samples are taken, the data should be given to cardiac specialist for further analysis of its usefulness diagnostic medicine. Also, the Principal Component Analysis should be completed to understand the discriminating features between various patients. Hopefully, the project will not only be found useful to find the blood pressure waveform, but also to be used as a diagnostic tool.

As a possible diagnostic tool, the LDV may be used to not only measure the skin velocity, but also the blood flow velocity. If a second laser vibrometer is used simultaneously, both aiming at the same artery, the blood flow velocity may be measured. Similarly, an investigation of circulation effects should be conducted, especially for

elderly diabetic patients. If, for example, there is a patient with poor circulation in the legs, measurements can be made over several points in the leg to visualize and hopefully discern of the point where the circulation worsens.

As an enhancement to the LDV, a tracker system may be added in using an additional laser. If such a system is used, the patient would not have to remain perfectly still, which is especially useful for an ER or for measurements of animals. An added benefit of the system would allow measurements to be made on subjects while they are in motion, (i.e. cardiovascular exercising). Using a treadmill or a bicycle, the patient may be in motion while the laser tracks the target artery, collecting useful data. This data could be used to determine the health of the heart, as well as a diagnostic tool.

For even further analysis of the data, future studies should be done to determine the relationship between the calculated displacement waveform and an actual systolic and diastolic reading. Blood pressure can be found by the following relationship:

$$\text{Blood Pressure} = \text{Cardiac Output} * \text{Total Peripheral Resistance} \quad (34)$$

The cardiac output is the blood flow, and can be changed by the heart rate and stroke volume. The total peripheral resistance is the opposition to blood flow, also defined as impedance. Although more work need to be conducted, it appears that the velocity waveform measured with the LDV is related to the derivative of the impedance waveform [7]. Knowing the impedance waveform would allow calculations of systolic and diastolic pressures to be done simply by multiplying the maximum and the minimum points on the waveform by the cardiac output, respectively [11]. There should also be

studies done in conjunction with a cardiac specialist to determine a systematic and simple way of determining the cardiac output of a patient so that determining the systolic and diastolic blood pressures may become part of the protocol.

VI. Conclusions:

The Fenwick Scholar project has undoubtedly been one of the best experiences of my life. I have found a whole new meaning of time management, I have found appreciation for independent motivation, and most importantly I have become a creative thinker. These qualities are essential for a successful future in medical school, especially for research, and I am glad that I have had the chance to prepare myself for this future in such a unique way. I would like to again thank Professor Matlak, the Fenwick Committee, Dr. Lynn Antonelli, and Dr. Edward Soares

VI. Appendices

Appendix A

References

- [1] Anderson, James E. Grant's Atlas of Anatomy. 7th ed. Baltimore: Williams & Wilkins Co., 1978.
- [2] Antonelli, Lynn T. Pressure Event Detection Based on the Dyadic Wavelet Transform. Ann Arbor: UMI Dissertation Services, 1995.
- [3] Antonelli, L., Desjardins, C., Soares, E., "A remote and non-contact method for obtaining the blood-pulse waveform with a laser Doppler vibrometer" submitted to the proceedings SPIE Photonics West: BIOS, January 2007
- [4] Berne, Robert, Matthew Levy. Cardiovascular Physiology. 8th ed., St. Louis: Mosby, 2001.
- [5] Brooks, Wendy C. "Hypertension (High Blood Pressure)." The Pet Health Library (2002). 22 July 2005
<<http://www.veterinarypartner.com/content.plx?P=A&A=1216>>.
- [6] Dorsey, Michael. "WPI - Transformations." On the Front Lines of Telemedicine. 02 September 2004. Worcester Polytechnic Institute. 7 July 2005
<<http://www.wpi.edu/News/Transformations/2003Spring/telemedicine.html>>.
- [7] Essue, Paul, David P. Beach, and Allen Shotwell. Applications of Lasers and Laser Systems. Englewood Cliffs: PTR Prentice-Hall, Inc., 1993.
- [8] Goldwasser, Samuel." Laser Safety Classifications." Sam's Laser FAQ. 1 May 2007.
<<http://www.repairfaq.org/sam/lasersaf.htm#safisc>>.
- [9] Hering, Peter, Jan Peter Lay, and Sandra Stry, ed. Laser in Environmental and Life Sciences. Berlin: Springer, 2004.
- [10] Lay, David C. Linear Algebra and It's Applications. 3rd ed. Boston: Addison-Wesley, 2003.
- [11] Lomba, John F. Non-Contact Measurement of the Carotid Artery Pulse Waveform Thesis. University of Rhode Island, 2004.
- [12] Newman, C.N. Hypertension in Dogs and Cats. Dec 1997. 04 Aug. 2005
<<http://www.newmanveterinary.com/hyperten.html#What%20Is%20Systemic%20Hypertension>>.

- [13] Niemz, Markolf H. Laser-Tissue Interactions. 3rd ed. Heidelberg: Springer, 2004.
- [14] Papoulis, Athanasios. Signal Analysis. New York: McGraw-Hill, 1977.
- [15] Phillips, Jr., Roger E. "Access Excellence Classic Collection." The Heart and Circulatory System. National Health Museum. 18 July 2005
<http://www.accessexcellence.org/AE/AEC/CC/heart_anatomy.html>.
- [16] Ross, John. Blood Vessels. 1999. 02 Aug. 2005
<<http://greenfield.fortunecity.com/rattler/46/bloodpressure.htm>>.
- [17] Schmidt-Nielsen, Knut. Animal Physiology: Adaptation and Environment. 5th ed. New York: Cambridge University Press, 1997.
- [18] Stewart, James. Single Variable Calculus: Concepts & Contexts. 3rd. ed., Belmont. CA: Thomson/Brooks-Cole, 2005.
- [19] Wadsworth, Kimberly. "Blood Pressures." E-mail to Candida Desjardins. 22 Jul 2005.
- [20] Winburn, D.C. What Every Engineer Should Know About Lasers. New York: Marcel Dekker, Inc., 1987.

Appendix B

Figures and Tables

	Page Number
Table 1 – He-Ne laser properties	9
Table 2 – Summary of Laser Safety Guidelines	15
Table 3 - Biostimulative Effects	26
Table 4 - Thermal Effects of laser irradiation	29
Figure 1 – Diagram of amplification by stimulated emission	7
Figure 2 (a) – Laser Scheme	8
(b) – Typical Resonant Cavity	8
Figure 3 – He-Ne laser scheme	9
Figure 4 - Modified Mach-Zehnder heterodyned interferometer configuration used in the Polytec Laser Doppler Vibrometer	18
Figure 5 - Simplified model of the skin with plane parallel epidermal and dermal layers	23
Figure 6 - Diagram of laser-tissue interactions	27
Figure 7 - Location of thermal effects in tissue	30
Figure 8 -	
(a) Uterine tissue of a rat coagulated with a CW Nd:YAG laser	30
(b) Human cornea coagulated with 120 pulses from an Er:YAG laser	30
Figure 9 -	
(a) Human tooth vaporized with 20 pulses from an Er:YAG laser	31
(b) Enlargement	31
Figure 10 -	
(a) Tumor metastases on human skin carbonized with a CW CO ₂ laser	31
(b) Human tooth carbonized with a CW CO ₂ laser	31

Figure 11 -	
(a) Human tooth melted with 100 pulses from a Ho:YAG laser	32
(b) Enlargement	32
Figure 12 - Computer simulation of photoablation	33
Figure 13 - Photoablation of corneal tissue with an ArF excimer laser	34
Figure 14 - Laser-induced plasma sparking on a tooth surface with a single pulse from a Nd:YLF laser	35
Figure 15 - Cavitation bubble with a human cornea induced by a single pulse from a Nd:YLF laser	36
Figure 16– Figure of the human heart	38
Figure 17 – Photograph of device and data acquisition system	47
Figure 18 –	
(a) Picture of velocity wave-form measurement of the carotid artery on a female subject	48
(b) Picture of a velocity waveform measurement of the carotid artery on a male subject	48
Figure 19 - Diagram of the human body arteriole system along with the target arteries labeled	49
Figure 20 –	
(a) - Carotid artery skin velocity measurement on a female subject	50
(b) - Facial artery skin velocity measurement on a female subject	51
(c) - Brachial artery skin velocity measurement on a male subject	51
(d) - Radial artery skin velocity measurement on a male subject	52
(e) - Femoral artery skin velocity measurement on a female subject	52
(f) - Pedal artery skin velocity measurement on a female subject	53
(g) - Posterior tibial artery skin velocity measurement on a female subject	53
Figure 21 - Integration of raw data from the pedal artery of a female subject	55
Figure 22 –	
(a) - Raw data from the pedal artery (black) and the filtered data (red)	56
(b) - Frequency spectrum of the unfiltered data (red) and filtered data (blue)	56
Figure 23 - Filtered data from the pedal artery (black) and the integrated filtered data (red)	57
Figure 24 - Integration of the filtered data (red) and the integration of	58

the raw data using the dy method (black)

Figure 25 - Measurement of the carotid artery on a female subject showing the breathing effects drawn above	59
Figure 26 - Measurement of the pedal artery on a female subject showing the similar amplitudes as drawn above	59
Figure 27 – Calculation of the heart rate on a pedal artery skin velocity waveform	60
Figure 28 – Two breathing cycles of a carotid artery skin velocity measurement demonstrating a sinus arrhythmia	61
Figure 29 - Measurement of the pedal artery on a female subject without using the retro-reflective tape	62
Figure 30 – Distribution of subjects	64
Figure 31 –	
(a) - Carotid artery skin velocity waveform of an 87 year old female subject	65
(b) - Carotid artery skin velocity waveform of an 18 year old male subject	65
(c) - Carotid artery skin velocity waveform of a 44 year old female subject	66
Figure 32 – Distribution of BMI's from Holy Cross subjects	67
Figure 33 -	
(a) - Carotid artery skin velocity measurement of an underweight male subject	68
(b) - Carotid artery skin velocity measurement of an obese male subject	68
(c) - Carotid artery skin velocity measurement of a female subject with cuff reading of 81/64	69
(d) - Carotid artery skin velocity measurement of a male subject with cuff reading of 176/113	70
(e) - Carotid artery skin velocity measurement of a male subject with skin caliper reading of 6mm	71
(f) - Carotid artery skin velocity measurement of a female subject with skin caliper reading of 16mm	71
(g) - Carotid artery skin velocity measurement of a female subject with a heart rate of 51 bpm	72
(h) - Carotid artery skin velocity measurement of a male subject with a heart rate of 100 bpm	72

Figure 34 – LDV system being used on a subject in the Electrophysiology Lab at UMASS Memorial Hospital	74
Figure 35 (a) Electrocardiogram (blue), Radial Arterial Blood Pressure Waveform, and the Carotid Artery Skin Velocity Waveform of a male subject	75
Figure 35 (b) Electrocardiogram (blue), Radial Arterial Blood Pressure Waveform (red), and the Carotid Artery Blood Pulse Waveform (green) of a male subject.	76
Figure 35 (c) Electrocardiogram (blue), Radial Arterial Blood Pressure Waveform (red), the Carotid Artery Skin Velocity Waveform and the Carotid Artery Blood Pulse Waveform (green) of a male subject with arrows drawn to demonstrate some of the relationships between the waveforms	77
Figure 36(a) – Carotid artery skin velocity waveform of a male subject with various distinguishable characteristics indicated	79
Figure 36(b) – Carotid artery skin velocity waveform of a female subject with various distinguishable characteristics indicated.	80
Figure 36(c) – Carotid artery skin velocity waveform of a female subject with various distinguishable characteristics indicated	81
Figure 36(d)– Carotid artery skin velocity waveform of a male subject with various distinguishable characteristics indicated	82
Figure 37 – single cycle waveform for patient, m	82
Figure 38 - Laser vibrometer velocity measurement on the carotid artery of a female subject (red) and the biosensor LED measurement on her right index finger	84
Figure 39 - Filtered data of the carotid artery measurement with the laser vibrometer (black) and the derivative of WPI biosensor measurement of the index finger (blue)	85
Figure 40 - WPI biosensor measurement of the index finger (blue) and the integration of the filtered laser vibrometer data from the carotid artery (red)	88
Figure 41 - Measurement from the WPI biosensor on the index finger (black) and the derivative of the biosensor data (blue). The dicrotic notch is labeled at several points with a black arrow from one waveform to another.	89
Figure 42 - Filtered data from the laser vibrometer of the carotid artery	90

(black) and the integration of the filtered data (red) .
The dicrotic notch is labeled at several points with a black arrow from one waveform to another.

- Figure 43 - Picture of the set-up used for velocity measurement of a dog 93
- Figure 44 - Additional picture of the set-up along with the placement of the retro-reflective tape for the target femoral artery 93
- Figure 45 - Filtered data from the measurement of the femoral artery on a Wheaton Terrier (black) and the integration of the filtered data (red) 94
- Figure 46 - Filtered data from the measurement of the femoral artery on a Wheaton Terrier (black) and the integration of the filtered data (red). The dicrotic notch is labeled with a black arrow from one waveform to another 95
- Figure 47 - Femoral artery measurement on a Wheaton Terrier with the breathing effects drawn above 96

Appendix C

A remote and non-contact method for obtaining the blood-pulse waveform with a laser Doppler vibrometer*Candida L. Desjardins¹, Lynn T. Antontelli², Edward Soares^{1,3}¹ Department of Mathematics and Computer Science, College of the Holy Cross, Worcester, MA² Naval Undersea Warfare Center, 1176 Howell St., Newport, R.I.³ Department of Radiology, University of Massachusetts Medical School, Worcester MA**ABSTRACT**

The use of lasers to remotely and non-invasively detect the blood pressure waveform of humans and animals would provide a powerful diagnostic tool. Current blood pressure measurement tools, such as a cuff, are not useful for burn and trauma victims, and animals require catheterization to acquire accurate blood pressure information. The purpose of our sensor method and apparatus invention is to remotely and non-invasively detect the blood pulse waveform of both animals and humans. This device is used to monitor an animal or human's skin in proximity to an artery using radiation from a laser Doppler vibrometer (LDV). This system measures the velocity (or displacement) of the pulsatile motion of the skin, indicative of physiological parameters of the arterial motion in relation to the cardiac cycle. Tests have been conducted that measures surface velocity with an LDV and a signal-processing unit, with enhanced detection obtained with optional hardware including a retro-reflector dot. The blood pulse waveform is obtained by integrating the velocity signal to get surface displacement using standard signal processing techniques. Continuous recording of the blood pulse waveform yields data containing information on cardiac health and can be analyzed to identify important events in the cardiac cycle, such as heart rate, the timing of peak systole, left ventricular ejection time and aortic valve closure. Experimental results are provided that demonstrates the current capabilities of the optical, non-contact sensor for the continuous, non-contact recording of the blood pulse waveform without causing patient distress.

Keywords: Blood Pulse Waveform, Laser Doppler Vibrometer, Carotid Artery, Dicrotic Notch, Arterial Pulse, Non-Contact

*Adopted from Antonelli, L., Lomba, J., and Ohley, W., "Non-Contact Measurement of the Carotid Artery Blood Pulse Waveform" submitted to IEEE Transactions on Biomedical Engineering, September 2006.

I. INTRODUCTION

A Laser Doppler Vibrometer (LDV) was used to remotely record the arterial, blood pulse waveform (BPW) by directing the laser beam onto the skin surface above an artery to measure the surface velocity. The waveforms can be monitored in real-time and recorded for subsequent analysis of the patient's physiological condition. Information on patient condition with regard to the shape of the waveform as a result of heart muscle contractions and valve operations, as well as the timing of various cardiac cycle events can be obtained from the waveform measurement. Additionally, monitoring the blood pulse waveform at multiple points along the arterial path can provide blood flow velocity information as well as reveal changes in the waveform due to the arterial path structure, possibly revealing arterial obstructions. This technique is non-invasive and has been used to measure the blood pulse waveform over various arteries including the pedal, radial, femoral, brachial, popliteal, facial, posterior tibial, and carotid arteries. The non-contact method of monitoring an arterial pulse waveform can be appreciated in cases where very limited contact to the patient is desired, such as with trauma or burn victims and neonatal patients.

Test results are presented where the laser beam from the LDV was directed onto the skin surface area above a subject's carotid artery. The laser light reflected from the skin surface undergoes a Doppler shift due to the surface motion that occurs along the axis of the laser beam. The reflected light, frequency modulated by the skin surface motion, is detected by the LDV interferometer and demodulated to obtain the velocity of the skin surface. The blood pulse waveform, characterized by the displacement of the skin surface, is obtained by integrating the velocity waveform that is measured directly as the artery under the skin contracts and expands.

Traditionally, blood pulse waveforms, or blood pressure waveforms are obtained invasively by inserting a catheter with a pressure sensor tip into an artery, such as the femoral artery¹. This technique provides reliable time history of the pressure waveform with calibrated blood pressure values. Although the time history of the blood pulse waveform is measured using the laser sensor, the actual pressure values that cause the arterial motion have not yet been realized from the data, since the distensibility, or impedance of the arterial wall is not known.

Other means of measuring the rhythmic pulsation of the heart at different locations within the circulatory system have been attempted. Impedance cardiography, for example, has also provided a way to non-invasively monitor the pump action of the heart. Systems that use laser light have been widely used as a tool to measure other physiological quantities. A photometric pulse detector (PPD), which works by reflectance principle, has been used to measure an arterial pulse at the temporal artery by making contact to the skin area². An optical method known as photoelectric plethysmography detects blood pulse waves as a change in the light intensity modulated by blood contents in the tissue. The operation of this system is based on the fact that the heartbeat causes the change of blood contents in tissue and the light penetrating the tissue is absorbed by the blood³.

Laser Doppler techniques have found considerable application in biology and medicine. One such application is in assessing blood flow velocity through the arteries and capillaries. Light is capable of measuring the velocities of red blood cells even at relatively slow speeds with which they move through the capillaries. The spectral purity of the laser makes it practical to detect even the slight frequency shifts produced by the interactions between photons and moving red blood cells⁴. Essex⁵ discussed the development of the laser Doppler scanner, and the use of such device to build an image of the skin in terms of its blood flow. Laser Doppler vibrometer techniques have also been employed to measure low surface vibration velocities produced when excitation forces, with low energy levels, were employed to put teeth into vibration⁶. Measurements of skin surface vibration have been demonstrated using an optical interferometer system that measures surface velocity based on the Doppler frequency shift principle. Such vibration is proportional to the pulsatility of the underlying blood vessel especially the arteries and the heart⁷. An optical stethoscope, also based on Doppler principle covers most of the auditory range of a conventional stethoscope and can also detect skin vibration due to pulse waves propagating through the vasculature⁸. Lee⁹ verified through both experiment and theory that skin surface motion can be related to

the underlying vascular movements. The underlying artery causes skin vibration in the order of few hundred microns. The mean displacement of the carotid arterial wall resulting from the pumping action of the heart was found to be about $520 \mu\text{m}^{10}$. Such displacement data can be used to estimate the order of magnitude expected of the skin vibration. Vibration velocity of the tissue surrounding certain blood vessels can also be estimated and compared with the information obtained by the Doppler shift.

The blood pulse waveform, associated with the velocity and displacement of the vibratory skin as blood moves through the arteries, can be analyzed to derive the timing of cardiac events, such as heart rate, the timing of peak systole, left ventricular ejection time and aortic valve closure (dicrotic notch). Additional timing information can also be resolved with simultaneously recording of the electrocardiogram (ECG) along with the blood pulse waveform (BPW). Analysis of the combination of the ECG and BPW can provide information on the systolic time interval (STI), including the Left Ventricular Ejection Time (LVET), Pre-ejection Period (PEP), and Electromechanical Systole (QS2). These time intervals are important for health care professionals to assess patient condition.

This study investigates the use of a Laser Doppler Vibrometer (LDV) for non-contact measurement of the arterial, blood pulse waveform. Experimental data is presented to demonstrate the feasibility of the non-contact, laser-based detection method of measuring the blood pulse waveform. Analytical results to extract the timing of several cardiac events from the recorded waveform, with and without the electrocardiogram signals, are shown to provide insight on the type of information that can be derived from the measured blood pulse waveform.

II. THEORETICAL DISCUSSION

2.1 Cardiac function and timing

The heart is the central organ of the circulatory system and consists of four chambers, including two separate pumps that simultaneously inject an equal quantity of blood for both the pulmonary and systemic circulation. Pulmonary circulation supplies deoxygenated blood to the lungs while systemic circulation supplies oxygenated blood to all other organs. Systemic circulation consists of the aorta, the arteries, the arterioles, the capillary network, and the veins¹¹. The carotid artery, whose pulsatile motion will be monitored with the LDV, branches off from the aorta and travels up through the neck. Transmission of the arterial pulse over the short distance from the aortic root to the carotid artery site takes approximately 40ms and introduces virtually no waveform distortion.

The pump action of the heart occurs primarily as a result of the ventricular contraction. The cardiac cycle is divided into two periods; ventricular contraction (systole) and ventricular relaxation (diastole). During systole, the beginning of ventricular contraction and resulting first rise in the pressure inside the two ventricular chambers causes the two atrioventricular valves to close. The pressure rises without moving blood from the ventricles until it exceeds the pressure in the aorta and pulmonary artery. At this point the two semilunar valves are forced open and the flow of blood into the arterial trunks begins.

Blood flow through an artery is influenced by several factors including the geometry of the artery, the roughness and compliance of the arterial wall, and other characteristics and acting forces. As the blood is pumped through the arteries, the pressure forcing the blood flow causes a pulsatile, lateral movement of the vessel walls. Both the effective length of the arterial system and the pulse wave velocity influence the timing of the return of the reflected pressure wave. Therefore, a decrease in the aortic length or an increase in the pulse wave velocity can have the same effect on the blood pulse waveform⁹.

At the termination of the ventricle contraction and the onset of diastole, pressure in the cavities begins to fall, causing immediate closure of the semilunar valves. Relaxation of the semilunar muscle now produces a rapid fall in pressure in the two ventricle cavities, and the moment the pressure falls below the atria pressures the two atrioventricular valves open, permitting the ventricles to fill with blood from the atria. During both systole and diastole, there is a short period of time, which no blood flow occurs. This occurs between the time one set of valves closes and the others open and it is known as the isometric contraction and relaxation of the cardiac muscle¹¹.

During the cardiac cycle, pulsatile blood flow is introduced into the arterial system. This flow and the arterial wall resistance against such flow define the arterial pressure wave. The sudden dilation of the aorta by the blood ejected from the left ventricle is transmitted along the arterial system as a wave of elastic displacement of the arterial wall. This represents the arterial pulse wave or the arterial blood pressure waveform, which is an index of the heart rate, and in addition reflects the quantity of blood injected into aorta, and elasticity of the large arteries¹¹. Meinders et al¹² shows relationship between arterial pressure waveform and arterial cross-section by deriving pressure waveforms from the change in arterial cross-sections in the left common carotid artery. After the arterial cross-section and pressure waveforms are known, compliance, distensibility, pulse wave velocity and elastic modulus can be derived as a function of the distending pressure. Therefore a study of the common carotid artery shows that as the pulsatile blood flow travels through the arteries, it causes expansion and contraction of these arteries and therefore change in the diameter occurs. The LDV system is used to measure the skin motion due to the arterial expansion and contraction.

2.2 Optical properties of the skin

The optical properties of skin tissue influence all biological signal measurements that employ light energy. Models that predict reflection and transmission of light by tissue have been developed. However the accuracy of these models depends on how well the optical properties of tissues are known. Optical parameters are obtained by converting measurements of observable quantities like reflection into parameters that characterize light propagation in tissue. Such conversion process is based on a particular theory of light transport in tissue¹³. The theory of light transport in tissue is preferred in tissue optics instead of analytical approaches using Maxwell equations because of the inhomogeneity of biological tissue.

The reflectance from the skin is dependent upon the optical properties of the skin structure including the blood-free epidermis, as well as dermis layers as shown in Figure 1. The thickness of epidermis including the stratum corneum is 10-150 μm . The dermis layer is approximately 1-4 mm thick and contains elastic collagen fibers and blood vessels of different sizes. The epidermal layer contributes about 6% to the total reflectance at wavelengths over range from 400 to 800 nm¹⁴. This is a specular reflectance at the air-stratum corneum interface, which suggests that minimal scattering occurs in the epidermis, so that it acts primarily as an absorptive medium. Van Gemert et al¹⁵ found that for wavelengths between about 300nm and 1000nm, light scattering from nonpigmented tissues dominates absorption. And for wavelengths between 240nm and 633nm skin layers are strongly forward scattering media, meaning that the greatest scattering happens at the zero degree to the incident light.

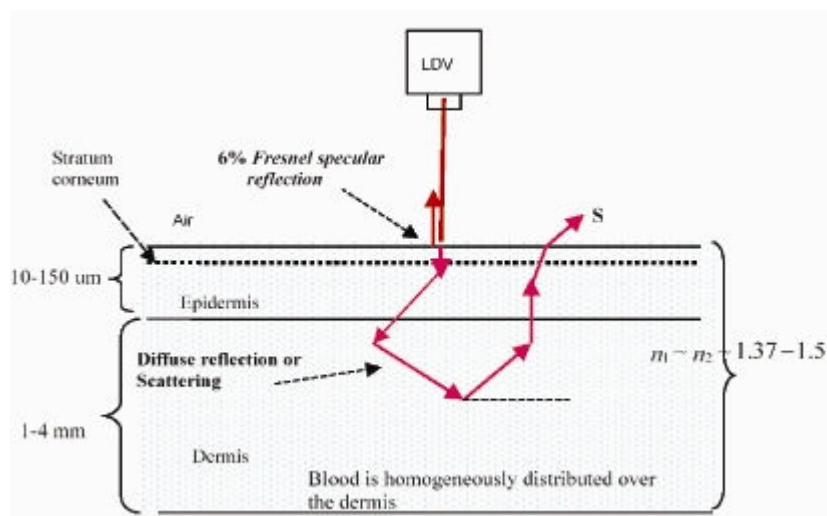


Fig. 1: Simplified model of the skin with plane parallel epidermal and dermal layers¹⁵.

Light penetration through tissue is important because the skin tissue is composed of several layers, which in turn can be broken down into sub-layers. Radiation at some wavelengths penetrates deeper than others and the absorption and scattering of such wavelengths in a tissue varies. Such scattered light once detected and demodulated provides information on the lateral displacement and velocity of the vessels and therefore the necessary information to show an arterial blood pulse waveform.

Measurements done during this study used an LDV to probe the surface area of the skin directly above the carotid artery on the neck of a person. Little skin preparation was needed, especially since this is an area with minimal hair growth. Any hair follicles that exist buried within the skin tissue layers will contribute to some extent to the absorption and scattering of the light and to the physiological noise present in the tissue. Such characteristics of light as it travels in a tissue should be accounted for and explained by the diffusion of light in tissue theory. Retro reflective tape at some instances was used to enhance the intensity of the reflected light at the detector, while preventing optical transmission into the skin layers.

2.3 Interferometer system description

One method to optically detect a small displacement or movement of an object is by means of interferometry. The principle of Laser Doppler Vibrometer (LDV) operation is based on the interference of two beams of light. The two laser (reference and measurement) beams arrive at the photodetector surface after one has undergone an optical path change and Doppler frequency shift. The measurement beam illuminates a surface and undergoes an optical path length change as the surface moves along the direction of the laser beam. This optical path difference is caused primarily by the vibration of the skin. The phase difference between the two beams inside the interferometer is represented by their beat frequency at the photodetector.

An LDV, Polytec PI model OFV-353 was used to obtain initial measurements of the blood pulse waveform by non-contact means at the subject's skin over the carotid artery. The system works on the basic principle of laser interferometry for Doppler shift velocity detection. Red light from a Helium Neon (HeNe) laser source is divided evenly by a beam splitter (BS1) into a reference beam and a measurement beam. The frequency of the reference beam is shifted using an acousto-optic modulator (Bragg cell) to introduce a 40 MHz signal. The modulation of the reference beam is desired in order to discern the direction (along the axis of the laser beam) of the movement obtained from Doppler shift of the returned signal. The measurement signal goes through the polarizing beam splitter (BS2) and Quarter Wave Plate (QWP), which behaves as a directional coupler. The light output from the vibrometer goes straight to the object under test, and the reflected beam is redirected to beam splitter (BS3). The reference beam and the return beam from the object are detected by detectors D1 and D2 and are subsequently combined and demodulated to obtain velocity and displacement information. Figure 2 shows a block representation of such a system, which is based on Mach-Zehnder interferometer¹⁶.

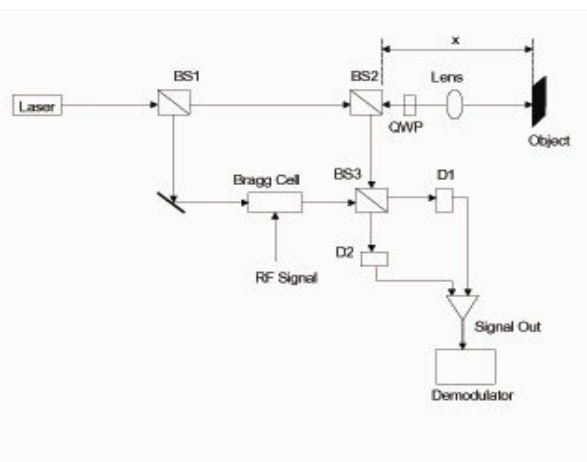


Fig. 2: Modified Mach-Zehnder heterodyned interferometer configuration used in the Polytec Laser Doppler Vibrometer¹⁶.

III. EXPERIMENTAL SETUP

A commercially available Laser Doppler Vibrometer (LDV) (Polytec PI model OFV353)¹⁶ was used to measure the blood pulse waveform by probing the skin surface above the carotid artery. The LDV system emits a continuous, low power, visible red light beam ($\lambda = 633 \text{ nm}$), which is directed onto the skin surface. The component of the scattered light that reflects back into the LDV interferometer, parallel to the incident beam, has undergone a Doppler shift due to the skin velocity. The detected signal is then demodulated by the system electronics to obtain the blood pulse waveform. A series of tests were conducted by measuring the skin motion on the neck region directly above the carotid artery, as illustrated by Figure 3. An optional piece of retro-reflective tape may be placed on the skin surface to enhance the signal. The LDV output signal was recorded along with the subject's ECG signal using a laptop computer based data acquisition system with a 1000 Hz sample rate. A 60 bpm signal represents a 1 Hz signal, and additional signal fluctuations were observed to be below 100 Hz, the 1000 Hz sample rate is above the Nyquist criterion for data sampling to prevent aliasing. The LDV sensitivity was set at 5 mm/s per Volt output. The velocity data was processed using a third order, high-pass Butterworth filter with a cutoff frequency of 0.0016 Hz to remove the DC offset that was imposed by the data acquisition system. The signal was then corrected to remove the imposed filter delay.

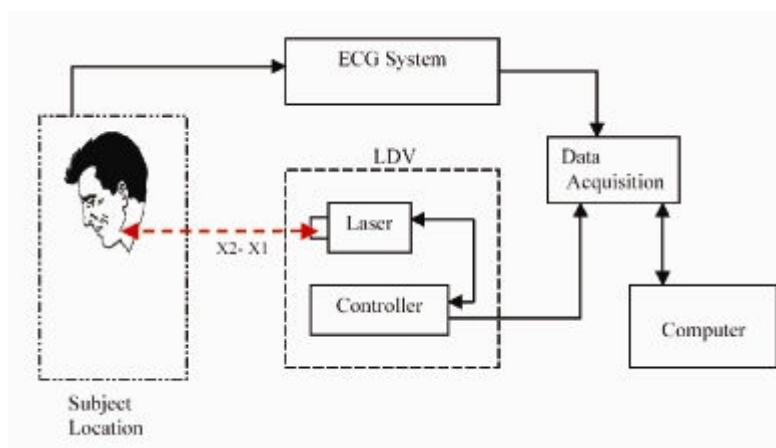


Fig. 3: Setup for simultaneous recording of ECG signal and carotid pressure waveform.

IV. RESULTS

The laser vibrometer system records surface velocity. During the cardiac cycle, variations in the blood pressure cause the artery to expand and contract. As the artery expands, the skin moves outward and the measured velocity signal increases. Likewise, the velocity is negative during contraction of the artery. As the artery motion changes direction, between a state of expansion and contraction, the velocity is zero. Zero velocity would occur at the point of maximum arterial expansion, such as at peak systole, during fluctuations in the blood flow direction such as during aortic valve closure and at the point of minimum arterial expansion at the start of left ventricular ejection. The blood pulse waveform is more clearly represented by the skin displacement, which is obtained by integrating the measured velocity signal. The skin displacement is comparable to traditional blood pulse waveforms. Two cardiac cycles of a blood pulse waveform measured on the carotid artery using the LDV are shown in Figure 4. The skin displacement waveform, calculated by integrating the measured velocity, is superimposed in Amplitude (V) in Figure 4. Two dotted vertical lines indicate (1) peak systole, which has a local maximum displacement and a zero velocity; and (2) the location of the dicrotic notch identifying aortic valve closure.

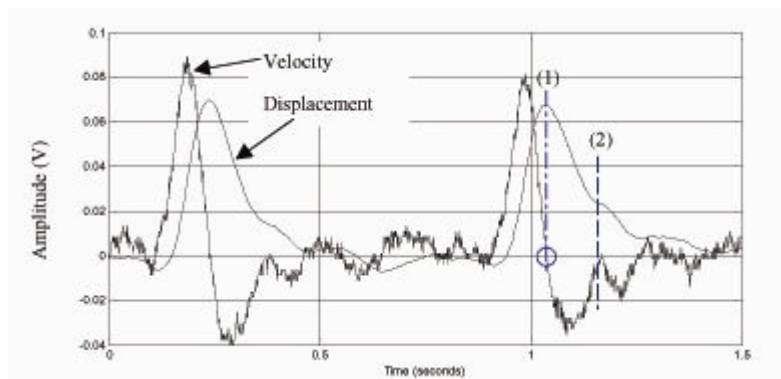


Fig. 4: LDV-measured velocity signal and the calculated displacement at the carotid artery.

A velocity waveform recorded by the LDV system on an adult male subject is shown in Figure 5a along with the calculated displacement signal in Figure 5b, which is the integral of the velocity signal that represents the blood pulse waveform and the simultaneously recorded ECG signal in figure 5c. The recording is 10 seconds long and contains 11 cardiac cycles. The amplitude scale for the velocity signal is in mm/s, which was converted from volts to velocity using the LDV sensitivity setting of 5 mm/s per Volt. The skin velocity ranges from approximately -5 to 8 mm/s. The skin displacement varies less than 0.4 mm. This test case was typical of the data that is repeatedly recorded using the laser vibrometer technique. The velocity and displacement signals do not identify the blood pressure quantity, only the time series waveform. The actual pressure values are not directly obtained from the remote velocity measurement. A calibration procedure would need to be developed, possibly by taking an independent reading of the actual pressure value such as with a cuff and relating the pressure to the voltage peak systolic amplitude.

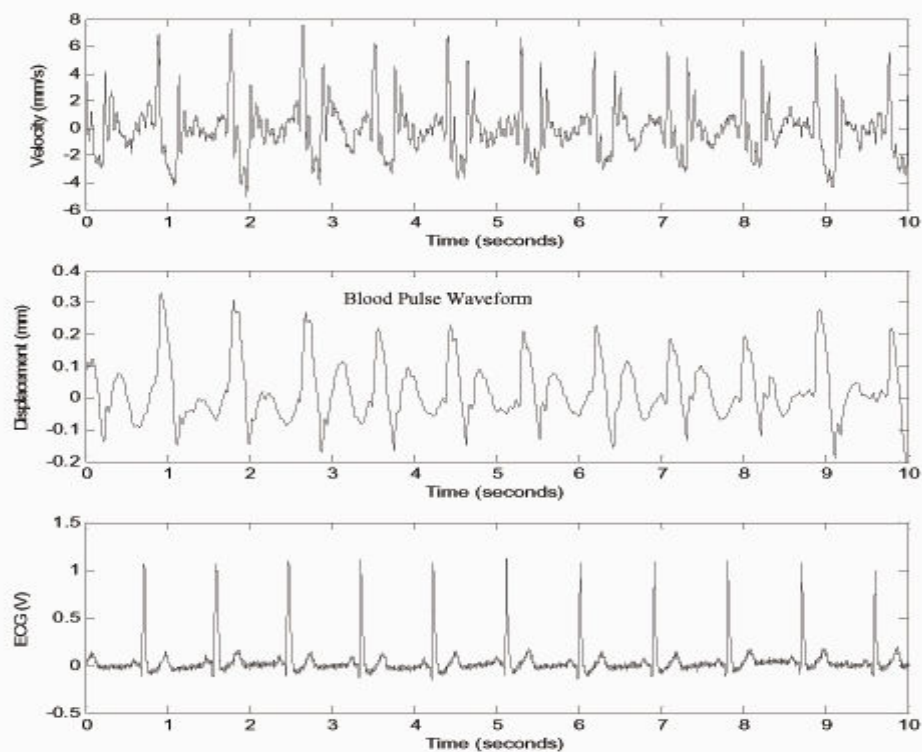


Fig. 5: Carotid artery pulse waveform (a) velocity signal measure by the LDV; (b) calculated displacement (blood pulse waveform); and (c) simultaneously measured ECG signal showing 11 cardiac cycles for an adult male subject.

The displacement waveform is similar to the impedance waveform and the velocity as the derivative of the impedance. Frey et al¹⁷ demonstrated that left ventricular ejection time measured from a carotid artery pulse wave recording and that of the impedance cardiogram are highly correlated. Electrical impedance cardiography (ICG) reflects instantaneous electrical impedance changes within the thorax area and these changes have been attributed to the dynamics of left ventricular ejection¹⁸. Figure 6 shows ICG plot recorded by electrodes contacting the skin and other cardiac signals of interest, which are used in identifying key parameters of the cardiac timing. On the first derivative (dZ/dt) plot, the onset of left ventricular ejection (O_a) and the closure of aortic valve (V_a) which defines LVET are shown. Such correlation was kept in mind during the analysis of the carotid pulse waveform obtained by means of LDV in this study.

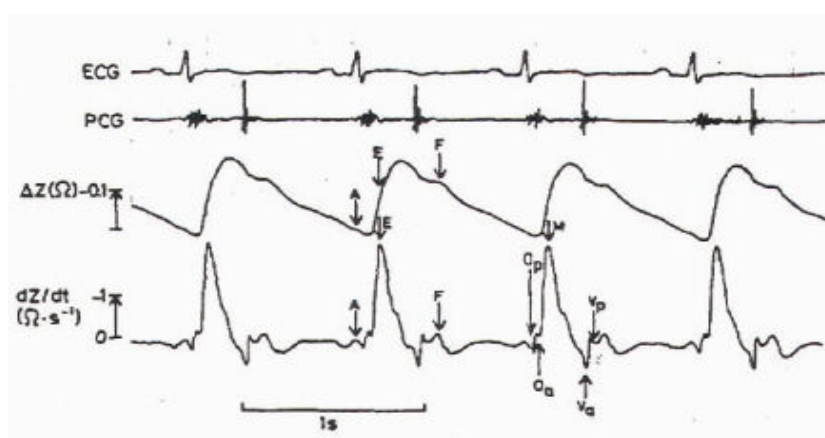


Fig. 6: Sample recording of electrocardiogram (ECG), phonocardiogram (PCG), and impedance cardiogram (Z) and its first derivative (dZ/dt) showing some cardiac timing intervals¹⁹.

V. CONCLUSION

A Laser Doppler Vibrometer (LDV) was used to measure the blood pulse waveform at several artery locations, including the carotid artery. This study shows that commercially available LDV systems can be used to directly probe person's skin surface area and record arterial blood pulse waveforms. The LDV measures the skin velocity above an underlying artery. The skin displacement, which corresponds to the blood pulse waveform was calculated by taking the integral of the recorded velocity signal and can also be measured by some commercial LDVs. This is a non-invasive and non-contact means of obtaining the blood pulse waveform. Blood pressure values are not directly obtained from the recorded waveform. A direct measurement of the blood pressure would be needed to calibrate the actual pressure with the recorded signal.

The onset of the upstroke and the dicrotic notch, which indicate the opening and closing of the aortic valve, respectively, are observed on the recorded blood pulse waveforms. Heart rate and the left ventricular ejection time can be determined from the timing of the characteristic events in the blood pulse waveform. Simultaneous ECG and LDV blood pulse measurements were recorded and used to estimate the systolic time intervals (QS2, LVET and PEP) and heart rate on a pulse-to-pulse basis.

The blood pulse data obtained shows potential for further use of such systems to provide information for assessing the health condition of a patient, particularly in trauma situations. In trauma situations the blood pulse waveform may provide physiological information that the systolic and diastolic pressure values alone do not provide. Other surface areas of the skin can be probed with the LDV in order to measure the blood pulse waveform at various arteries including the pedal, radial, femoral, brachial, popliteal, facial, posterior tibial, and carotid arteries. Simultaneous recording of the artery at several locations can be used to determine the propagation delay of the pulse waveform through the artery and to evaluate the change in waveform characteristics that may indicate possible obstructions or arterial condition. Further evaluation of this non-contact method of measuring the blood pulse waveform from a larger number of test subjects is currently being done. The College of the Holy Cross' Human Participant Committee has approved human subject trials to be conducted at the college through May 2007. The capability of this measurement method can then be evaluated versus a patient's physical characteristics, such as size, weight, and skin condition. Finally, a comprehensive medical evaluation of the measured, carotid artery, blood pulse waveforms need to be done to relate waveform characteristics to physiological condition.

VI. REFERENCES

1. Massachusetts General Hospital MGH/MF Waveform Database and Patient Guide, MIT, 1992.
2. Brown, T.R.M. and MacGregor, J., "An infra-red reflectance system for ambulatory characterization of left ventricular function," *Journal of Biomedical Engineering*, v. 4. n. 2, pp. 142-148, April 1982.
3. Tonooka, K., Yabe, K., Nishimura, O., and Kawabata, J. "Analysis of blood pulse wave measured by reflective optical sensor," *Proceedings of the 10th Annual International Conference of the IEEE, Engineering in Medicine and Biology Society*, v. 1, pp.84-85, 4-7 November 1988.
4. *Laser Doppler Blood Flowmetry (Developments in Cardiovascular Medicine S.)*, Ed.,Shepherd, A. P., and Oberg, P.A., Kluwer Academic Publishers, Norwell MA, 1990.
5. Essex, T.J.H., "Laser doppler imaging of skin blood flow," *The Institution of Electrical Engineers Colloquium on Functional Imaging*, pp. 8/1-8/2, 5 January 1994.
6. Castellini, P. and Scalise L., *Teeth mobility measurement by Laser Doppler Vibrometer*, American Institute of Physics, pp. 2850-2855, 1999.
7. Hong, H., and Fox, M. D., "Optical interferometric sensing of skin vibration," *Proceedings of the 15th Annual International Conference of the IEEE Engineering in Medicine and Biology*, pp. 894-895, 28-31 October 1993.
8. Hong, H., and Fox, M. D., "Detection of skin displacement and capillary flow using an optical stethoscope," *Proceedings of the 1993 IEEE 19th Annual Northeast Bioengineering Conference*, pp. 189-190, 1993.
9. Lee, C., and Mark, R. G., "Study of arterial pressure waves using a simple tube model of the ventriculo-arterial system." *IEEE*, 18-19 March 1993.
10. Hoeks, A. P., Brands, P. J., Smeets, F. A., and Reneman, R. S., "Assessment of the distensibility of superficial arteries," *Ultrasound in Medicine and Biology*, v. 16, n. 2, pp. 121-128, 1990.
11. Selzer, Arthur, *The Heart: Its Function in Health and Disease*. University of California Press, Berkeley and Los Angeles, 1966.
12. Meinders, Jan M., and Hoeks, A.P., "Simultaneous assessment of diameter and pressure waveforms in the carotid artery," *Ultrasound in Medicine & Biology*, v.30, n.2, pp.147-154, February 2004.
13. Cheong, W. F., Prael, S. A., and Welch, A. J., " A review of the optical properties of biological tissues," *IEEE Journal of Quantum Electronics*. v. 26. n. 12, pp. 2166-2185, December 1990.
14. Cui, W., Ostrander, L. E. and Lee, B.Y., "In vivo reflectance of blood tissue as a function of light wavelength," *IEEE Transaction on Biomedical Engineering*, v. 37. n. 6, pp. 632-639, June 1990.
15. Van Gemert, M. J. C., Jacques, S. L., Sterenborg, H. J. C. M., and Star, W. M., "Skin optics," *IEEE Transactions on Biomedical Engineering*, v. 36. n. 12, pp. 1146-1154, December 1989.
16. Polytec PI LDV manual OFV353 with interferometer drawing.
17. Frey, M. A. B., Doerr, B. M., Mann, B. L., and Miles, D. S. "Comparison of impedance ventricular function indices with systolic time intervals". *IEEE*, pp. 1086-1093, 1981.

18. Kizakevich, P. N., Gollan, F., McDermott, J. and Aranda, J. “ Continuous noninvasive cardiac monitoring of cardiac function,” Veterans Administration Hospital, University of Miami School of Medicine.
19. Visser, K.R., Mook, G. A., van der Wall, E., and Zijlstra, W.G., “Systolic time intervals by impedance cardiography,” Proceedings of the Annual International Conference of the IEEE Engineering in Medicine and Biology Society, v. 13. n. 2, pp.812-814, 31 October – 3 November 1991.

Appendix D

HUMAN PARTICIPANT CONSENT FORM

Title of Study: Remote detection of the blood pulse waveform

Purpose of Study:

The use of lasers to remotely and non-invasively detect the blood pressure waveform of both humans and animals will provide a powerful diagnostic tool. Currently, blood pressure measurement tools are not useful for burn and trauma victims, and animals require catheterization to acquire accurate blood pressure information. The purpose of the sensor method and apparatus invention is to remotely and non-invasively detect the blood pulse waveform of both animals and humans. This system will be used to measure the velocity (or displacement) of the pulsatile motion of the skin, indicative of physiological parameters of the arterial motion in relation to the cardiac cycle. Biological signals are important factor in helping to determine health condition. Continuous recording of the blood pulse waveform allows data containing information on the cardiac health and can be analyzed to identify important events in the cardiac cycle, such as heart rate, and the timing of peak systole and of the diastolic notch.

This is a study, not a diagnostic procedure.

Participation in the Demonstration:

You may take part in the study on a voluntary basis. If you are under 18 years of age you must have a parent sign this consent form in order to be able to participate. The risks to you are negligible. A low power (< 1 mW), visible light Class II laser is used and is considered a low risk for eye injury. If directly viewed for greater than 15 minutes, a Class II laser could be damaging to the eyes. The Class II laser used in this study will only be turned on for periods of 30 seconds when measurements are being taken, otherwise the laser will be shut-off. Avoid looking into a Class II laser beam, particularly with telescopic devices. The bright light of a Class II laser directed into the eyes will cause an instinctive reaction to look away or to close your eyes. This response is expected to protect you from any laser damage to the eyes; however, **you will be given eye protection as additional safety protection.** Measurements can be taken from areas of the body that are fully accessible (e.g. neck, face, arm) and/or areas that are normally covered by clothing (e.g. groin, knee, foot). **You are free to decide which areas of the body you are comfortable having measured.** Measurements will be taken behind closed doors with only the researcher and participant in Swords 201, with an additional curtain provided to ensure complete privacy. **You may stop participation at any time.**

Description of the procedure to be followed:

The demonstration participant will be seated and fitted with laser safety goggles. Blood pressure will be measured with a standard automatic blood pressure cuff, a skin caliper will be used to measure the amount of tissue that lies on top of the artery, and weight will be taken with a standard scale. A low power, 1 mW laser beam will be directed at the piece of retro-reflective tape placed on the target artery of the participant. The laser-detected blood pulse waveform will be viewed on a monitor and recorded. The blood pulse signal will be temporarily stored on a computer for video playback. The laser is shut off once the data has been recorded. The data file will be removed from the computer upon completion of the testing. The data will be stored as a hard copy with an associated subject number and will be locked in a file cabinet. **At no point in the study will your name be recorded, and a diagnosis will not be made.**

Expected duration of participation: 10 - 15 minutes **Location of study:**
Swords 201

Use and Confidentiality of Data: Participants are entitled to view the data taken at any point during the testing, which includes their blood pressure, weight, and blood pulse waveform. At no point in the study will the participant's name be recorded. All data will be saved under a subject number and locked in a file cabinet. All data taken will be used for further analysis and may be presented in the future.

Points of contact: **Candida (Didi) Desjardins**
College of the Holy Cross
Box 700
cldesj07@holycross.edu
508-728-5310

Prof. Edward Soares (advisor)
College of the Holy Cross
Box 73A
esoares@holycross.edu
508-793-3040

Statement of consent:

Please confirm that:

- 1) you have read the above information;
- 2) you have had the opportunity to ask questions, and they have been answered;
- 3) you understand that you do not have to fill out this form;
- 4) you do not have to participate in this study
- 5) you have the right to stop participation at any point in the study and;
- 6) you voluntarily consent to participate in the study.

Signature of Volunteer

Date

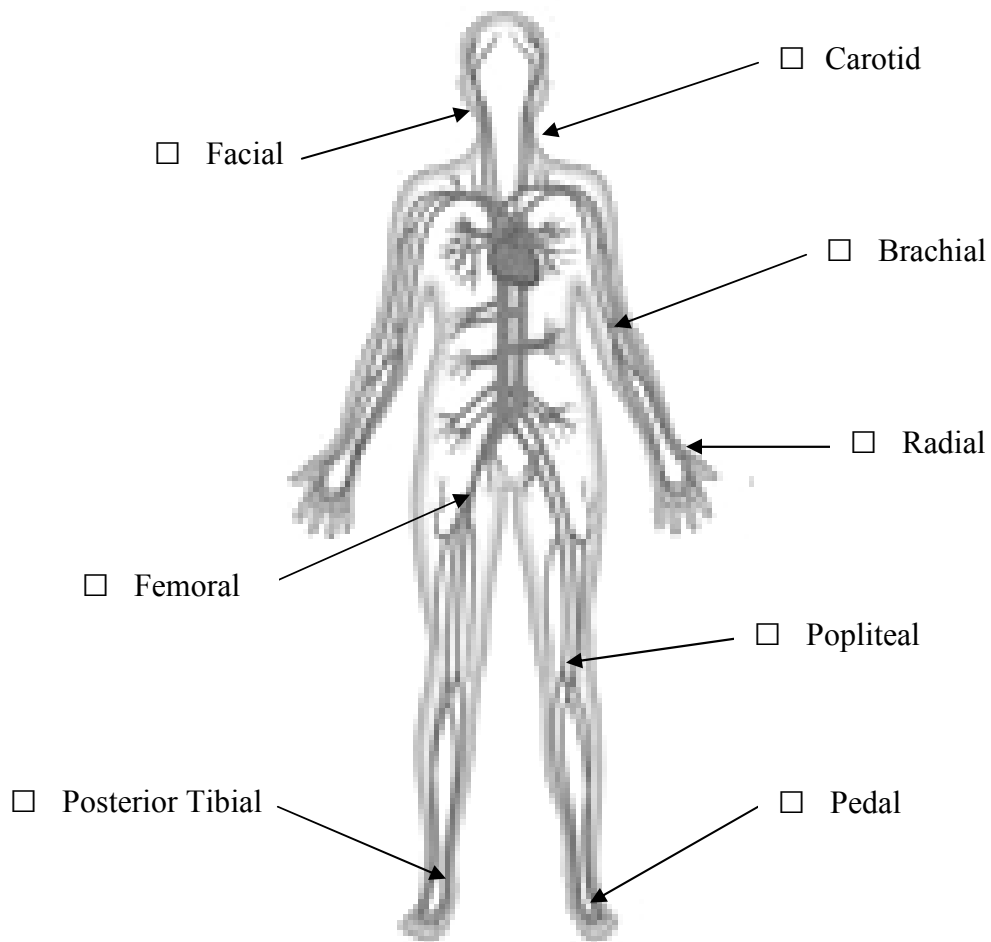
Signature of Principal Investigator

Date

Participant has agreed to have data recorded

Check
box

Arteries to be Measured: (please check)



courtesy of <http://www.dorlingkindersley-uk.co.uk/.html>

Skin Caliper Measurements:

Carotid Artery _____

Facial Artery _____

Brachial Artery _____

Radial Artery _____

Femoral Artery _____

Popliteal Artery _____

Posterior Tibial Artery _____

Pedal Artery _____

Appendix F

List of Equipment Used

- Tektronix TDS 1002 Two Channel Digital Storage Oscilloscope
- Polytec PDV-100 He-Ne Laser Doppler Vibrometer
- National Instruments 4-channel Hi-Speed USB Carrier (NI USB-9162)
- Naval Undersea Warfare Center (NUWC) Laptop 66604381139
- Omron HEM-780 *Intelli-sense* blood pressure monitor